N73-25276

NASA TECHNICAL NOTE

NASA TN D-7220

NASA TN D-7220

LOCAL SKIN FRICTION COEFFICIENTS AND BOUNDARY-LAYER PROFILES OBTAINED IN FLIGHT FROM THE XB-70-1 AIRPLANE AT MACH NUMBERS UP TO 2.5

by David F. Fisher and Edwin J. Saltzman

Flight Research Center

Edwards, Calif. 93523

NATIONAL AERONAUTICS AND SPACE ADMINISTRATION • WASHINGTON, D. C. • JUNE 1973

1. Report No.	2. Government Accession No.	3. Recipient's Catalog No.
NASA TN D-7220		
4. Title and Subtitle LOCAL SKIN FRICTION COEFFICIENTS AND BOUNDARY-LAYER PROFILES OBTAINED IN FLIGHT FROM THE XB-70-1 AIRPLANE AT MACH NUMBERS UP TO 2.5		5. Report Date June 1973 6. Performing Organization Code
7. Author(s) David F. Fisher and Edwin J. Saltzman		8. Performing Organization Report No. H-710
9. Performing Organization Name and Address NASA Flight Research Center P. O. Box 273 Edwards, California 93523		10. Work Unit No. 501-06-08-00-24 11. Contract or Grant No.
12. Sponsoring Agency Name and Address National Aeronautics and Space Administration Washington, D. C. 20546		13. Type of Report and Period Covered Technical Note 14. Sponsoring Agency Code
15. Supplementary Notes		

16. Abstract

Boundary-layer and local skin friction data for Mach numbers up to 2.5 and Reynolds numbers up to 3.6×10^8 were obtained in flight at three locations on the XB-70-1 airplane: the lower forward fuselage centerline (nose), the upper rear fuselage centerline, and the upper surface of the right wing.

Local skin friction coefficients were derived at each location by using (1) a skin friction force balance, (2) a Preston probe, and (3) an adaptation of Clauser's method which derives skin friction from the rake velocity profile. These three techniques provided consistent results that agreed well with the von Kármán-Schoenherr relationship for flow conditions that are quasi-two-dimensional.

At the lower angles of attack, the nose-boom and flow-direction vanes are believed to have caused the momentum thickness at the nose to be larger than at the higher angles of attack.

The boundary-layer data and local skin friction coefficients are tabulated. The wind-tunnel-model surface-pressure distribution ahead of the three locations and the flight surface-pressure distribution ahead of the wing location are included.

17. Key Words (Suggested by Author(s))	18. Distribution Statement
Turbulent boundary layer Skin friction XB-70-1 airplane	Unclassified - Unlimited

19. Security Classif. (of this report)	20. Security Classif. (of this page)	21. No. of Pages	22. Price*
Unclassified	Unclassified	68	$3.00

*For sale by the Clearinghouse for Federal Scientific and Technical Information
Springfield, Virginia 22151

* For sale by the National Technical Information Service, Springfield, Virginia 22151

LOCAL SKIN FRICTION COEFFICIENTS AND BOUNDARY-LAYER PROFILES OBTAINED IN FLIGHT FROM THE XB-70-1 AIRPLANE AT MACH NUMBERS UP TO 2.5

David F. Fisher and Edwin J. Saltzman
Flight Research Center

INTRODUCTION

Accurate prediction of skin friction drag is extremely important in the design of supersonic cruise aircraft. On a typical supersonic cruise airplane, for example, skin friction can account for as much as 30 percent to 40 percent of the total drag at cruise conditions. Because the range of an airplane is directly dependent on its lift-drag ratio, a seemingly small underestimation of the skin friction drag would result in the actual range of the vehicle being smaller than expected.

In the past, skin friction estimates were based on wind-tunnel-derived data and semiempirical expressions. These data and expressions covered a wide range of Mach numbers, Reynolds numbers, and stagnation temperatures, but usually did not account for effects of longitudinal pressure gradients, surface roughnesses, or upstream flow conditions. In addition, wind tunnels could not simultaneously simulate the Mach number, Reynolds number, and stagnation temperature conditions that would be experienced in flight by a supersonic cruise vehicle.

Because of these simulation deficiencies, the NASA Flight Research Center conducted a flight-test program with the XB-70-1 airplane to measure local skin friction and the associated turbulent boundary layer in a "real" environment. The large size and Mach number capability of the airplane enabled these measurements to be made at flow conditions that would be encountered by a supersonic cruise vehicle. Thus the flight data taken during this investigation will supplement existing wind-tunnel data and semiempirical expressions which have been extrapolated to the flight conditions of a supersonic cruise vehicle.

This report presents the skin friction coefficients and turbulent boundary-layer profile data obtained in the flight study. The flights were made at Mach numbers up to 2.5 and Reynolds numbers up to 3.6×10^8 based on the length of the run. Stagnation temperatures were as high as 488° K (878° R). Also included are the in-flight surface-pressure distributions obtained on the right wing for the region ahead of the boundary-layer sensor complex, and the skin temperature measured at each sensor complex. Wind-tunnel surface-pressure-distribution data obtained from an XB-70-1 model at locations corresponding to the regions directly ahead of each boundary-layer sensor complex are also presented.

The in-flight local skin friction coefficients and boundary-layer data are compared with the flat plate relationship of von Kármán-Schoenherr. The basic velocity profile data are tabulated so that other prediction techniques may be applied and the results compared with the flight measurements.

SYMBOLS

Physical quantities in this report are given in the International System of Units (SI) and parenthetically in U. S. Customary Units. The measurements were taken in U. S. Customary Units. Factors relating the two systems are presented in reference 1.

C_f	local skin friction coefficient, $\frac{\tau}{q_1}$
C_p	pressure coefficient, $\frac{p - p_\infty}{q_\infty}$
c	chord length, m (ft)
d	diameter of rake pitot probe, cm (in.)
H_f	flight-measured boundary-layer shape factor, $\frac{\delta^*}{\theta}$
$\bar{H}$	boundary-layer shape factor for a flat plate
k	constant, $20.05 \frac{\text{m/sec}}{(°\text{K})^{1/2}}$ $\left(49.02 \frac{\text{ft/sec}}{(°\text{R})^{1/2}}\right)$
l	length of airplane, 56.62 m (185.75 ft)
M	Mach number
p	static pressure, N/m^2 (lb/ft^2)
q	dynamic pressure, $(\gamma/2)M^2p$, N/m^2 (lb/ft^2)
R_x	Reynolds number based on distance, x
R_θ	Reynolds number based on momentum thickness
r	radius of surface at rear fuselage boundary-layer rake location, 45.7 cm (18 in.)
T	local static temperature, except when used with subscript or superscript, °K (°R)
T'	reference temperature (ref. 2), °K (°R)
T_r	recovery temperature, $T_1\left(1 + 0.176M_1^2\right)$, °K (°R)

T_t	total or stagnation temperature, °K (°R)
T_w	wall (skin) temperature, °K (°R)
t	time during flight, hr:min
u	local velocity, m/sec (ft/sec)
u'_τ	friction velocity, $(\tau/\rho')^{1/2}$, m/sec (ft/sec)
w	width of rake strut
x	distance from nose apex along airplane centerline or from wing leading edge along a chord line, m (ft)
y	distance from surface to rake probe centerline, cm (in.)
α	indicated airplane angle of attack, deg
γ	ratio of specific heats for air, 1.4
δ^+	boundary-layer thickness where $\frac{u}{u_1} = 1.00$, cm (in.)
δ^*	displacement thickness of boundary layer, cm (in.)
Θ	momentum thickness of boundary layer, cm (in.)
μ'	absolute viscosity based on reference temperature
μ_1	absolute viscosity based on edge temperature
ν'	kinematic viscosity based on reference temperature, $\frac{\mu'}{\rho'}$
ρ	local mass density
ρ'	mass density based on reference temperature
ρ_1	mass density based on edge temperature
τ	surface friction stress, N/m^2 (lb/ft^2)
$-$	over a quantity denotes flat plate and zero longitudinal pressure gradient
$\frown$	over a quantity indicates a curved surface

Subscripts:

c	for curved surface
fb	determined using skin friction force balance method

i	incompressible
pp	determined using Preston probe method
rake	determined using rake method
1	edge condition
∞	free-stream condition

TEST FACILITY

Aircraft Description

The XB-70-1 airplane, designed as a long-range, supersonic cruise airplane, was the testbed for this experiment. The airplane was 56.62 meters (185.75 feet) long and had a wingspan of 32 meters (105 feet). Although it was capable of speeds up to Mach 3 at an altitude of 21,000 meters (70,000 feet), it was limited to a Mach number of approximately 2.5 for the flights of this study. Gross takeoff weight was approximately 227,000 kilograms (500,000 pounds). The airplane had a thin, low-aspect-ratio, 65.6° sweptback delta wing with folding tips, twin vertical stabilizers, and a movable canard with trailing-edge flaps. Its propulsion system consisted of a twin-inlet, six-jet-engine package mounted on the undersurface of the wing and fuselage. A more detailed description of the airplane is included in reference 3. A photograph of the airplane is shown in figure 1, and a three-view drawing, with pertinent dimensions, is presented in figure 2.

Location of Boundary-Layer Sensor Complexes

Skin friction boundary-layer complexes were installed at three locations on the airplane: two on the fuselage (one on the lower surface of the nose and another on the upper surface of the rear fuselage); and a third on the upper surface of the right wing. The locations of these complexes are shown in figure 2.

Upstream Surface Areas

Photographs of the surface areas on the airplane ahead of the three sensor complexes are shown in figure 3. The principal surface protuberances ahead of the nose complex are the nose boom, the flow-direction vanes, and their supporting shafts (fig. 3(a)). The lower fuselage skin (fig. 3(b)) was quite smooth.

Ahead of the rear fuselage complex, protuberances that would disturb the flow included a canard and three rear-facing vents (figs. 3(c) and 3(d)), the canopy and nose visor, and the nose-boom and flow-direction vanes mentioned before. The surface forward of this complex had many screwheads, some of which protruded approximately 1.2 millimeters (3/64 inch) (figs. 3(e) and 3(f)). However, the surface 6.7 meters (22 feet) immediately ahead of the complex was smooth, painted metal without screwheads.

Directly ahead of the wing rake, a chordwise distribution of flush static orifices was provided by an installation and fairing technique described in reference 4. This faired surface was very smooth, with no gaps, lap joints, or protuberances. However, about 45 centimeters (18 inches) on each side of the row of orifices, the aircraft skin had various types of lap joints, rivet heads, and other roughnesses, some protruding as much as 1.6 millimeters (1/16 inch). These surfaces are shown in figures 3(c), 3(f), and 3(g).

INSTRUMENTATION

Air Data Parameters

On the XB-70-1 airplane, Mach number was measured with a pitot-static probe mounted on the nose boom. This probe and its flight calibration are described in reference 5. Also mounted on the nose boom were balsa vanes that measured angle of attack and angle of sideslip. A photograph of the nose boom showing the pitot-static probe and the balsa vanes is presented in figure 3(a). Free-stream total temperature was measured with a dual-range total-temperature probe mounted beneath the engine inlet.

Description of Boundary-Layer Sensor Complexes

Each of the three skin friction boundary-layer complexes consisted of a boundary-layer rake, a Preston probe, a skin friction force balance, a flush static-pressure orifice, and a thermocouple.

The boundary-layer rake at the nose sensor complex was mounted on the lower centerline of the forward fuselage, 5.5 meters (18.2 feet) behind the juncture of the nose boom and fuselage. This rake, the Preston probe, the static-pressure orifices, and the skin friction force balance are shown in figures 4(a) and 4(b). The friction force balance was approximately 28 centimeters (11 inches) directly forward of the Preston probe. The thermocouple that measured skin temperature was nearby on the inside skin surface.

At the rear fuselage complex (figs. 5(a) and 5(b)), the boundary-layer rake was mounted on the upper fuselage centerline 43.5 meters (142.8 feet) behind the nose-boom–fuselage juncture. The skin friction force balance and the Preston probe were, respectively, to the left and right of the rake looking rearward. The flush static-pressure orifice was between the Preston probe and the rake, and the skin temperature thermocouple was nearby on the inside skin surface.

The rake at the wing sensor complex was on the right wing, 4.4 meters (14.3 feet) from the airplane centerline and 15.6 meters (51.1 feet) behind the wing chord leading edge. A photograph of this sensor complex is shown in figure 6. At this complex, two different locations were used for the friction force balance, but only one was used at a time. The Preston probe and static-pressure orifice are also shown in the photograph. The skin temperature thermocouple was slightly inboard of the Preston probe on the inside surface of the skin.

Pressures from the rake, Preston probe, and static-pressure orifices, the force balance and thermocouple outputs, and many other aircraft parameters were recorded by a pulse code modulation (PCM) and a magnetic tape data recording system. The data acquisition system is described in detail in references 6 to 10.

Skin Friction Force Balance

A small, commercially developed, liquid-cooled force balance was used in this investigation. The balance was calibrated before and after each flight, using the airplane's recording system, by applying known forces along the sensitive axis of the balance. The balances had a sensitive area of 0.694 square centimeter (0.108 square inch). The sensitivity of the balances for the flights of this study was 1 gram per square centimeter (2.05 pounds per square foot) for the nose and rear fuselage sensor complexes and usually 2 grams per square centimeter (4.10 pounds per square foot) for the wing complex. Previous use of this type of skin friction force balance in flight is described in reference 11.

Boundary-Layer Rakes

A drawing of the wing rake, which was similar to the other rakes used in this experiment, is shown with some design criteria in figure 7. The rake consisted of a stainless steel strut with a 15°-wedge-angle leading edge and a semicircular trailing edge. The wing and rear fuselage rakes had 11 probes with an outer diameter of 0.318 centimeter (0.125 inch) and a pitot-static probe with an outer diameter of 0.475 centimeter (0.187 inch). The nose rake had nine probes with an outer diameter of 0.152 centimeter (0.060 inch). The leading edges of all the probes on the wing and rear fuselage rakes were chamfered internally 30°. The distances of the probes from the airplane skin for these rakes are presented in table 1. A rake with the same dimensions as the wing rake and two smaller rakes with the same proportions were evaluated in the NASA Ames Research Center's Unitary Plan Wind Tunnel. Parameters derived from these rakes in supersonic flow compared well with data from a single traversing probe, as reported in reference 12.

Preston Probes

The Preston probes (figs. 4 to 6) used in this flight investigation were surface impact-pressure tubes similar to those suggested by Preston in reference 13 and used in the study of reference 14. The leading edges of the cylindrical tubes or probes were squared off perpendicular to the tube axis and were free of burrs. The probes had an outer diameter of 0.635 centimeter (0.250 inch) with an inside-to-outside-diameter ratio of 0.6; they were 6.35 centimeters (2.5 inches) long. The calibration in reference 14 was used to derive the skin friction coefficients.

Pressure Transducers

Because relatively high temperatures were experienced, special differential-pressure transducers of the linear variable differential transformer type were used. These transducers were designed to withstand and operate reliably at temperatures up to 316° C (600° F). They were mounted beneath the airplane skin close to each rake to keep the pressure lines short and to minimize lag effects.

The transducers were referenced to a nose-boom static pressure. This pressure was monitored by a high-resolution absolute-pressure transducer, which was kept in a carefully controlled temperature environment.

Thermocouples

Chromel-alumel thermocouples were placed at each complex to measure local skin temperature. Thermocouples were also used to measure the temperature of one pressure transducer of each cluster of transducers as well as the temperature of each skin friction balance. Thus it was assured that these instruments remained within tolerable temperature limits during the flights of this study.

DATA REDUCTION

Data for processing were selected from steady-state flight (that is, time segments when aircraft velocity and altitude were essentially constant) to minimize the effects of lag. After the steady-state portions of the flights were identified, digital data were selected at the rate of four data points per second. These data were then averaged for 30 time points, or a total of 7.5 seconds for each data point presented in table 1.

Using the information given in reference 15, the impact pressures within and beyond the boundary layer were combined with the corresponding local surface static pressure to obtain values of local Mach number. The usual assumption was made that static pressure was constant through the boundary layer. Evidence to support this assumption was obtained by comparing the pressure values obtained from the flush orifice with those from the rake tip pitot-static probe for the wing and aft fuselage sensor complexes. Local velocities were computed from Mach numbers by using the following expression and assuming that the total-temperature distribution through the boundary layer was constant and equal to the free-stream value:

$$u = kM\left(\frac{T_t}{1 + \frac{\gamma - 1}{2} M^2}\right)^{1/2}$$

where

u is in m/sec (ft/sec)

$k = 20.05 \; \frac{\text{m/sec}}{(°\text{K})^{1/2}} \; \left(49.02 \frac{\text{ft/sec}}{(°\text{R})^{1/2}}\right)$

T_t is in °K (°R)

Momentum thickness, Θ, and displacement thickness, δ^*, were calculated from the following flat plate relationships for the nose and the wing sensor complexes:

$$\Theta = \int_0^{\delta^+} \frac{\rho u}{\rho_1 u_1}\left(1 - \frac{u}{u_1}\right)dy$$

$$\delta^* = \int_0^{\delta^+} \left(1 - \frac{\rho u}{\rho_1 u_1}\right)dy$$

At the nose and wing complexes, the boundary-layer thicknesses were small in comparison to the local surface radius of curvature; therefore, negligible error was introduced by using flat plate relationships. However, at the rear fuselage complex the boundary-layer thicknesses were not small compared to the local surface radius of curvature, so it was necessary to use the following three-dimensional relationships:

$$\Theta_c = \int_0^{\delta^+} \frac{\rho u}{\rho_1 u_1}\left(1 - \frac{u}{u_1}\right)\left(\frac{r + y}{r}\right)dy$$

$$\delta_c^* = \int_0^{\delta^+} \left(1 - \frac{\rho u}{\rho_1 u_1}\right)\left(\frac{r + y}{r}\right)dy$$

Local skin friction coefficients were obtained from the flight data by three different methods. In the first method, a direct measurement, a small force balance measured the drag of a small exposed element set flush in the skin. In the second method, the Preston probe technique described in reference 13 was combined with the calibration for compressible flow effects given in reference 14. In the third method, which made use of the rake, local skin friction was determined through an adaptation of the Clauser technique (ref. 16) in which local skin friction is derived from boundary-layer profiles. The charts in reference 17 were used to adapt this method to compressible flow conditions. The latter two methods depended on the universal nature of the wall law to provide local friction coefficients.

RESULTS AND DISCUSSION

The measured boundary-layer velocity profiles and the values calculated from these profiles are tabulated in tables 1 and 2.

Comparison of Methods Used To Determine Local Skin Friction

The flight-derived values of skin friction determined by using the three methods—force balance, Preston probe, and rake—are presented and compared in figure 8. In the data from the nose sensor complex (fig. 8(a)), the values from the Preston probe tend to be higher than those from either the force balance or the rake. As was shown in figure 4(a), the Preston probe and friction force balance were displaced slightly from the lower centerline, whereas the rake was on the centerline. This, combined with the blunt (not chamfered) leading edge of the Preston probe, may have caused some crossflow effects in the Preston probe data. When the rake-determined coefficients were plotted against the force balance results, the data were scattered about the line of perfect agreement; however, the scatter was large.

At the rear fuselage location (fig. 8(b)), the values found with the three methods agreed well, but only a few data points were obtained using the force balance. The values for the rake method and those for the Preston probe method were in good agreement, even though the Preston probe was displaced from the centerline. This agreement would seem to indicate that crossflow was not a factor at this location.

At the wing location (fig. 8(c)), the data were scattered about the line of perfect agreement when the skin friction coefficients determined with the Preston probe and rake methods were plotted against the force balance results. The scatter is quite large for the relationships that include the force balance results, probably because the force balance used for most of the measurements at the wing was less sensitive than those installed at the nose or rear fuselage. The use of this balance was unintentional, but necessitated by the schedule of flights and the unavailability of other balances. The agreement between the results from the rake and Preston methods was excellent.

Small skin friction force balances like those used in this experiment must be kept free of dust, lint, water, and fuel to operate reliably. Where it has not been possible to maintain this degree of cleanliness or where sufficient cooling has not been available, data and experience have shown that the Preston probe and rake techniques could be substituted for the more direct balance approach on a full-scale vehicle. In addition, the installation of a friction force balance requires space to a depth of about 5 centimeters (2 inches) below the skin. Where this space is not available, use of the Preston probe and rake would be advantageous.

Velocity Profiles

Typical turbulent velocity profiles for the three locations are presented in figures 9(a) to 9(c). These velocity profiles were time-averaged from 30 discrete time points lasting 7.5 seconds during steady-state flight. Thus any short-period pressure fluctuations were eliminated.

In figures 10(a) to 10(c) representative data are plotted in the Sommer and Short T' form of the law of the wall. These plots represent profiles from the three complexes; the data are plotted three times for each complex, once for each method of determining skin friction. The friction coefficients determined from the results of the rake method were derived by using the velocity profiles. Since the rake method is based on the law of the wall, it was not surprising to find good agreement between the flight data and the values predicted by the theory of reference 18 in the logarithmic portion of the boundary layer. These plots distinctly show the logarithmic portion of the boundary layer. The tendency of the data in the semilogarithmic region to agree in magnitude with the theoretical data, instead of being below and parallel with them, suggests, according to Clauser (ref. 16) and Prandtl (ref. 19), that surface roughness was not a significant factor in the local skin friction coefficient.

Momentum Thickness Results

In figure 11 the incompressible momentum thickness parameter, $\frac{\Theta}{x}\frac{T'}{T_1}$, is plotted for the three locations as a function of incompressible Reynolds number. At the nose location (fig. 11(a)) the low-angle-of-attack data (square symbols) have higher momentum thicknesses than the higher angle-of-attack data. These results are similar to those reported in reference 20. When the nose-boom length of 1.97 meters (77.75 inches) is included in the length of the run, x, the low-angle-of-attack data correspond better with the higher angle-of-attack data but are still approximately 25 percent higher than the von Kármán-Schoenherr flat plate curve (ref. 21). As in reference 20, it is thought that the higher momentum thicknesses for the low-angle-of-attack data were caused chiefly by the nose boom and its accompanying protuberances. This suggests that more of the flow over the nose boom and its protuberances travels along the lower fuselage centerline at the low angles of attack, causing the boundary layer to be thicker and to have a larger momentum thickness at the nose sensor complex location than at the higher angles of attack.

Values of momentum thickness obtained at the rear fuselage location are shown in figure 11(b). These data are presented with the von Kármán-Schoenherr curve for a flat plate to illustrate how much momentum thickness can deviate from flat plate values. At the higher Reynolds numbers the data were about 25 percent below the von Kármán-Schoenherr curve, and at the lower Reynolds numbers the measured values were as much as 60 percent lower. Reference 22 reports that the three vents shown in figures 3(c) and 3(d) exhaust low momentum flow into the boundary layer, which would tend to increase the momentum thickness rather than decrease it. The canard and other three-dimensional forebody effects may result in relatively high energy flow being directed to the upper fuselage region, causing the apparent momentum thickness to be lower than the flat plate curve.

At the wing location (fig. 11(c)), the data are scattered about the von Kármán-Schoenherr curve, tending to be slightly higher at the lower Reynolds numbers and slightly lower at the higher Reynolds numbers.

Possibly a more explicit way to evaluate the influence of angle of attack and nose-boom protuberances on the nose momentum thickness data is shown in figure 12. The ordinate is a ratio of the values of momentum thickness determined for the data from the nose location (fig. 11(a)) to the values of momentum thickness predicted by the von Kármán-Schoenherr flat plate theory for corresponding Reynolds numbers. For comparison, a curve derived from a method used by Allen and Monta (ref. 23) is included. This curve approximates the influence of the lower centerline contour of the fuselage from the nose back to the boundary-layer complex. It also approximates the effects of angle of attack. In this instance, as in reference 20, liberties were taken with the method to permit the effects of angle of attack to be treated like deformations of the body cross-sectional area. Thus the lower centerline contour of the fuselage relative to the free-stream flow is accounted for in the prediction at any angle of attack, although the local body radius is not properly simulated.

Comparison of the flight-derived data with the reference 23 curve shows that below an angle of attack of 4° the subsonic and supersonic data are higher than the theory, suggesting the influence of the nose boom and the accompanying protuberances. Above an angle of attack of 4°, the subsonic data agree with the theory, but the supersonic data are below the theory.

The momentum thickness data from the rear fuselage location were relatively insensitive to angle of attack and are not shown.

At the wing location, angle of attack had a significant effect on momentum thickness at supersonic speeds, as shown in figure 13. At a free-stream Mach number of approximately 2.5 (flagged symbols), the leading edge is not yet experiencing supersonic flow, so the increase in momentum loss with angle of attack might represent a rolled-up vortex that grows with angle of attack. At subsonic speeds, leading edge separation would also be expected to produce increasing losses with angle of attack; however, this was not evident in the data.

Local Skin Friction Results

The local skin friction coefficients obtained in flight from the nose, rear fuselage, and wing locations are presented as a function of Reynolds number based on momentum thickness in figure 14. These data, representing the three methods of determining local friction, were transposed to incompressible conditions by using the reference temperature method described in reference 2.

For both the nose (fig. 14(a)) and rear fuselage (fig. 14(b)) locations, the local friction coefficients at the higher Reynolds numbers tend to agree with the flat plate values given by the von Kármán-Schoenherr curve (ref. 21). The only exception is the Preston probe data from the nose location. At the lower Reynolds numbers, however, the friction levels for these locations are significantly above the flat plate prediction.

A detailed history of the flow ahead of these locations would aid in explaining the difference in the levels of friction at the lower and higher Reynolds numbers. Although this history is not available, of related interest are the shape factor levels associated with the local friction coefficients shown in figures 14(a) and 14(b). The shape factors of the data for the higher Reynolds numbers, where the friction coefficients tend to agree with the flat plate values, are similar to those for a flat plate ($\frac{H_f}{\bar{\bar{H}}} \approx 1$). Where the friction data are significantly higher than the von Kármán-Schoenherr curve, that is, for the lower Reynolds numbers, the shape factors are lower than for flat plate values $(\frac{H_f}{\overline{\overline{H}}} < 1)$. Qualitatively, this would be expected.

At the wing location (fig. 14(c)), where the flow would tend to be more two-dimensional than at the nose or rear fuselage, the local skin friction coefficients agreed well with the von Kármán-Schoenherr flat plate theory. However, the measured shape factors were higher than would be predicted for a flat plate $(\frac{H_f}{\overline{\overline{H}}} > 1)$, and lower friction levels would be expected. This benefit was not achieved, however.

It is sometimes preferable to plot skin friction coefficients as a function of Reynolds number based on the assumed length of the turbulent run, x, as in figure 15. Again, as before, the data were transformed to incompressible conditions. This figure shows essentially the same results as figure 14. The data from the nose (fig. 15(a)) and rear fuselage (fig. 15(b)) locations are higher than the von Kármán-Schoenherr curve, as they were in figure 14, for the lower Reynolds numbers. Also, for the wing location (fig. 15(c)), where the flow is most nearly two-dimensional, the data agree well with the two-dimensional von Kármán-Schoenherr theory.

CONCLUDING REMARKS

In a flight investigation with the XB-70-1 airplane at Mach numbers up to 2.5 and Reynolds numbers up to 3.6×10^8, skin friction boundary-layer measurements were made at three locations: (1) the lower forward fuselage centerline (nose), (2) the upper rear fuselage centerline, and (3) the upper surface of the right wing. Three different methods were used at each location. Skin friction force balances, Preston probes, and boundary-layer rakes were used in conjunction with appropriate calibrations for compressible flow.

For a quasi-two-dimensional flow (wing location) the local skin friction coefficients agreed with the von Kármán-Schoenherr theory when transposed to incompressible conditions by using the reference temperature method of Sommer and Short.

The results from the three methods were in agreement except for the Preston probe data obtained at the nose. A slight displacement of the probe from the lower centerline may have been responsible for the discrepancy.

The influence of the nose-boom and flow-direction vanes on momentum thickness was evident at the nose location with change in angle of attack. At the lower angles of attack, momentum thickness was significantly higher than theoretical values because of the thickening of the boundary layer caused by the nose-boom and flow-direction vanes. At the higher angles of attack more of the flow was diverted away from the lower centerline, causing the momentum thickness to be less than at the lower angles of attack.

Flight Research Center
National Aeronautics and Space Administration
Edwards, Calif., November 10, 1972

APPENDIX

PRESSURE DISTRIBUTIONS

One of the quantities necessary to accurately predict skin friction and other boundary-layer parameters is the pressure distribution along the flow streamline. In this investigation, it was assumed that the flow streamline was parallel to the longitudinal body axis; that is, that the flow streamline at the nose and rear fuselage locations started at the nose and continued along the lower and upper fuselage centerlines, respectively. It was also assumed that the flow streamline for the wing location started at the wing leading edge at butt plane 172, approximately 15.6 meters (51 feet) forward of the boundary-layer complex.

Figure 16 shows the pressure distribution on the wing for several Mach numbers as measured in flight and on a wind-tunnel model (unpublished data). The agreement between the data is fair.

In figure 17 wind-tunnel pressure-distribution data for the fuselage lower surface (ref. 24) are presented for several Mach numbers. No flight data in terms of the distribution of pressure were available for this location; however, flight results from an orifice near the sensor complex are included for comparison and showed good agreement.

The wind-tunnel pressure distribution for the upper fuselage, also from reference 24, is shown in figure 18. Again, data are presented for several Mach numbers. As on the lower fuselage, no flight data were available other than those taken near the sensor complex. These data showed good agreement with the wind-tunnel results except at Mach 0.95.

REFERENCES

1. Mechtly, E. A.: The International System of Units - Physical Constants and Conversion Factors. NASA SP-7012, 1969.

2. Sommer, Simon C.; and Short, Barbara J.: Free-Flight Measurements of Turbulent-Boundary-Layer Skin Friction in the Presence of Severe Aerodynamic Heating at Mach Numbers From 2.8 to 7.0. NACA TN 3391, 1955.

3. Andrews, William H.: Summary of Preliminary Data Derived From the XB-70 Airplanes. NASA TM X-1240, 1966.

4. Taillon, Norman V.: A Method for the Surface Installation and Fairing of Static-Pressure Orifices on a Large Supersonic-Cruise Airplane. NASA TM X-1530, 1968.

5. Webb, Lannie D.; and Washington, Harold P.: Flight Calibration of Compensated and Uncompensated Pitot-Static Airspeed Probes and Application of the Probes to Supersonic Cruise Vehicles. NASA TN D-6827, 1972.

6. Edwards, E. L.: An Airborne Data Acquisition System for Use in Flight Testing the XB-70 Airplane. Selected Instrumentation Application Papers From AGARD Flight Mechanics Panel - Twenty-Sixth Meeting, AGARD Rept. 507, June 1965, pp. 23-48.

7. Edwards, E. L.: A Data Processing Facility for the XB-70 Flight Test Program. Flight Test Instrumentation, AGARD Conf. Proc. No. 32, 1967, pp. 243-258.

8. Ince, D. B.: Application Experience With the B-70 Flight Test Data System. Aerospace Instrumentation. Vol. 4 - Proceedings of the Fourth International Aerospace Symposium, College of Aeronautics, Cranfield, Eng., March 21-24, 1966, M. A. Perry, ed., Pergamon Press, Ltd., 1967, pp. 195-208.

9. Arnaiz, Henry H.; and Schweikhard, William G.: Validation of the Gas Generator Method of Calculating Jet-Engine Thrust and Evaluation of the XB-70-1 Airplane Engine Performance at Ground Static Conditions. NASA TN D-7028, 1970.

10. Saltzman, Edwin J.; Goecke, Sheryll A.; and Pembo, Chris: Base Pressure Measurements on the XB-70 Airplane at Mach Numbers From 0.4 to 3.0. NASA TM X-1612, 1968.

11. Garringer, Darwin J.; and Saltzman, Edwin J.: Flight Demonstration of a Skin-Friction Gage to a Local Mach Number of 4.9. NASA TN D-3830, 1967.

12. Keener, Earl R.; and Hopkins, Edward J.: Accuracy of Pitot-Pressure Rakes for Turbulent Boundary-Layer Measurements in Supersonic Flow. NASA TN D-6229, 1971.

13. Preston, J. H.: The Determination of Turbulent Skin Friction by Means of Pitot Tubes. No. 15,758, British A.R.C., March 31, 1953.

14. Hopkins, Edward J. ; and Keener, Earl R. : Study of Surface Pitots for Measuring Turbulent Skin Friction at Supersonic Mach Numbers - Adiabatic Wall. NASA TN D-3478, 1966.

15. Ames Research Staff: Equations, Tables, and Charts for Compressible Flow. NACA Rept. 1135, 1953. (Supersedes NACA TN 1428.)

16. Clauser, Francis H. : Turbulent Boundary Layers in Adverse Pressure Gradients. J. Aeron. Sci., vol. 21, no. 2, 1954, pp. 91-108.

17. Allen, Jerry M. ; and Tudor, Dorothy H. : Charts for the Interpolation of Local Skin Friction From Experimental Turbulent Velocity Profiles. NASA SP-3048, 1969.

18. Smith, Donald W. ; and Walker, John H. : Skin-Friction Measurements in Incompressible Flow. NASA TR R-26, 1959. (Supersedes NACA TN 4231.)

19. Prandtl, L. : The Mechanics of Viscous Fluids. Vol. III of Aerodynamic Theory, div. G, sec. 22, W. F. Durand, ed., Dover Publications, Inc., 1963, pp. 135-145.

20. Saltzman, Edwin J. ; and Fisher, David F. : Some Turbulent Boundary-Layer Measurements Obtained From the Forebody of an Airplane at Mach Numbers up to 1.72. NASA TN D-5838, 1970.

21. Locke, F. W. S., Jr. : Recommended Definition of Turbulent Friction in Incompressible Fluids. DR Rept. No. 1415, Navy Dept., Bur. of Aeronautics, Res Div., June 1952.

22. Wykes, John H. ; and Lawrence, Robert E. : Estimated Performance and Stability and Control Data for Correlation With XB-70-1 Flight Test Data. North American Rockwell Corp. (NASA CR 114335), 1971.

23. Allen, Jerry M. ; and Monta, William J. : Turbulent-Boundary-Layer Characteristics of Pointed Slender Bodies of Revolution at Supersonic Speeds. NASA TN D-4193, 1967.

24. Anon. : Trisonic Wind Tunnel Tests of an .03 Scale XB-70 Pressure Model To Determine Pressure Distribution at Mach Numbers .60 to 3.0. North American Aviation, Inc., Rept. No. NA-62-1275, vol. I, Oct. 1, 1962.

TABLE 1.– MEASURED BOUNDARY-LAYER VELOCITY PROFILES

(a) Nose location; x = 5.54 m (18.2 ft)

Flight identification	
1-79, t = 1 hr 40 min	
Flight conditions	
$M_1 = 1.97$, $\alpha = 3.4°$, $T_t = 389°$ K (700° R), $T_w = 362°$ K (651° R)	
y, cm (in.)	$\frac{u}{u_1}$
0.076 (0.030)	0.5909
.381 (.150)	.6960
.762 (.300)	.7517
1.080 (.425)	.7800
1.709 (.673)	.8199
4.420 (1.740)	.9201
7.399 (2.913)	.9497
10.02 (3.945)	.9660
16.33 (6.430)	1.0000

Flight identification	
1-79, t = 1 hr 42 min	
Flight conditions	
$M_1 = 2.10$, $\alpha = 3.1°$, $T_t = 393°$ K (707° R), $T_w = 362°$ K (651° R)	
y, cm (in.)	$\frac{u}{u_1}$
0.076 (0.030)	0.6240
.381 (.150)	.7243
.762 (.300)	.7724
1.080 (.425)	.7989
1.709 (.673)	.8370
4.420 (1.740)	.9286
7.399 (2.913)	.9570
10.02 (3.945)	.9711
16.33 (6.430)	1.0000

Flight identification	
1-79, t = 1 hr 57 min	
Flight conditions	
$M_1 = 1.57$, $\alpha = 2.8°$, $T_t = 328°$ K (591° R), $T_w = 321°$ K (577° R)	
y, cm (in.)	$\frac{u}{u_1}$
0.076 (0.030)	0.5518
.381 (.150)	.6471
.762 (.300)	.6986
1.080 (.425)	.7238
1.709 (.673)	.7642
4.420 (1.740)	.8844
7.399 (2.913)	.9467
10.02 (3.945)	.9799
16.33 (6.430)	1.0000

Flight identification	
1-79, t = 2 hr 15 min	
Flight conditions	
$M_1 = 0.85$, $\alpha = 3.5°$, $T_t = 284°$ K (512° R), $T_w = 305°$ K (549° R)	
y, cm (in.)	$\frac{u}{u_1}$
0.076 (0.030)	0.6018
.381 (.150)	.6952
.762 (.300)	.7486
1.080 (.425)	.7721
1.709 (.673)	.8140
4.420 (1.740)	.8977
7.399 (2.913)	.9594
10.02 (3.945)	1.0000
16.33 (6.430)	1.0000

Flight identification	
1-82, t = 1 hr 40 min	
Flight conditions	
$M_1 = 2.24$, $\alpha = 4.4°$, $T_t = 481°$ K (865° R), $T_w = 406°$ K (731° R)	
y, cm (in.)	$\frac{u}{u_1}$
0.076 (0.030)	0.5935
.381 (.150)	.7001
.762 (.300)	.7572
1.080 (.425)	.7886
1.709 (.673)	.8276
4.420 (1.740)	.9361
7.399 (2.913)	.9786
10.02 (3.945)	.9888
16.33 (6.430)	1.0000

Flight identification	
1-82, t = 1 hr 48 min	
Flight conditions	
$M_1 = 2.28$, $\alpha = 4.5°$, $T_t = 488°$ K (878° R), $T_w = 426°$ K (766° R)	
y, cm (in.)	$\frac{u}{u_1}$
0.076 (0.030)	0.6263
.381 (.150)	.7439
.762 (.300)	.7996
1.080 (.425)	.8299
1.709 (.673)	.8691
4.420 (1.740)	.9700
7.399 (2.913)	.9853
10.02 (3.945)	.9884
16.33 (6.430)	1.0000

Flight identification	
1-82, t = 1 hr 55 min	
Flight conditions	
$M_1 = 2.22$, $\alpha = 4.9°$, $T_t = 460°$ K (828° R), $T_w = 426°$ K (766° R)	
y, cm (in.)	$\frac{u}{u_1}$
0.076 (0.030)	0.6229
.381 (.150)	.7461
.762 (.300)	.7987
1.080 (.425)	.8312
1.709 (.673)	.8703
4.420 (1.740)	.9666
7.399 (2.913)	.9745
10.02 (3.945)	.9780
16.33 (6.430)	1.0000

Flight identification	
1-82, t = 2 hr 02 min	
Flight conditions	
$M_1 = 2.18$, $\alpha = 4.9°$, $T_t = 458°$ K (825° R), $T_w = 422°$ K (759° R)	
y, cm (in.)	$\frac{u}{u_1}$
0.076 (0.030)	0.6152
.381 (.150)	.7377
.762 (.300)	.7954
1.080 (.425)	.8298
1.709 (.673)	.8682
4.420 (1.740)	.9714
7.399 (2.913)	.9749
10.02 (3.945)	.9778
16.33 (6.430)	1.0000

Flight identification	
1-82, t = 2 hr 08 min	
Flight conditions	
$M_1 = 2.17$, $\alpha = 4.6°$, $T_t = 450°$ K (810° R), $T_w = 416°$ K (748° R)	
y, cm (in.)	$\frac{u}{u_1}$
0.076 (0.030)	0.6133
.381 (.150)	.7369
.762 (.300)	.7944
1.080 (.425)	.8279
1.709 (.673)	.8671
4.420 (1.740)	.9744
7.399 (2.913)	.9769
10.02 (3.945)	.9783
16.33 (6.430)	1.0000

TABLE 1.– (Continued)

(a) (Concluded)

Flight identification	
1-82, $t \approx 2$ hr 16 min	
Flight conditions	
$M_1 = 2.15$, $\alpha = 4.4°$, $T_t = 447°$ K (805° R), $T_w = 414°$ K (746° R)	
y, cm (in.)	$\frac{u}{u_1}$
0.076 (0.030)	0.6549
.381 (.150)	.7226
.762 (.300)	.7790
1.080 (.425)	.8134
1.709 (.673)	.8508
4.420 (1.740)	.9618
7.399 (2.913)	.9755
10.02 (3.945)	.9785
16.33 (6.430)	1.0000

Flight identification	
1-82, $t = 2$ hr 20 min	
Flight conditions	
$M_1 = 2.13$, $\alpha = 4.1°$, $T_t = 449°$ K (809° R), $T_w = 413°$ K (744° R)	
y, cm (in.)	$\frac{u}{u_1}$
0.076 (0.030)	0.5902
.381 (.150)	.7033
.762 (.300)	.7585
1.080 (.425)	.7932
1.709 (.673)	.8333
4.420 (1.740)	.9446
7.399 (2.913)	.9743
10.02 (3.945)	.9783
16.33 (6.430)	1.0000

Flight identification	
1-82, $t = 1$ hr 50 min	
Flight conditions	
$M_1 = 2.26$, $\alpha = 4.7°$, $T_t = 479°$ K (863° R), $T_w = 426°$ K (767° R)	
y, cm (in.)	$\frac{u}{u_1}$
0.076 (0.030)	0.6207
.381 (.150)	.7465
.762 (.300)	.8053
1.080 (.425)	.8365
1.709 (.673)	.8753
4.420 (1.740)	.9764
7.399 (2.913)	.9836
10.02 (3.945)	.9852
16.33 (6.430)	1.0000

Flight identification	
1-83, $t \approx 1$ hr 21 min	
Flight conditions	
$M_1 = 0.86$, $\alpha = 5.3°$, $T_t = 284°$ K (511° R), $T_w = 281°$ K (506° R)	
y, cm (in.)	$\frac{u}{u_1}$
0.076 (0.030)	0.6562
.381 (.150)	.7420
.762 (.300)	.7979
1.080 (.425)	.8275
1.709 (.673)	.8716
7.399 (2.913)	.9715
10.22 (3.945)	.9860
16.33 (6.430)	1.0000

Flight identification	
1-83, $t = 2$ hr 06 min	
Flight conditions	
$M_1 = 0.88$, $\alpha = 5.7°$, $T_t = 281°$ K (506° R), $T_w = 273°$ K (492° R)	
y, cm (in.)	$\frac{u}{u_1}$
0.076 (0.030)	0.6510
.381 (.150)	.7404
.762 (.300)	.7937
1.080 (.425)	.8231
1.709 (.673)	.8689
7.399 (2.913)	.9728
10.22 (3.945)	.9866
16.33 (6.430)	1.0000

Flight identification	
1-83, $t = 2$ hr 40 min	
Flight conditions	
$M_1 = 0.89$, $\alpha = 4.8°$, $T_t = 273°$ K (491° R), $T_w = 270°$ K (486° R)	
y, cm (in.)	$\frac{u}{u_1}$
0.076 (0.030)	0.6508
.381 (.150)	.7378
.762 (.300)	.7910
1.080 (.425)	.8237
1.709 (.673)	.8677
7.399 (2.913)	.9746
10.22 (3.945)	.9880
16.33 (6.430)	1.0000

TABLE 1.– (Continued)

(b) Rear fuselage location; x = 43.5 m (142.8 ft)

Flight identification	
1-68, t = 1 hr 57 min	
Flight conditions	
$M_1 = 2.20$, $\alpha = 3.7°$, $T_t = 427°$ K (768° R), $T_W = 378°$ K (681° R)	
y, cm (in.)	$\frac{u}{u_1}$
0.262 (0.103)	0.7188
1.303 (.513)	.8205
2.522 (.993)	.8716
4.648 (1.830)	.9181
7.132 (2.808)	.9447
10.85 (4.273)	.9612
16.04 (6.313)	.9694
22.39 (8.813)	.9784
30.00 (11.81)	.9860
37.54 (14.78)	.9904
46.51 (18.31)	.9958
55.40 (21.81)	1.0000

Flight identification	
1-68, t = 2 hr 14 min	
Flight conditions	
$M_1 = 2.29$, $\alpha = 3.7°$, $T_t = 442°$ K (795° R), $T_W = 388°$ K (698° R)	
y, cm (in.)	$\frac{u}{u_1}$
0.262 (0.103)	0.7215
1.303 (.513)	.8214
2.522 (.993)	.8734
4.648 (1.830)	.9204
7.132 (2.808)	.9456
10.85 (4.273)	.9601
16.04 (6.313)	.9695
22.39 (8.813)	.9764
30.00 (11.81)	.9844
37.54 (14.78)	.9886
46.51 (18.31)	.9949
55.40 (21.81)	1.0000

Flight identification	
1-69, t = 1 hr 47 min	
Flight conditions	
$M_1 = 2.39$, $\alpha = 5.4°$, $T_t = 467°$ K, (841° R), $T_W = 402°$ K (723° R)	
y, cm (in.)	$\frac{u}{u_1}$
0.262 (0.103)	0.6881
1.303 (.513)	.8115
2.522 (.993)	.8592
4.648 (1.830)	.9100
7.132 (2.808)	.9430
10.85 (4.273)	.9709
16.04 (6.313)	.9848
22.39 (8.813)	.9926
30.00 (11.81)	.9985
46.51 (18.31)	.9985
55.40 (21.81)	1.0000

Flight identification	
1-69, t = 1 hr 55 min	
Flight conditions	
$M_1 = 2.44$, $\alpha = 4.8°$, $T_t = 475°$ K (855° R), $T_W = 403°$ K (725° R)	
y, cm (in.)	$\frac{u}{u_1}$
0.262 (0.103)	0.6916
1.303 (.513)	.8127
2.522 (.993)	.8624
4.648 (1.830)	.9139
7.132 (2.808)	.9450
10.85 (4.273)	.9677
16.04 (6.313)	.9807
22.39 (8.813)	.9867
30.00 (11.81)	.9933
46.51 (18.31)	.9961
55.40 (21.81)	1.0000

Flight identification	
1-69, t = 2 hr 08 min	
Flight conditions	
$M_1 = 2.39$, $\alpha = 4.2°$, $T_t = 466°$ K (838° R), $T_W = 402°$ K (723° R)	
y, cm (in.)	$\frac{u}{u_1}$
0.262 (0.103)	0.6977
1.303 (.513)	.8188
2.522 (.993)	.8693
4.648 (1.830)	.9199
7.132 (2.808)	.9474
10.85 (4.273)	.9641
16.04 (6.313)	.9729
22.39 (8.813)	.9802
30.00 (11.81)	.9888
46.51 (18.31)	.9931
55.40 (21.81)	1.0000

Flight identification	
1-70, t = 1 hr 57 min	
Flight conditions	
$M_1 = 2.43$, $T_t = 479°$ K (863° R), $T_W = 403°$ K (726° R)	
y, cm (in.)	$\frac{u}{u_1}$
0.262 (0.103)	0.7124
1.303 (.513)	.8264
2.522 (.993)	.8732
4.648 (1.830)	.9241
7.132 (2.808)	.9522
10.85 (4.273)	.9707
16.04 (6.313)	.9806
22.39 (8.813)	.9868
30.00 (11.81)	.9916
37.54 (14.78)	.9943
46.51 (18.31)	.9977
55.40 (21.81)	1.0000

TABLE 1.– (Continued)

(b) (Continued)

Flight identification	
1-70, t = 2 hr 07 min	
Flight conditions	
M_1 = 2.43, T_t = 477° K (858° R), T_w = 406° K (730° R)	
y, cm (in.)	$\frac{u}{u_1}$
0.262 (0.103)	0.7079
1.303 (.513)	.8186
2.522 (.993)	.8665
4.648 (1.830)	.9185
7.132 (2.808)	.9489
10.85 (4.273)	.9715
16.04 (6.313)	.9841
22.39 (8.813)	.9894
30.00 (11.81)	.9946
37.54 (14.78)	.9954
46.51 (18.31)	.9992
55.40 (21.81)	1.0000

Flight identification	
1-70, t = 2 hr 16 min	
Flight conditions	
M_1 = 2.35, T_t = 464° K (835° R), T_w = 403° K (725° R)	
y, cm (in.)	$\frac{u}{u_1}$
0.262 (0.103)	0.7210
1.303 (.513)	.8304
2.522 (.993)	.8784
4.648 (1.830)	.9265
7.132 (2.808)	.9508
10.85 (4.273)	.9658
16.04 (6.313)	.9745
22.39 (8.813)	.9801
30.00 (11.81)	.9875
37.54 (14.78)	.9901
46.51 (18.31)	.9971
55.40 (21.81)	1.0000

Flight identification	
1-74, t = 1 hr 24 min	
Flight conditions	
M_1 = 0.49, α = 8.3°, T_t = 323° K (581° R), T_w = 301° K (541° R)	
y, cm (in.)	$\frac{u}{u_1}$
0.262 (0.103)	0.6364
1.303 (.513)	.7320
2.522 (.993)	.7761
4.648 (1.830)	.8229
7.132 (2.808)	.8505
10.85 (4.273)	.8898
16.04 (6.313)	.9074
22.39 (8.813)	.9622
30.00 (11.81)	.9735
37.54 (14.78)	1.0000
46.51 (18.31)	1.0000
55.40 (21.81)	1.0000

Flight identification	
1-74, t = 1 hr 56 min	
Flight conditions	
M_1 = 0.48, α = 8.1°, T_t = 317° K (570° R), T_w = 293° K (527° R)	
y, cm (in.)	$\frac{u}{u_1}$
0.262 (0.103)	0.8042
1.303 (.513)	.8205
2.522 (.993)	.8237
4.648 (1.830)	.8395
7.132 (2.808)	.8458
10.85 (4.273)	.8877
16.04 (6.313)	.9050
22.39 (8.813)	.9672
30.00 (11.81)	.9749
37.54 (14.78)	1.0000
46.51 (18.31)	1.0000
55.40 (21.81)	1.0000

Flight identification	
1-74, t = 2 hr 05 min	
Flight conditions	
M_1 = 0.44, α = 8.2°, T_t = 323° K (581° R), T_w = 301° K (541° R)	
y, cm (in.)	$\frac{u}{u_1}$
0.262 (0.103)	0.6169
1.303 (.513)	.7221
2.522 (.993)	.7648
4.648 (1.830)	.8118
7.132 (2.808)	.8425
10.85 (4.273)	.8845
16.04 (6.313)	.9031
22.39 (8.813)	.9645
30.00 (11.81)	.9700
37.54 (14.78)	1.0000
46.51 (18.31)	1.0000
55.40 (21.81)	1.0000

Flight identification	
1-74, t = 2 hr 26 min	
Flight conditions	
M_1 = 0.39, α = 8.7°, T_t = 324° K (584° R), T_w = 301° K (541° R)	
y, cm (in.)	$\frac{u}{u_1}$
0.262 (0.103)	0.6241
1.303 (.513)	.7288
2.522 (.993)	.7708
4.648 (1.830)	.8187
7.132 (2.808)	.8475
10.85 (4.273)	.8868
16.04 (6.313)	.9019
22.39 (8.813)	.9630
30.00 (11.81)	.9560
37.54 (14.78)	1.0000
46.51 (18.31)	1.0000
55.40 (21.81)	1.0000

TABLE 1.– (Continued)

(b) (Continued)

Flight identification	
1-77, t = 1 hr 56 min	
Flight conditions	
$M_1 = 2.12$, $\alpha = 3.7°$, $T_t = 444°$ K (800° R), $T_w = 386°$ K (694° R)	
y, cm (in.)	$\frac{u}{u_1}$
0.262 (0.103)	0.7293
1.303 (.513)	.8219
2.522 (.993)	.8718
4.648 (1.830)	.9225
7.132 (2.808)	.9481
10.85 (4.273)	.9649
16.04 (6.313)	.9712
22.39 (8.813)	.9845
30.00 (11.81)	.9892
37.54 (14.78)	.9952
46.51 (18.31)	.9989
55.40 (21.81)	1.0000

Flight identification	
1-77, t = 2 hr 00 min	
Flight conditions	
$M_1 = 2.20$, $\alpha = 4.1°$, $T_t = 458°$ K (824° R), $T_w = 397°$ K (714° R)	
y, cm (in.)	$\frac{u}{u_1}$
0.262 (0.103)	0.7308
1.303 (.513)	.8198
2.522 (.993)	.8699
4.648 (1.830)	.9203
7.132 (2.808)	.9472
10.85 (4.273)	.9657
16.04 (6.313)	.9721
22.39 (8.813)	.9847
30.00 (11.81)	.9921
37.54 (14.78)	.9948
46.51 (18.31)	.9985
55.40 (21.81)	1.0000

Flight identification	
1-77, t = 2 hr 07 min	
Flight conditions	
$M_1 = 2.30$, $\alpha = 3.9°$, $T_t = 481°$ K (865° R), $T_w = 408°$ K (734° R)	
y, cm (in.)	$\frac{u}{u_1}$
0.262 (0.103)	0.7408
1.303 (.513)	.8284
2.522 (.993)	.8789
4.648 (1.830)	.9293
7.132 (2.808)	.9530
10.85 (4.273)	.9659
16.04 (6.313)	.9703
22.39 (8.813)	.9807
30.00 (11.81)	.9859
37.54 (14.78)	.9924
46.51 (18.31)	.9966
55.40 (21.81)	1.0000

Flight identification	
1-78, t = 1 hr 50 min	
Flight conditions	
$M_1 = 2.26$, $\alpha = 5.1°$, $T_t = 449°$ K (808° R), $T_w = 388°$ K (699° R)	
y, cm (in.)	$\frac{u}{u_1}$
0.262 (0.103)	0.7124
1.303 (.513)	.8146
2.522 (.993)	.8657
4.648 (1.830)	.9179
7.132 (2.808)	.9481
10.85 (4.273)	.9703
16.04 (6.313)	.9809
22.39 (8.813)	.9909
30.00 (11.81)	.9919
37.54 (14.78)	.9967
46.51 (18.31)	.9991
55.40 (21.81)	1.0000

Flight identification	
1-78, t = 1 hr 55 min	
Flight conditions	
$M_1 = 2.30$, $\alpha = 5.3°$, $T_t = 452°$ K (814° R), $T_w = 392°$ K (705° R)	
y, cm (in.)	$\frac{u}{u_1}$
0.262 (0.103)	0.7087
1.303 (.513)	.8094
2.522 (.993)	.8618
4.648 (1.830)	.9133
7.132 (2.808)	.9448
10.85 (4.273)	.9674
16.04 (6.313)	.9794
22.39 (8.813)	.9897
30.00 (11.81)	.9921
37.54 (14.78)	.9973
46.51 (18.31)	.9982
55.40 (21.81)	1.0000

Flight identification	
1-78, t = 2 hr 03 min	
Flight conditions	
$M_1 = 2.27$, $\alpha = 4.8°$, $T_t = 448°$ K (807° R), $T_w = 396°$ K (713° R)	
y, cm (in.)	$\frac{u}{u_1}$
0.262 (0.103)	0.7165
1.303 (.513)	.8166
2.522 (.993)	.8683
4.648 (1.830)	.9207
7.132 (2.808)	.9494
10.85 (4.273)	.9693
16.04 (6.313)	.9789
22.39 (8.813)	.9885
30.00 (11.81)	.9900
37.54 (14.78)	.9953
46.51 (18.31)	.9995
55.40 (21.81)	1.0000

TABLE 1.– (Continued)

(b) (Continued)

Flight identification	
1-78, t = 2 hr 09 min	
Flight conditions	
$M_1 = 2.41$, $\alpha = 4.5°$, $T_t = 473°$ K (852° R), $T_w = 407°$ K (733° R)	
y, cm (in.)	$\frac{u}{u_1}$
0.262 (0.103)	0.7313
1.303 (.513)	.8220
2.522 (.993)	.8748
4.648 (1.830)	.9268
7.132 (2.808)	.9534
10.85 (4.273)	.9683
16.04 (6.313)	.9763
22.39 (8.813)	.9853
30.00 (11.81)	.9892
37.54 (14.78)	.9934
46.51 (18.31)	.9963
55.40 (21.81)	1.0000

Flight identification	
1-79, t = 1 hr 14 min	
Flight conditions	
$M_1 = 0.97$, $\alpha = 4.9°$, $T_t = 268°$ K (483° R), $T_w = 268°$ K (483° R)	
y, cm (in.)	$\frac{u}{u_1}$
0.300 (0.118)	0.6271
1.270 (.500)	.7274
2.464 (.970)	.7727
4.605 (1.813)	.8153
7.145 (2.813)	.8413
10.32 (4.063)	.8725
15.34 (6.038)	.8982
22.39 (8.813)	.9310
30.00 (11.81)	.9491
37.59 (14.80)	.9729
46.48 (18.30)	.9867
55.32 (21.78)	1.0000

Flight identification	
1-79, t = 1 hr 40 min	
Flight conditions	
$M_1 = 1.94$, $\alpha = 3.4°$, $T_t = 389°$ K (700° R), $T_w = 355°$ K (639° R)	
y, cm (in.)	$\frac{u}{u_1}$
0.300 (0.118)	0.7142
1.270 (.500)	.8095
2.464 (.970)	.8590
4.605 (1.813)	.9087
7.145 (2.813)	.9343
10.32 (4.063)	.9523
15.34 (6.038)	.9623
22.39 (8.813)	.9742
30.00 (11.81)	.9812
37.59 (14.80)	.9914
46.48 (18.30)	.9980
55.32 (21.78)	1.0000

Flight identification	
1-82, t = 1 hr 40 min	
Flight conditions	
$M_1 = 2.35$, $\alpha = 4.4°$, $T_t = 481°$ K (865° R), $T_w = 399°$ K (719° R)	
y, cm (in.)	$\frac{u}{u_1}$
0.300 (0.118)	0.7285
1.270 (.500)	.8274
2.464 (.970)	.8790
4.605 (1.813)	.9306
7.145 (2.813)	.9565
10.32 (4.063)	.9708
15.34 (6.038)	.9778
22.39 (8.813)	.9866
30.00 (11.81)	.9930
37.59 (14.80)	.9954
46.48 (18.30)	.9981
55.32 (21.78)	1.0000

Flight identification	
1-82, t = 1 hr 48 min	
Flight conditions	
$M_1 = 2.42$, $\alpha = 4.5°$, $T_t = 488°$ K (878° R), $T_w = 409°$ K (736° R)	
y, cm (in.)	$\frac{u}{u_1}$
0.300 (0.118)	0.7281
1.270 (.500)	.8243
2.464 (.970)	.8739
4.605 (1.813)	.9254
7.145 (2.813)	.9537
10.32 (4.063)	.9703
15.34 (6.038)	.9793
22.39 (8.813)	.9883
30.00 (11.81)	.9931
37.59 (14.80)	.9964
46.48 (18.30)	.9979
55.32 (21.78)	1.0000

Flight identification	
1-82, t = 1 hr 50 min	
Flight conditions	
$M_1 = 2.39$, $\alpha = 4.7°$, $T_t = 479°$ K (863° R), $T_w = 408°$ K (735° R)	
y, cm (in.)	$\frac{u}{u_1}$
0.300 (0.118)	0.7258
1.270 (.500)	.8209
2.464 (.970)	.8699
4.605 (1.813)	.9215
7.145 (2.813)	.9510
10.32 (4.063)	.9704
15.34 (6.038)	.9810
22.39 (8.813)	.9909
30.00 (11.81)	.9945
37.59 (14.80)	.9977
46.48 (18.30)	.9992
55.32 (21.78)	1.0000

TABLE 1.– (Continued)

(b) (Concluded)

Flight identification	
1-82, t = 1 hr 55 min	
Flight conditions	
$M_1 = 2.28$, $\alpha = 4.9^\circ$, $T_t = 460^\circ$ K (828° R), $T_w = 403^\circ$ K (726° R)	
y, cm (in.)	$\frac{u}{u_1}$
0.300 (0.118)	0.7182
1.270 (.500)	.8124
2.464 (.970)	.8628
4.605 (1.813)	.9145
7.145 (2.813)	.9446
10.32 (4.063)	.9669
15.34 (6.038)	.9783
22.39 (8.813)	.9894
30.00 (11.81)	.9939
37.59 (14.80)	.9991
46.48 (18.30)	1.0000
55.32 (21.78)	1.0000

Flight identification	
1-82, t = 2 hr 02 min	
Flight conditions	
$M_1 = 2.27$, $\alpha = 4.9^\circ$, $T_t = 458^\circ$ K (825° R), $T_w = 400^\circ$ K (720° R)	
y, cm (in.)	$\frac{u}{u_1}$
0.300 (0.118)	0.7134
1.270 (.500)	.8103
2.464 (.970)	.8614
4.605 (1.813)	.9138
7.145 (2.813)	.9439
10.32 (4.063)	.9660
15.34 (6.038)	.9768
22.39 (8.813)	.9880
30.00 (11.81)	.9929
37.59 (14.80)	.9981
46.48 (18.30)	1.0000
55.32 (21.78)	1.0000

Flight identification	
1-82, t = 2 hr 08 min	
Flight conditions	
$M_1 = 2.27$, $\alpha = 4.6^\circ$, $T_t = 450^\circ$ K (810° R), $T_w = 397^\circ$ K (715° R)	
y, cm (in.)	$\frac{u}{u_1}$
0.300 (0.118)	0.7183
1.270 (.500)	.8127
2.464 (.970)	.8637
4.605 (1.813)	.9158
7.145 (2.813)	.9441
10.32 (4.063)	.9648
15.34 (6.038)	.9745
22.39 (8.813)	.9852
30.00 (11.81)	.9901
37.59 (14.80)	.9967
46.48 (18.30)	1.0000
55.32 (21.78)	1.0000

Flight identification	
1-82, t = 2 hr 16 min	
Flight conditions	
$M_1 = 2.29$, $\alpha = 4.4^\circ$, $T_t = 447^\circ$ K (805° R), $T_w = 397^\circ$ K (714° R)	
y, cm (in.)	$\frac{u}{u_1}$
0.300 (0.118)	0.7411
1.270 (.500)	.8259
2.464 (.970)	.8730
4.605 (1.813)	.9218
7.145 (2.813)	.9478
10.32 (4.063)	.9662
15.34 (6.038)	.9740
22.39 (8.813)	.9845
30.00 (11.81)	.9894
37.59 (14.80)	.9954
46.48 (18.30)	.9995
55.32 (21.78)	1.0000

Flight identification	
1-82, t = 2 hr 20 min	
Flight conditions	
$M_1 = 2.24$, $\alpha = 4.1^\circ$, $T_t = 449^\circ$ K (809° R), $T_w = 397^\circ$ K (714° R)	
y, cm (in.)	$\frac{u}{u_1}$
0.300 (0.118)	0.7228
1.270 (.500)	.8168
2.464 (.970)	.8687
4.605 (1.813)	.9206
7.145 (2.813)	.9467
10.32 (4.063)	.9634
15.34 (6.038)	.9705
22.39 (8.813)	.9815
30.00 (11.81)	.9870
37.59 (14.80)	.9943
46.48 (18.30)	.9986
55.32 (21.78)	1.0000

TABLE 1.– (Continued)

(c) Wing location; x = 15.6 m (51.1 ft)

Flight identification	
1-66, t = 2 hr 01 min	
Flight conditions	
$M_1 = 2.12$, $\alpha = 4.3°$, $T_t = 410°$ K (738° R), $T_w = 371°$ K (667° R)	
y, cm (in.)	$\frac{u}{u_1}$
1.300 (0.512)	0.7301
1.913 (.753)	.7623
2.527 (.995)	.7842
3.132 (1.233)	.8017
3.726 (1.467)	.8191
6.167 (2.428)	.8741
9.238 (3.637)	.9219
15.40 (6.061)	.9771
22.03 (8.673)	.9873
31.04 (12.22)	1.0000

Flight identification	
1-66, t = 2 hr 04 min	
Flight conditions	
$M_1 = 2.15$, $\alpha = 4.3°$, $T_t = 411°$ K (739° R), $T_w = 364°$ K (655° R)	
y, cm (in.)	$\frac{u}{u_1}$
1.300 (0.512)	0.7495
1.913 (.753)	.7801
2.527 (.995)	.7994
3.132 (1.233)	.8166
3.726 (1.467)	.8311
6.167 (2.428)	.8836
9.238 (3.637)	.9288
15.40 (6.061)	.9824
22.03 (8.673)	.9916
31.04 (12.22)	1.0000

Flight identification	
1-66, t = 2 hr 18 min	
Flight conditions	
$M_1 = 1.72$, $\alpha = 3.4°$, $T_t = 340°$ K (612° R), $T_w = 331°$ K (595° R)	
y, cm (in.)	$\frac{u}{u_1}$
1.300 (0.512)	0.7411
1.913 (.753)	.7697
2.527 (.995)	.7885
3.132 (1.233)	.8093
3.726 (1.467)	.8207
6.167 (2.428)	.8772
9.238 (3.637)	.9293
15.40 (6.061)	.9890
22.03 (8.673)	.9971
31.04 (12.22)	1.0000

Flight identification	
1-68, t = 2 hr 14 min	
Flight conditions	
$M_1 = 2.41$, $\alpha = 3.7°$, $T_t = 442°$ K (795° R), $T_w = 371°$ K (668° R)	
y, cm (in.)	$\frac{u}{u_1}$
0.699 (0.275)	0.6905
1.303 (.513)	.7323
1.913 (.753)	.7546
2.527 (.995)	.7734
3.132 (1.233)	.7948
3.726 (1.467)	.7971
6.167 (2.428)	.8598
9.238 (3.637)	.9124
12.26 (4.828)	.9465
15.40 (6.061)	.9556
22.03 (8.673)	1.0000
31.04 (12.22)	1.0000

Flight identification	
1-69, t = 1 hr 47 min	
Flight conditions	
$M_1 = 2.48$, $\alpha = 5.4°$, $T_t = 467°$ K (841° R), $T_w = 329°$ K (593° R)	
y, cm (in.)	$\frac{u}{u_1}$
0.699 (0.275)	0.6980
1.303 (.513)	.7363
1.913 (.753)	.7604
2.527 (.995)	.7786
3.132 (1.233)	.7946
3.726 (1.467)	.8044
6.167 (2.428)	.8526
9.238 (3.637)	.8947
12.26 (4.828)	.9438
15.40 (6.061)	.9610
22.03 (8.673)	.9962
31.04 (12.22)	1.0000

Flight identification	
1-69, t = 1 hr 56 min	
Flight conditions	
$M_1 = 2.53$, $\alpha = 4.8°$, $T_t = 475°$ K (855° R), $T_w = 346°$ K (622° R)	
y, cm (in.)	$\frac{u}{u_1}$
0.699 (0.275)	0.6940
1.303 (.513)	.7351
1.913 (.753)	.7567
2.527 (.995)	.7705
3.132 (1.233)	.7921
3.726 (1.467)	.7931
6.167 (2.428)	.8474
9.238 (3.637)	.8850
12.26 (4.828)	.9309
15.40 (6.061)	.9411
22.03 (8.673)	.9902
31.04 (12.22)	1.0000

TABLE 1.– (Continued)

(c) (Continued)

Flight identification	
1-69, t = 2 hr 08 min	
Flight conditions	
$M_1 = 2.51$, $\alpha = 4.1°$, $T_t = 464°$ K (836° R), $T_w = 368°$ K (662° R)	
y, cm (in.)	$\frac{u}{u_1}$
0.699 (0.275)	0.7265
1.303 (.513)	.7666
1.913 (.753)	.7901
2.527 (.995)	.8052
3.132 (1.233)	.8269
3.726 (1.467)	.8284
6.167 (2.428)	.8848
9.238 (3.637)	.9252
12.26 (4.828)	.9665
15.40 (6.061)	.9735
22.03 (8.673)	1.0000
31.04 (12.22)	1.0000

Flight identification	
1-70, t = 1 hr 57 min	
Flight conditions	
$M_1 = 2.50$, $T_t = 481°$ K (865° R), $T_w = 418°$ K (753° R)	
y, cm (in.)	$\frac{u}{u_1}$
0.699 (0.275)	0.7083
1.303 (.513)	.7418
1.913 (.753)	.7673
2.527 (.995)	.7849
3.132 (1.233)	.7996
3.726 (1.467)	.8159
6.167 (2.428)	.8534
9.238 (3.637)	.8892
12.26 (4.828)	.9240
15.40 (6.061)	.9509
22.03 (8.673)	.9907
31.04 (12.22)	1.0000

Flight identification	
1-70, t = 2 hr 07 min	
Flight conditions	
$M_1 = 2.53$, $T_t = 477°$ K (858° R), $T_w = 423°$ K (762° R)	
y, cm (in.)	$\frac{u}{u_1}$
0.699 (0.275)	0.6965
1.303 (.513)	.7330
1.913 (.753)	.7547
2.527 (.995)	.7693
3.132 (1.233)	.7892
3.726 (1.467)	.7942
6.167 (2.428)	.8470
9.238 (3.637)	.8865
12.26 (4.828)	.9241
15.40 (6.061)	.9448
22.03 (8.673)	.9885
31.04 (12.22)	1.0000

Flight identification	
1-70, t = 2 hr 16 min	
Flight conditions	
$M_1 = 2.51$, $T_t = 466°$ K (838° R), $T_w = 417°$ K (751° R)	
y, cm (in.)	$\frac{u}{u_1}$
0.699 (0.275)	0.7134
1.303 (.513)	.7491
1.913 (.753)	.7713
2.527 (.995)	.7853
3.132 (1.233)	.8045
3.726 (1.467)	.8118
6.167 (2.428)	.8694
9.238 (3.637)	.9176
12.26 (4.828)	.9618
15.40 (6.061)	.9828
22.03 (8.673)	1.0000
31.04 (12.22)	1.0000

Flight identification	
1-74, t = 1 hr 24 min	
Flight conditions	
$M_1 = 0.51$, $\alpha = 8.3°$, $T_t = 323°$ K (581° R), $T_w = 303°$ K (546° R)	
y, cm (in.)	$\frac{u}{u_1}$
0.699 (0.275)	0.7190
1.303 (.513)	.7672
1.913 (.753)	.7900
2.527 (.995)	.8119
3.726 (1.467)	.8357
6.167 (2.428)	.8784
9.238 (3.637)	.9342
12.26 (4.828)	.9474
15.40 (6.061)	.9774
22.03 (8.673)	1.0000
31.04 (12.22)	1.0000

Flight identification	
1-74, t = 1 hr 55 min	
Flight conditions	
$M_1 = 0.49$, $\alpha = 8.1°$, $T_t = 317°$ K (570° R), $T_w = 295°$ K (531° R)	
y, cm (in.)	$\frac{u}{u_1}$
0.699 (0.275)	0.6850
1.303 (.513)	.7418
1.913 (.753)	.7735
2.527 (.995)	.7971
3.726 (1.467)	.8230
6.167 (2.428)	.8689
9.238 (3.637)	.9255
12.26 (4.828)	.9442
15.40 (6.061)	.9752
22.03 (8.673)	1.0000
31.04 (12.22)	1.0000

TABLE 1.– (Continued)

(c) (Continued)

Flight identification	
1-74, t = 2 hr 05 min	
Flight conditions	
$M_1 = 0.46$, $\alpha = 8.2°$, $T_t = 323°$ K (581° R), $T_w = 303°$ K (546° R)	
y, cm (in.)	$\frac{u}{u_1}$
0.699 (0.275)	0.7145
1.303 (.513)	.7643
1.913 (.753)	.7877
2.527 (.995)	.8072
3.726 (1.467)	.8322
6.167 (2.428)	.8738
9.238 (3.637)	.9265
12.26 (4.828)	.9450
15.40 (6.061)	.9730
22.03 (8.673)	1.0000
31.04 (12.22)	1.0000

Flight identification	
1-74, t = 2 hr 26 min	
Flight conditions	
$M_1 = 0.41$, $\alpha = 8.7°$, $T_t = 324°$ K (584° R), $T_w = 303°$ K (546° R)	
y, cm (in.)	$\frac{u}{u_1}$
0.699 (0.275)	0.6906
1.303 (.513)	.7572
1.913 (.753)	.7861
2.527 (.995)	.8138
3.726 (1.467)	.8366
6.167 (2.428)	.8731
9.238 (3.637)	.9344
12.26 (4.828)	.9473
15.40 (6.061)	.9726
22.03 (8.673)	1.0000
31.04 (12.22)	1.0000

Flight identification	
1-75, t = 0 hr 32 min	
Flight conditions	
$M_1 = 0.53$, $\alpha = 8.9°$, $T_t = 305°$ K (549° R), $T_w = 303°$ K (545° R)	
y, cm (in.)	$\frac{u}{u_1}$
0.699 (0.275)	0.6940
1.303 (.513)	.7367
1.913 (.753)	.7645
2.527 (.995)	.7881
3.132 (1.233)	.8024
3.726 (1.467)	.8137
6.167 (2.428)	.8618
9.238 (3.637)	.9183
12.26 (4.828)	.9391
15.40 (6.061)	.9768
22.03 (8.673)	1.0000
31.04 (12.22)	1.0000

Flight identification	
1-75, t = 0 hr 46 min	
Flight conditions	
$M_1 = 0.95$, $\alpha = 5.2°$, $T_t = 303°$ K (545° R), $T_w = 298°$ K (537° R)	
y, cm (in.)	$\frac{u}{u_1}$
0.699 (0.275)	0.7200
1.303 (.513)	.7543
1.913 (.753)	.7859
2.527 (.995)	.8078
3.132 (1.233)	.8250
3.726 (1.467)	.8391
6.167 (2.428)	.8933
9.238 (3.637)	.9525
12.26 (4.828)	.9728
15.40 (6.061)	.9930
22.03 (8.673)	1.0000
31.04 (12.22)	1.0000

Flight identification	
1-75, t = 1 hr 05 min	
Flight conditions	
$M_1 = 0.94$, $\alpha = 5.5°$, $T_t = 293°$ K (527° R), $T_w = 288°$ K (519° R)	
y, cm (in.)	$\frac{u}{u_1}$
0.699 (0.275)	0.7247
1.303 (.513)	.7578
1.913 (.753)	.7899
2.527 (.995)	.8110
3.132 (1.233)	.8269
3.726 (1.467)	.8408
6.167 (2.428)	.8932
9.238 (3.637)	.9450
12.26 (4.828)	.9685
15.40 (6.061)	.9917
22.03 (8.673)	1.0000
31.04 (12.22)	1.0000

Flight identification	
1-75, t = 1 hr 14 min	
Flight conditions	
$M_1 = 0.93$, $\alpha = 5.4°$, $T_t = 292°$ K (526° R), $T_w = 289°$ K (520° R)	
y, cm (in.)	$\frac{u}{u_1}$
0.699 (0.275)	0.7274
1.303 (.513)	.7587
1.913 (.753)	.7894
2.527 (.995)	.8107
3.132 (1.233)	.8266
3.726 (1.467)	.8406
6.167 (2.428)	.8898
9.238 (3.637)	.9423
12.26 (4.828)	.9642
15.40 (6.061)	.9906
22.03 (8.673)	1.0000
31.04 (12.22)	1.0000

TABLE 1.– (Continued)

(c) (Continued)

Flight identification	
1-75, t = 1 hr 21 min	
Flight conditions	
$M_1 = 0.94$, $\alpha = 5.4°$, $T_t = 293°$ K (527° R), $T_w = 289°$ K (521° R)	
y, cm (in.)	$\frac{u}{u_1}$
0.699 (0.275)	0.7285
1.303 (.513)	.7611
1.913 (.753)	.7913
2.527 (.995)	.8122
3.132 (1.233)	.8294
3.726 (1.467)	.8431
6.167 (2.428)	.8962
9.238 (3.637)	.9474
12.26 (4.828)	.9706
15.40 (6.061)	.9926
22.03 (8.673)	1.0000
31.04 (12.22)	1.0000

Flight identification	
1-76, t = 1 hr 21 min	
Flight conditions	
$M_1 = 0.96$, $\alpha = 5.7°$, $T_t = 277°$ K (499° R), $T_w = 277°$ K (499° R)	
y, cm (in.)	$\frac{u}{u_1}$
0.699 (0.275)	0.7341
1.303 (.513)	.7622
1.913 (.753)	.7904
2.527 (.995)	.8113
3.132 (1.233)	.8258
3.726 (1.467)	.8398
6.617 (2.428)	.8868
9.238 (3.637)	.9356
12.26 (4.828)	.9591
15.40 (6.061)	.9884
22.03 (8.673)	1.0000
31.04 (12.22)	1.0000

Flight identification	
1-76, t = 2 hr 27 min	
Flight conditions	
$M_1 = 0.92$, $\alpha = 3.4°$, $T_t = 291°$ K (523° R), $T_w = 287°$ K (517° R)	
y, cm (in.)	$\frac{u}{u_1}$
0.699 (0.275)	0.7498
1.303 (.513)	.7752
1.913 (.753)	.8022
2.527 (.995)	.8232
3.132 (1.233)	.8376
3.726 (1.467)	.8502
6.167 (2.428)	.8992
9.238 (3.637)	.9495
12.26 (4.828)	.9715
15.04 (6.061)	.9952
22.03 (8.673)	1.0000
31.04 (12.22)	1.0000

Flight identification	
1-77, t = 1 hr 30 min	
Flight conditions	
$M_1 = 0.95$, $\alpha = 8.2°$, $T_t = 257°$ K (463° R), $T_w = 274°$ K (494° R)	
y, cm (in.)	$\frac{u}{u_1}$
0.699 (0.275)	0.6966
1.303 (.513)	.7353
1.913 (.753)	.7683
2.527 (.995)	.7873
3.132 (1.233)	.8055
3.726 (1.467)	.8207
6.167 (2.428)	.8671
9.238 (3.637)	.9172
12.26 (4.828)	.9431
15.40 (6.061)	.9719
22.03 (8.673)	1.0000
31.04 (12.22)	1.0000

Flight identification	
1-77, t = 1 hr 56 min	
Flight conditions	
$M_1 = 2.26$, $\alpha = 3.7°$, $T_t = 444°$ K (800° R), $T_w = 392°$ K (705° R)	
y, cm (in.)	$\frac{u}{u_1}$
0.699 (0.275)	0.6944
1.303 (.513)	.7239
1.913 (.753)	.7538
2.527 (.995)	.7717
3.132 (1.233)	.7879
3.726 (1.467)	.8010
6.167 (2.428)	.8502
9.238 (3.637)	.9011
12.26 (4.828)	.9344
15.40 (6.061)	.9681
22.03 (8.673)	.9986
31.04 (12.22)	1.0000

Flight identification	
1-77, t = 2 hr 00 min	
Flight conditions	
$M_1 = 2.32$, $\alpha = 4.1°$, $T_t = 458°$ K (824° R), $T_w = 406°$ K (730° R)	
y, cm (in.)	$\frac{u}{u_1}$
0.699 (0.275)	0.7536
1.303 (.513)	.7841
1.913 (.753)	.8156
2.527 (.995)	.8346
3.132 (1.233)	.8541
3.726 (1.467)	.8659
6.167 (2.428)	.9132
9.238 (3.637)	.9541
12.26 (4.828)	.9716
15.40 (6.061)	.9826
22.03 (8.673)	.9969
31.04 (12.22)	1.0000

TABLE 1.– (Continued)

(c) (Continued)

Flight identification	
1-77, t = 2 hr 07 min	
Flight conditions	
$M_1 = 2.44$, $\alpha = 3.9°$, $T_t = 481° K (865° R)$, $T_w = 425° K (765° R)$	
y, cm (in.)	$\frac{u}{u_1}$
0.699 (0.275)	0.7187
1.303 (.513)	.7499
1.913 (.753)	.7800
2.527 (.995)	.7984
3.132 (1.233)	.8136
3.726 (1.467)	.8298
6.167 (2.428)	.8773
9.238 (3.637)	.9239
12.26 (4.828)	.9515
15.40 (6.061)	.9787
22.03 (8.673)	1.0000
31.04 (12.22)	1.0000

Flight identification	
1-78, t = 1 hr 50 min	
Flight conditions	
$M_1 = 2.30$, $\alpha = 5.1°$, $T_t = 449° K (808° R)$, $T_w = 401° K (721° R)$	
y, cm (in.)	$\frac{u}{u_1}$
0.699 (0.275)	0.6759
1.303 (.513)	.7160
1.913 (.753)	.7459
2.527 (.995)	.7661
3.132 (1.233)	.7838
3.726 (1.467)	.7953
6.167 (2.428)	.8315
9.238 (3.637)	.8709
15.40 (6.061)	.8933
22.03 (8.673)	.9776
31.04 (12.22)	1.0000

Flight identification	
1-78, t = 1 hr 55 min	
Flight conditions	
$M_1 = 2.35$, $\alpha = 5.3°$, $T_t = 452° K (814° R)$, $T_w = 404° K (727° R)$	
y, cm (in.)	$\frac{u}{u_1}$
0.699 (0.275)	0.6787
1.303 (.513)	.7171
1.913 (.753)	.7482
2.527 (.995)	.7682
3.132 (1.233)	.7858
3.726 (1.467)	.7972
6.167 (2.428)	.8348
9.238 (3.637)	.8764
15.40 (6.061)	.9372
22.03 (8.673)	.9839
31.04 (12.22)	1.0000

Flight identification	
1-78, t = 2 hr 03 min	
Flight conditions	
$M_1 = 2.34$, $\alpha = 4.8°$, $T_t = 448° K (807° R)$, $T_w = 406° K (731° R)$	
y, cm (in.)	$\frac{u}{u_1}$
0.699 (0.275)	0.6893
1.303 (.513)	.7287
1.913 (.753)	.7595
2.527 (.995)	.7774
3.132 (1.233)	.7973
3.726 (1.467)	.8062
6.167 (2.428)	.8406
9.238 (3.637)	.8730
15.40 (6.061)	.9149
22.03 (8.673)	.9703
31.04 (12.22)	1.0000

Flight identification	
1-78, t = 2 hr 09 min	
Flight conditions	
$M_1 = 2.52$, $\alpha = 4.5°$, $T_t = 473° K (852° R)$, $T_w = 426° K (767° R)$	
y, cm (in.)	$\frac{u}{u_1}$
0.699 (0.275)	0.7179
1.303 (.513)	.7532
1.913 (.753)	.7832
2.527 (.995)	.8037
3.132 (1.233)	.8185
3.726 (1.467)	.8331
6.167 (2.428)	.8742
9.238 (3.637)	.9153
15.40 (6.061)	.9663
22.03 (8.673)	.9986
31.04 (12.22)	1.0000

Flight identification	
1-79, t = 1 hr 40 min	
Flight conditions	
$M_1 = 2.06$, $\alpha = 3.4°$, $T_t = 389° K (700° R)$, $T_w = 363° K (653° R)$	
y, cm (in.)	$\frac{u}{u_1}$
0.739 (0.291)	0.6945
1.303 (.513)	.7291
1.890 (.744)	.7591
2.454 (.966)	.7782
3.134 (1.234)	.7954
3.736 (1.471)	.8103
6.167 (2.428)	.8614
9.258 (3.645)	.9153
15.40 (6.063)	.9844
21.52 (8.474)	1.0000
30.71 (12.09)	1.0000

TABLE 1.– (Continued)

(c) (Continued)

Flight identification	
1-79, t = 1 hr 42 min	
Flight conditions	
$M_1 = 2.06$, $\alpha = 3.1°$, $T_t = 393°$ K (707° R), $T_w = 361°$ K (650° R)	
y, cm (in.)	$\frac{u}{u_1}$
0.739 (0.291)	0.7050
1.303 (.513)	.7361
1.890 (.744)	.7655
2.454 (.966)	.7846
3.134 (1.234)	.8024
3.736 (1.471)	.8170
6.167 (2.428)	.8681
9.258 (3.645)	.9231
15.40 (6.063)	.9887
21.52 (8.474)	1.0000
30.71 (12.09)	1.0000

Flight identification	
1-79, t = 2 hr 15 min	
Flight conditions	
$M_1 = 0.92$, $\alpha = 3.5°$, $T_t = 284°$ K (512° R), $T_w = 302°$ K (543° R)	
y, cm (in.)	$\frac{u}{u_1}$
0.739 (0.291)	0.7425
1.303 (.513)	.7750
1.890 (.744)	.8051
2.454 (.966)	.8274
3.134 (1.234)	.8458
3.736 (1.471)	.8595
6.167 (2.428)	.9146
9.258 (3.645)	.9622
15.40 (6.063)	1.0000
21.52 (8.474)	1.0000
30.71 (12.09)	1.0000

Flight identification	
1-82, t = 1 hr 40 min	
Flight conditions	
$M_1 = 2.48$, $\alpha = 4.4°$, $T_t = 481°$ K (865° R), $T_w = 409°$ K (736° R)	
y, cm (in.)	$\frac{u}{u_1}$
0.739 (0.291)	0.7152
1.303 (.513)	.7499
1.890 (.744)	.7778
2.454 (.966)	.7970
3.134 (1.234)	.8124
3.736 (1.471)	.8262
6.167 (2.428)	.8677
9.258 (3.645)	.9058
15.40 (6.063)	.9590
21.52 (8.474)	.9952
30.71 (12.09)	1.0000

Flight identification	
1-82, t = 1 hr 48 min	
Flight conditions	
$M_1 = 2.51$, $\alpha = 4.5°$, $T_t = 488°$ K (878° R), $T_w = 424°$ K (763° R)	
y, cm (in.)	$\frac{u}{u_1}$
0.739 (0.291)	0.7019
1.303 (.513)	.7359
1.890 (.744)	.7659
2.454 (.966)	.7858
3.134 (1.234)	.8009
3.736 (1.471)	.8137
6.167 (2.428)	.8547
9.258 (3.645)	.8933
15.40 (6.063)	.9506
21.52 (8.474)	.9934
30.71 (12.09)	1.0000

Flight identification	
1-82, t = 1 hr 50 min	
Flight conditions	
$M_1 = 2.48$, $\alpha = 4.7°$, $T_t = 479°$ K (863° R), $T_w = 424°$ K (764° R)	
y, cm (in.)	$\frac{u}{u_1}$
0.739 (0.291)	0.6773
1.303 (.513)	.7131
1.890 (.744)	.7435
2.454 (.966)	.7626
3.134 (1.234)	.7784
3.736 (1.471)	.7896
6.167 (2.428)	.8316
9.258 (3.645)	.8718
15.40 (6.063)	.9350
21.52 (8.474)	.9872
30.71 (12.09)	1.0000

Flight identification	
1-82, t = 1 hr 55 min	
Flight conditions	
$M_1 = 2.34$, $\alpha = 4.9°$, $T_t = 460°$ K (828° R), $T_w = 416°$ K (748° R)	
y, cm (in.)	$\frac{u}{u_1}$
0.739 (0.291)	0.6690
1.303 (.513)	.7061
1.890 (.744)	.7374
2.454 (.966)	.7568
3.134 (1.234)	.7717
3.736 (1.471)	.7839
6.167 (2.428)	.8258
9.258 (3.645)	.8667
15.40 (6.063)	.9308
21.52 (8.474)	.9784
30.71 (12.09)	1.0000

TABLE 1.– (Concluded)

(c) (Concluded)

Flight identification	
1-82, t = 2 hr 02 min	
Flight conditions	
M_1 = 2.34, α = 4.9°, T_t = 458° K (825° R), T_w = 412° K (742° R)	
y, cm (in.)	$\frac{u}{u_1}$
0.739 (0.291)	0.6627
1.303 (.513)	.7003
1.890 (.744)	.7318
2.454 (.966)	.7518
3.134 (1.234)	.7681
3.736 (1.471)	.7791
6.167 (2.428)	.8210
9.258 (3.645)	.8616
15.40 (6.063)	.9287
21.52 (8.474)	.9758
30.71 (12.09)	1.0000

Flight identification	
1-82, t = 2 hr 08 min	
Flight conditions	
M_1 = 2.36, α = 4.6°, T_t = 450° K (810° R), T_w = 408° K (735° R)	
y, cm (in.)	$\frac{u}{u_1}$
0.739 (0.291)	0.6922
1.303 (.513)	.7291
1.890 (.744)	.7580
2.454 (.966)	.7778
3.134 (1.234)	.7922
3.736 (1.471)	.8030
6.167 (2.428)	.8396
9.258 (3.645)	.8677
15.40 (6.063)	.9131
21.52 (8.474)	.9694
30.71 (12.09)	1.0000

Flight identification	
1-82, t = 2 hr 16 min	
Flight conditions	
M_1 = 2.36, α = 4.4°, T_t = 447° K (805° R), T_w = 407° K (733° R)	
y, cm (in.)	$\frac{u}{u_1}$
0.739 (0.291)	0.7105
1.303 (.513)	.7428
1.890 (.744)	.7716
2.454 (.966)	.7915
3.134 (1.234)	.8081
3.736 (1.471)	.8183
6.167 (2.428)	.8521
9.258 (3.645)	.8953
15.40 (6.063)	.9444
21.52 (8.474)	.9815
30.71 (12.09)	1.0000

Flight identification	
1-82, t = 2 hr 20 min	
Flight conditions	
M_1 = 2.41, α = 4.1°, T_t = 449 K (809° R), T_w = 407° K (732° R)	
y, cm (in.)	$\frac{u}{u_1}$
0.739 (0.291)	0.7434
1.303 (.513)	.7775
1.890 (.744)	.8066
2.454 (.966)	.8277
3.134 (1.234)	.8447
3.736 (1.471)	.8554
6.167 (2.428)	.8995
9.258 (3.645)	.9352
15.40 (6.063)	.9721
21.52 (8.474)	.9932
30.71 (12.09)	1.0000

Flight identification	
1-83, t = 1 hr 21 min	
Flight conditions	
M_1 = 0.91, α = 5.3°, T_t = 284° K (511° R), T_w = 282° K (507° R)	
y, cm (in.)	$\frac{u}{u_1}$
0.739 (0.291)	0.7413
1.303 (.513)	.7748
1.890 (.744)	.8059
2.454 (.966)	.8262
3.134 (1.234)	.8432
3.736 (1.471)	.8561
6.167 (2.428)	.9082
9.258 (3.645)	.9544
15.40 (6.063)	.9951
21.52 (8.474)	1.0000
30.71 (12.09)	1.0000

Flight identification	
1-83, t = 2 hr 06 min	
Flight conditions	
M_1 = 0.90, α = 5.7°, T_t = 281° K (506° R), T_w = 279° K (503° R)	
y, cm (in.)	$\frac{u}{u_1}$
0.739 (0.291)	0.7156
1.303 (.513)	.7537
1.890 (.744)	.7857
2.454 (.966)	.8086
3.134 (1.234)	.8264
3.736 (1.471)	.8395
6.167 (2.428)	.8952
9.258 (3.645)	.9424
15.40 (6.063)	.9947
21.52 (8.474)	1.0000
30.71 (12.09)	1.0000

Flight identification	
1-83, t = 2 hr 40 min	
Flight conditions	
M_1 = 0.93, α = 4.8°, T_t = 273° K (491° R), T_w = 272° K (489° R)	
y, cm (in.)	$\frac{u}{u_1}$
0.739 (0.291)	0.7265
1.303 (.513)	.7632
1.890 (.744)	.7939
2.454 (.966)	.8156
3.134 (1.234)	.8334
3.736 (1.471)	.8467
6.167 (2.428)	.9004
9.258 (3.645)	.9457
15.40 (6.063)	.9955
21.52 (8.474)	1.0000
30.71 (12.09)	1.0000

TABLE 2. – CALCULATED FREE-STREAM AND BOUNDARY-LAYER PARAMETERS

(a) Nose location; x = 5.54 m (18.2 ft)

Flight	t, hr:min	M_∞	M_1	u_1, m/sec	u_1, (ft/sec)	R_x	R_Θ	Θ, cm	Θ, (in.)	δ^*, cm	δ^*, (in.)	$C_{f,pp}$	$C_{f,fb}$	$C_{f,rake}$	T_w/T_r
1-79	1:40	2.08	1.97	585	(1919)	39.7×10^6	6.02×10^4	0.841	(0.331)	2.451	(0.965)	0.180×10^{-2}	0.157×10^{-2}	0.157×10^{-2}	0.982
	1:42	2.09	2.10	608	(1995)	45.2	6.17	.754	(.297)	2.352	(.926)	.180	.150	.157	.976
	1:57	1.63	1.57	466	(1529)	51.8	9.03	.965	(.380)	2.304	(.907)	.174	.141	.140	1.016
	2:15	.87	.85	269	(883)	48.5	7.48	.853	(.336)	1.356	(.534)	.201	.194	.180	1.089
1-82	1:40	2.48	2.24	695	(2279)	24.8×10^6	2.75×10^4	0.615	(0.242)	2.123	(0.836)	0.210×10^{-2}	0.165×10^{-2}	0.203×10^{-2}	0.899
	1:48	2.50	2.28	706	(2317)	25.9	2.25	.483	(.190)	1.681	(.662)	.200	.197	.185	.929
	1:50	2.48	2.26	698	(2290)	25.0	2.16	.478	(.188)	1.648	(.649)	.202	.201	.187	.946
	1:55	2.38	2.22	677	(2220)	25.7	2.61	.561	(.221)	1.869	(.736)	.204	.202	.185	.984
	2:02	2.38	2.18	670	(2197)	23.9	2.40	.556	(.219)	1.819	(.716)	.206	.204	.185	.977
	2:08	2.39	2.17	661	(2170)	24.6	2.42	.546	(.215)	1.770	(.697)	.198	.197	.184	.980
	2:16	2.37	2.15	657	(2157)	24.0	2.58	.597	(.235)	1.923	(.757)	.198	.195	.180	.984
	2:20	2.39	2.13	656	(2152)	23.8	2.83	.658	(.259)	2.118	(.834)	.203	.198	.170	.975
1-83	1:21	0.86	0.86	272	(893)	59.2×10^6	7.87×10^4	0.737	(0.290)	1.135	(0.447)	0.195×10^{-2}	0.177×10^{-2}	0.197×10^{-2}	1.006
	2:06	.88	.88	275	(901)	57.0	7.58	.737	(.290)	1.148	(.452)	.195	.178	.195	.988
	2:40	.89	.89	274	(898)	55.4	7.26	.726	(.286)	1.143	(.450)	.202	.175	.197	1.006

TABLE 2. – (Continued)

(b) Rear fuselage location; x = 43.5 m (142.8 ft)

Flight	t, hr:min	M_∞	M_1	u_1, m/sec	u_1, (ft/sec)	R_x	R_{θ_c}	θ_c, cm	θ_c, (in.)	δ^*, cm	δ^*, (in.)	$C_{f,pp}$	$C_{f,fb}$	$C_{f,rake}$	T_w/T_r
1-68	1:57	2.34	2.20	649	(2130)	2.59×10^8	10.2×10^4	1.72	(0.677)	5.44	(2.14)	0.156×10^{-2}	- - -	0.165×10^{-2}	0.942
	2:14	2.42	2.29	673	(2209)	2.34	9.56	1.78	(.701)	5.92	(2.33)	.155	- - -	.165	.935
1-69	1:47	2.48	2.39	707	(2321)	1.97×10^8	5.04×10^4	1.12	(0.440)	4.14	(1.63)	0.151×10^{-2}	- - -	0.161×10^2	0.919
	1:55	2.53	2.44	720	(2362)	1.87	5.82	1.35	(.533)	5.05	(1.99)	.149	- - -	.160	.908
	2:08	2.52	2.39	706	(2316)	2.01	7.67	1.65	(.651)	5.77	(2.27)	.151	- - -	.161	.922
1-70	1:57	2.52	2.43	722	(2368)	1.93×10^8	5.73×10^4	1.30	(0.511)	4.70	(1.85)	0.152×10^{-2}	- - -	0.164×10^{-2}	0.900
	2:07	2.51	2.43	721	(2364)	1.76	4.85	1.20	(.472)	4.42	(1.74)	.154	- - -	.164	.910
	2:16	2.49	2.35	700	(2295)	2.16	7.72	1.55	(.612)	5.38	(2.12)	.150	- - -	.164	.927
1-74	1:24	0.46	0.49	172	(565)	3.61×10^8	28.1×10^4	3.38	(1.33)	4.37	(1.72)	0.154×10^{-2}	0.159×10^{-2}	0.165×10^{-2}	0.936
	1:56	.45	.48	169	(553)	3.30	23.9	3.15	(1.24)	4.04	(1.59)	.151	.162	- - -	.930
	2:05	.41	.44	156	(511)	3.31	26.5	3.48	(1.37)	4.57	(1.80)	.154	.158	.161	.935
	2:26	.37	.39	140	(459)	3.06	25.5	3.63	(1.43)	4.62	(1.82)	.150	.159	.167	.930
1-77	1:56	2.27	2.12	650	(2131)	2.40×10^8	8.12×10^4	1.47	(0.580)	4.47	(1.76)	0.165×10^{-2}	- - -	0.174×10^{-2}	0.920
	2:00	2.33	2.20	673	(2208)	2.23	7.31	1.43	(.563)	4.62	(1.82)	.168	- - -	.170	.921
	2:07	2.45	2.30	705	(2312)	2.19	7.88	1.57	(.617)	5.26	(2.07)	.165	- - -	.170	.904
1-78	1:50	2.35	2.26	675	(2214)	1.77×10^8	5.09×10^4	1.25	(0.494)	4.19	(1.65)	0.180×10^{-2}	- - -	0.176×10^{-2}	0.921
	1:55	2.37	2.30	683	(2241)	1.77	5.56	1.36	(.536)	4.52	(1.78)	.178	- - -	.175	.923
	2:03	2.36	2.27	676	(2218)	1.77	5.37	1.32	(.520)	4.45	(1.75)	.178	- - -	.177	.941
	2:09	2.49	2.41	714	(2344)	1.83	6.01	1.43	(.564)	5.08	(2.00)	.173	- - -	.170	.920
1-79	1:14	0.95	0.97	292	(959)	3.18×10^8	32.8×10^4	4.47	(1.76)	7.03	(2.77)	0.144×10^{-2}	0.138×10^{-2}	0.156×10^{-2}	1.019
	1:40	2.08	1.94	579	(1899)	2.77	12.3	1.93	(.761)	5.28	(2.08)	.159	.148	.169	.962
1-82	1:40	2.48	2.35	712	(2335)	1.93×10^8	5.54×10^4	1.25	(0.493)	4.37	(1.72)	0.177×10^{-2}	- - -	0.172×10^{-2}	0.887
	1:48	2.50	2.42	727	(2386)	1.99	5.59	1.23	(.483)	4.42	(1.74)	.174	- - -	.169	.896
	1:50	2.48	2.39	716	(2350)	1.43	5.00	1.15	(.452)	4.14	(1.63)	.176	- - -	.170	.910
	1:55	2.38	2.28	686	(2251)	1.86	5.20	1.22	(.480)	4.14	(1.63)	.179	- - -	.171	.934
	2:02	2.38	2.27	683	(2242)	1.71	5.04	1.28	(.503)	4.32	(1.70)	.180	- - -	.172	.929
	2:08	2.39	2.27	677	(2222)	1.79	5.63	1.38	(.542)	4.60	(1.81)	.177	- - -	.172	.940
	2:16	2.37	2.29	678	(2223)	1.83	5.85	1.39	(.549)	4.67	(1.84)	.169	- - -	.175	.945
	2:20	2.39	2.24	673	(2208)	1.79	6.20	1.52	(.597)	5.00	(1.97)	.174	- - -	.176	.939

TABLE 2.– (Concluded)

(c) Wing location; x = 15.6 m (51.1 ft)

Flight	t, hr:min	M_∞	M_1	u_1, m/sec	u_1, (ft/sec)	R_x	R_θ	θ, cm	θ, (in.)	δ^*, cm	δ^*, (in.)	$C_{f,pp}$	$C_{f,fb}$	$C_{f,rake}$	T_w/T_r
1-66	2:01	2.20	2.12	624	(2046)	8.18×10^7	6.90×10^4	1.31	(0.517)	4.72	(1.86)	0.153×10^{-2}	- - -	0.139×10^{-2}	0.958
	2:04	2.20	2.15	630	(2067)	8.35	6.38	1.19	(.468)	4.42	(1.74)	.147	- - -	.141	.941
	2:18	1.81	1.72	504	(1654)	12.5	9.77	1.21	(.478)	3.66	(1.44)	.139	- - -	.142	1.018
1-68	2:14	2.42	2.41	691	(2266)	9.89×10^7	8.51×10^4	1.34	(0.527)	5.36	(2.11)	0.127×10^{-2}	- - -	0.122×10^{-2}	0.898
1-69	1:47	2.48	2.48	719	(2359)	7.77×10^7	6.89×10^4	1.37	(0.539)	5.64	(2.22)	0.123×10^{-2}	- - -	0.122×10^{-2}	0.755
	1:56	2.53	2.53	732	(2400)	7.50	7.34	1.53	(.602)	6.40	(2.52)	.123	- - -	.120	.777
	2:08	2.51	2.51	722	(2370)	8.42	6.29	1.16	(.458)	4.88	(1.92)	.133	- - -	.130	.846
1-70	1:57	2.52	2.51	732	(2402)	7.63×10^7	7.37×10^4	1.50	(0.592)	6.22	(2.45)	0.131×10^{-2}	0.115×10^{-2}	0.127×10^{-2}	0.935
	2:07	2.51	2.51	731	(2397)	6.89	6.75	1.53	(.601)	6.35	(2.50)	.129	.115	.127	.952
	2:16	2.49	2.52	721	(2367)	9.24	6.09	1.03	(.404)	4.37	(1.72)	.137	.110	.131	.968
1-74	1:24	0.46	0.51	178	(585)	13.3×10^7	10.8×10^4	1.26	(0.498)	1.96	(0.770)	0.184×10^{-2}	- - -	0.177×10^{-2}	0.945
	1:55	.45	.49	170	(558)	11.8	10.3	1.36	(.536)	2.10	(.825)	.175	- - -	.173	.937
	2:05	.41	.46	164	(538)	12.4	10.6	1.34	(.526)	2.02	(.797)	.181	- - -	.179	.944
	2:26	.37	.41	147	(481)	11.4	9.54	1.31	(.515)	1.97	(.777)	.188	- - -	.185	.939
1-75	0:32	0.50	0.53	181	(595)	13.0×10^7	13.5×10^4	1.61	(0.634)	2.53	(0.977)	0.170×10^{-2}	- - -	0.168×10^{-2}	0.999
	0:46	.92	.95	304	(998)	15.7	12.0	1.19	(.469)	2.23	(.878)	.160	- - -	.161	1.004
	1:05	.89	.94	296	(971)	14.1	11.1	1.22	(.482)	2.26	(.891)	.166	- - -	.166	1.003
	1:14	.88	.93	294	(965)	14.1	11.4	1.25	(.494)	2.30	(.906)	.167	- - -	.168	1.006
	1:21	.89	.94	296	(971)	14.1	10.9	1.20	(.471)	2.21	(.872)	.167	- - -	.168	1.007
1-76	1:21	0.89	0.96	294	(966)	11.6×10^7	9.70×10^4	1.30	(0.511)	2.39	(0.942)	0.165×10^{-2}	0.174×10^{-2}	0.173×10^{-2}	1.019
	2:27	.86	.92	291	(955)	14.1	10.4	1.14	(.450)	2.11	(.829)	.165	.145	.172	1.006
1-77	1:30	0.89	0.95	281	(923)	11.0×10^7	11.0×10^4	1.55	(0.612)	2.82	(1.11)	0.167×10^{-2}	0.156×10^{-2}	0.166×10^{-2}	1.087
	1:56	2.27	2.26	671	(2203)	10.5	9.38	1.40	(.550)	5.16	(2.03)	.115	.138	.125	.938
	2:00	2.33	2.32	691	(2267)	9.19	5.75	.973	(.383)	3.71	(1.46)	.148	.158	.147	.945
	2:07	2.45	2.44	724	(2376)	9.35	6.96	1.16	(.457)	4.70	(1.85)	.129	.148	.131	.946
1-78	1:50	2.35	2.30	681	(2234)	7.00×10^7	8.78×10^4	1.95	(0.767)	7.21	(2.84)	0.133×10^{-2}	0.150×10^{-2}	0.131×10^{-2}	0.951
	1:55	2.37	2.35	690	(2263)	7.00	7.68	1.70	(.670)	6.48	(2.55)	.131	.150	.130	.953
	2:03	2.36	2.34	686	(2251)	7.15	8.62	1.88	(.739)	7.04	(2.77)	.138	.155	.133	.966
	2:09	2.49	2.49	729	(2391)	7.56	6.01	1.24	(0.488)	5.18	(2.04)	.139	.145	.135	.965
1-79	1:40	2.08	2.06	599	(1965)	12.1×10^7	9.89×10^4	1.27	(0.501)	4.27	(1.68)	0.125×10^{-2}	- - -	0.129×10^{-2}	0.987
	1:42	2.09	2.06	603	(1977)	13.6	10.5	1.21	(.475)	4.06	(1.60)	.124	- - -	.129	.973
	2:15	.87	.92	287	(943)	14.6	9.43	1.01	(.398)	1.93	(.758)	.173	- - -	.173	1.080
1-82	1:40	2.48	2.48	730	(2394)	8.02×10^7	6.90×10^4	1.34	(0.526)	5.49	(2.16)	0.134×10^{-2}	0.140×10^{-2}	0.132×10^{-2}	0.911
	1:48	2.50	2.50	739	(2425)	8.02	7.41	1.44	(.566)	5.99	(2.36)	.129	.137	.126	.931
	1:50	2.48	2.48	729	(2391)	7.61	8.05	1.65	(.648)	6.78	(2.67)	.122	.135	.122	.948
	1:55	2.38	2.34	695	(2279)	7.36	8.49	1.79	(.705)	6.83	(2.69)	.123	.140	.128	.964
	2:02	2.38	2.34	693	(2274)	6.90	8.15	1.84	(.723)	7.01	(2.76)	.123	.143	.123	.960
	2:08	2.39	2.36	689	(2262)	7.30	8.80	1.87	(.738)	7.11	(2.80)	.133	.146	.133	.969
	2:16	2.37	2.36	689	(2259)	7.36	7.45	1.58	(.622)	6.05	(2.38)	.136	.144	.138	.972
	2:20	2.39	2.41	696	(2285)	7.66	5.60	1.14	(.449)	4.50	(1.77)	.148	.149	.146	.967
1-83	1:21	0.86	0.91	285	(934)	17.3×10^7	12.1×10^4	1.09	(0.430)	2.04	(0.802)	0.165×10^{-2}	0.142×10^{-2}	0.167×10^{-2}	1.009
	2:06	.88	.90	281	(921)	16.4	12.8	1.22	(.479)	2.25	(.885)	.156	.141	.162	1.011
	2:40	.89	.93	284	(933)	16.0	12.0	1.17	(.459)	2.18	(.860)	.164	.135	.164	1.014

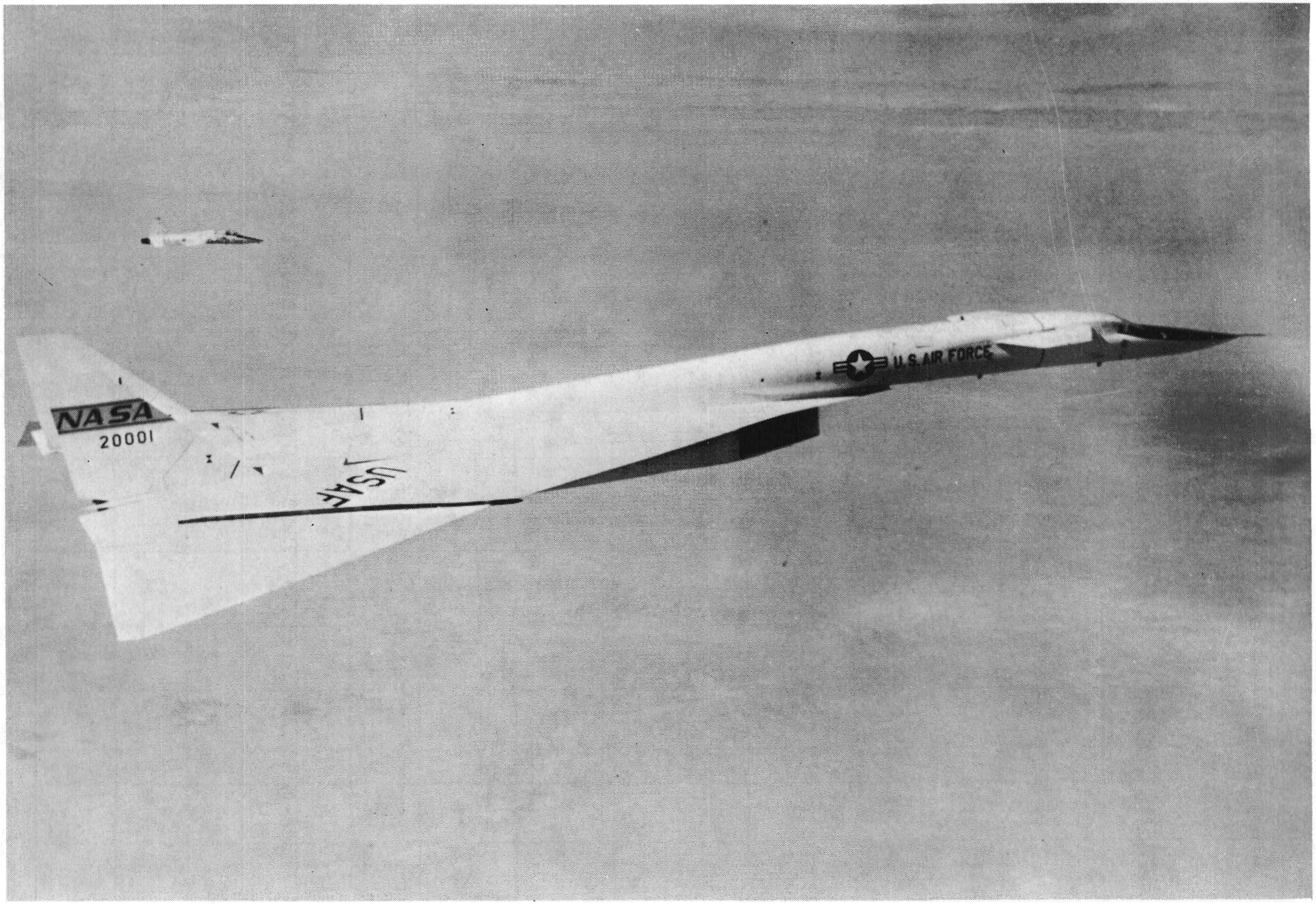

E-17463

Figure 1. XB-70-1 airplane in flight.

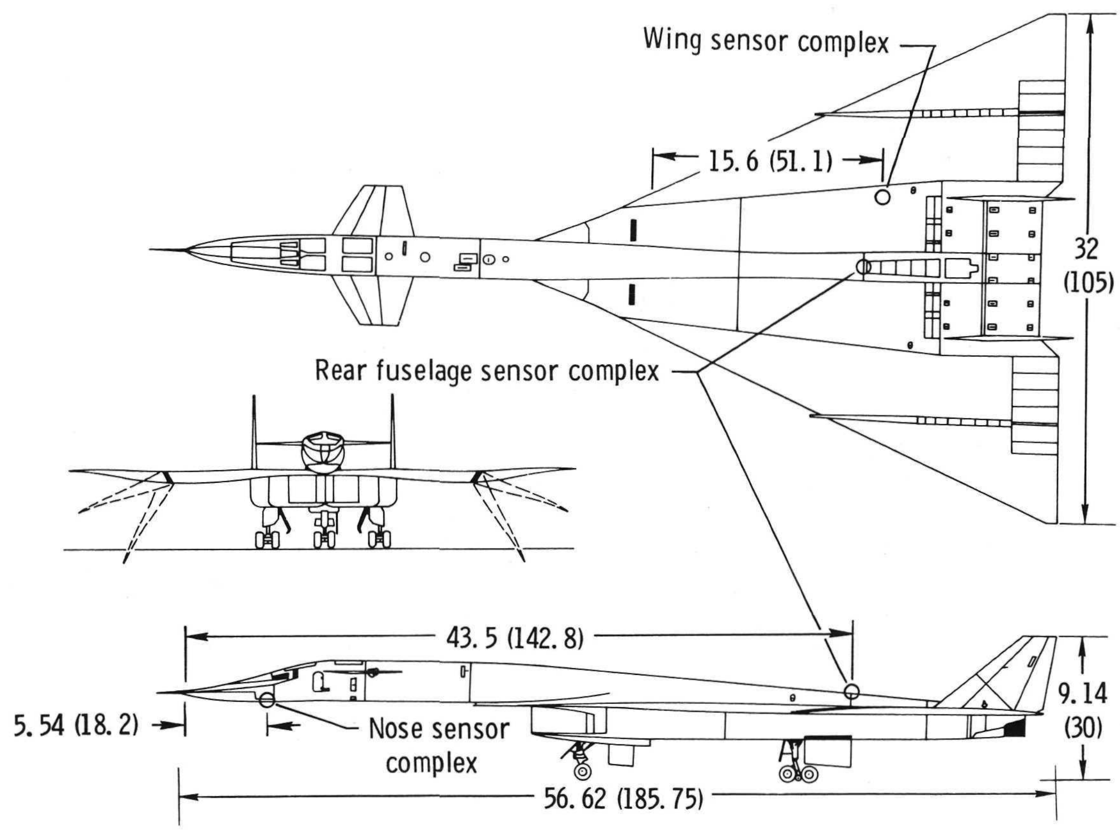

Figure 2. Three-view drawing of the XB-70-1 airplane. Dimensions in meters (feet).

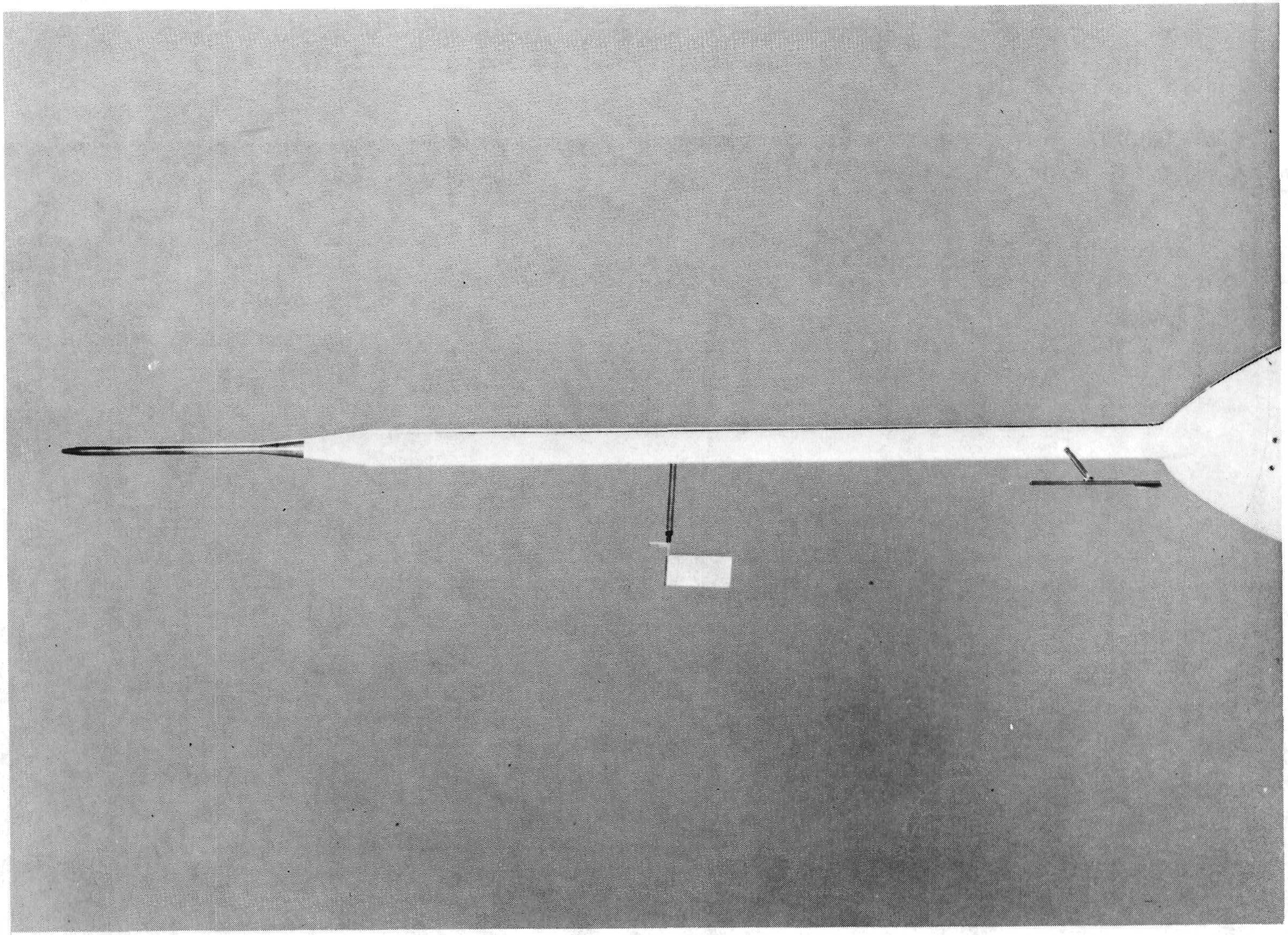

E-17042

(a) Nose boom with protuberances ahead of lower forward fuselage (nose) complex.

Figure 3. Surface areas ahead of the sensor complexes.

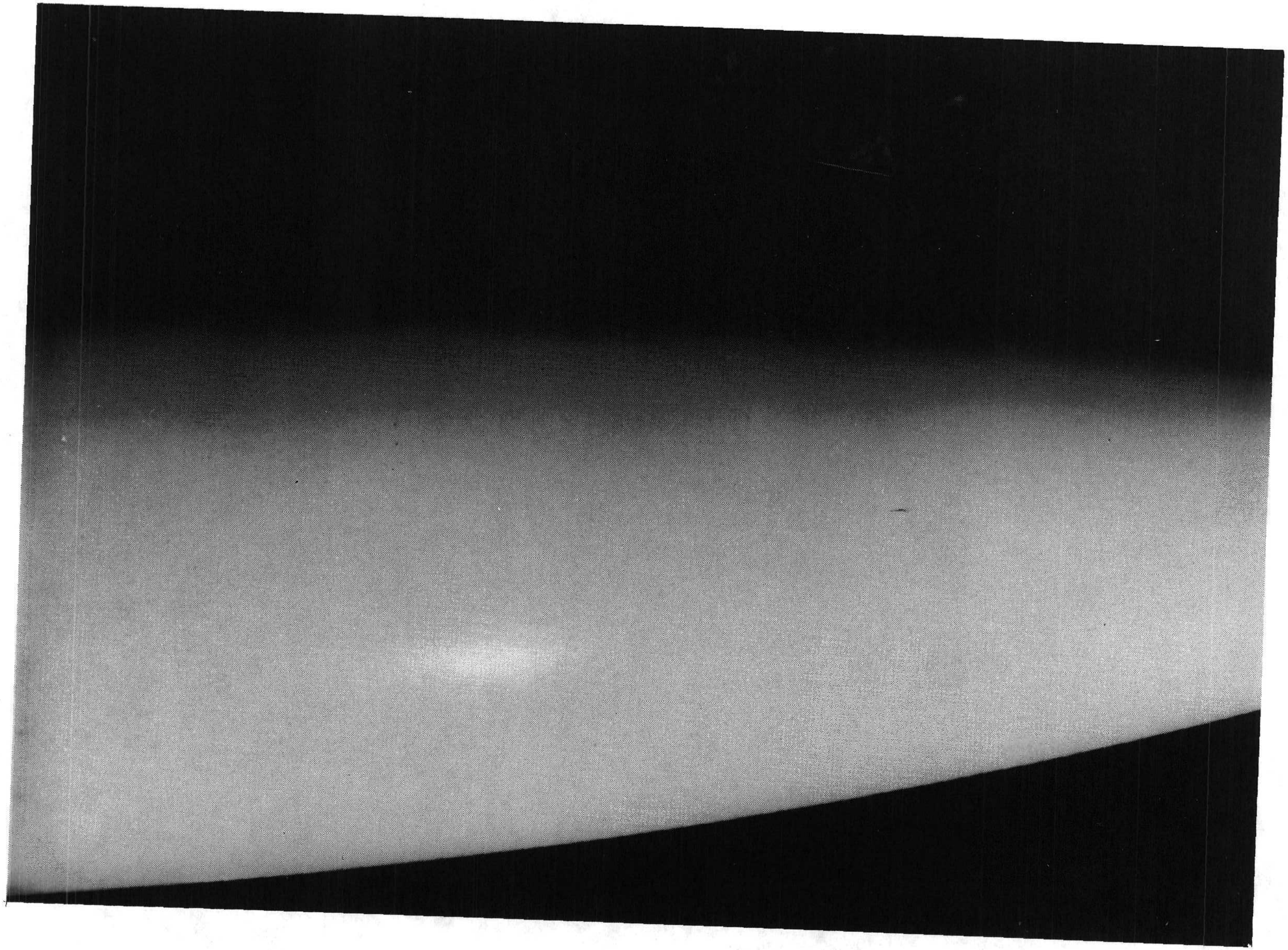

E-19823

(b) Surface ahead of nose complex.

Figure 3. Continued.

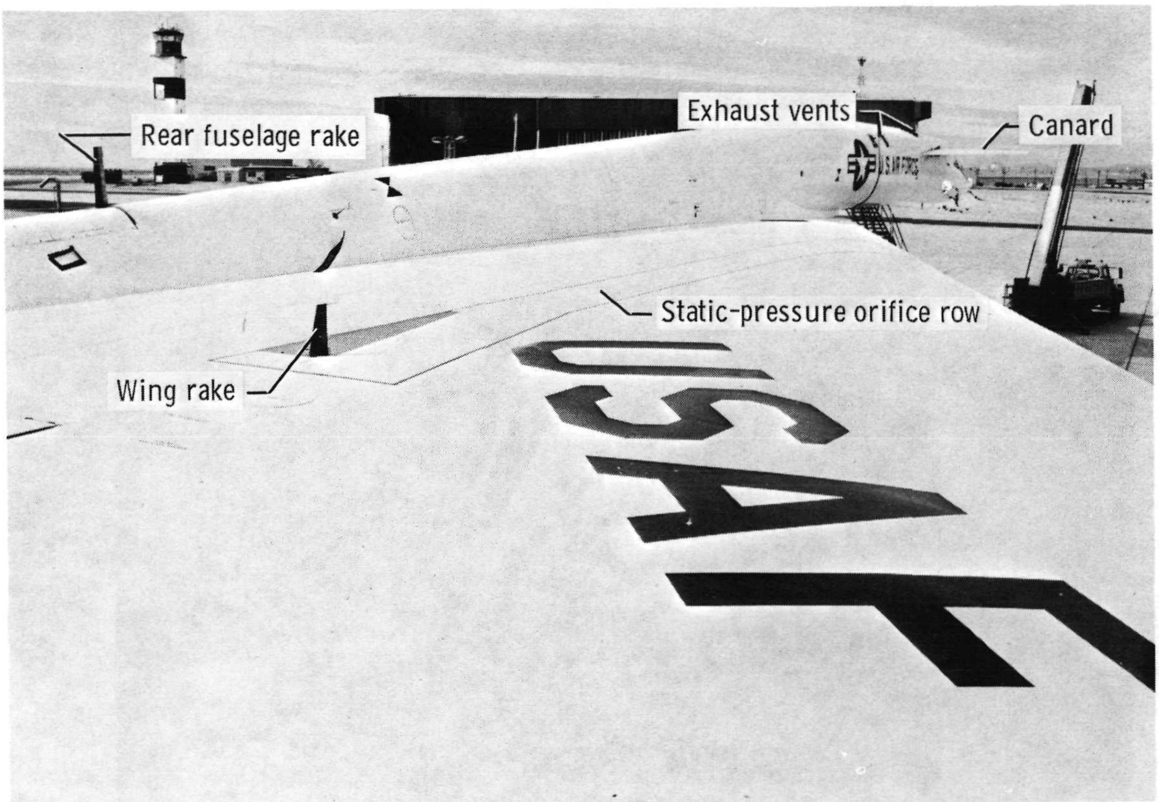

E-16566

(c) View looking forward, on right side, to area ahead of rear fuselage and wing complexes.

Figure 3. Continued

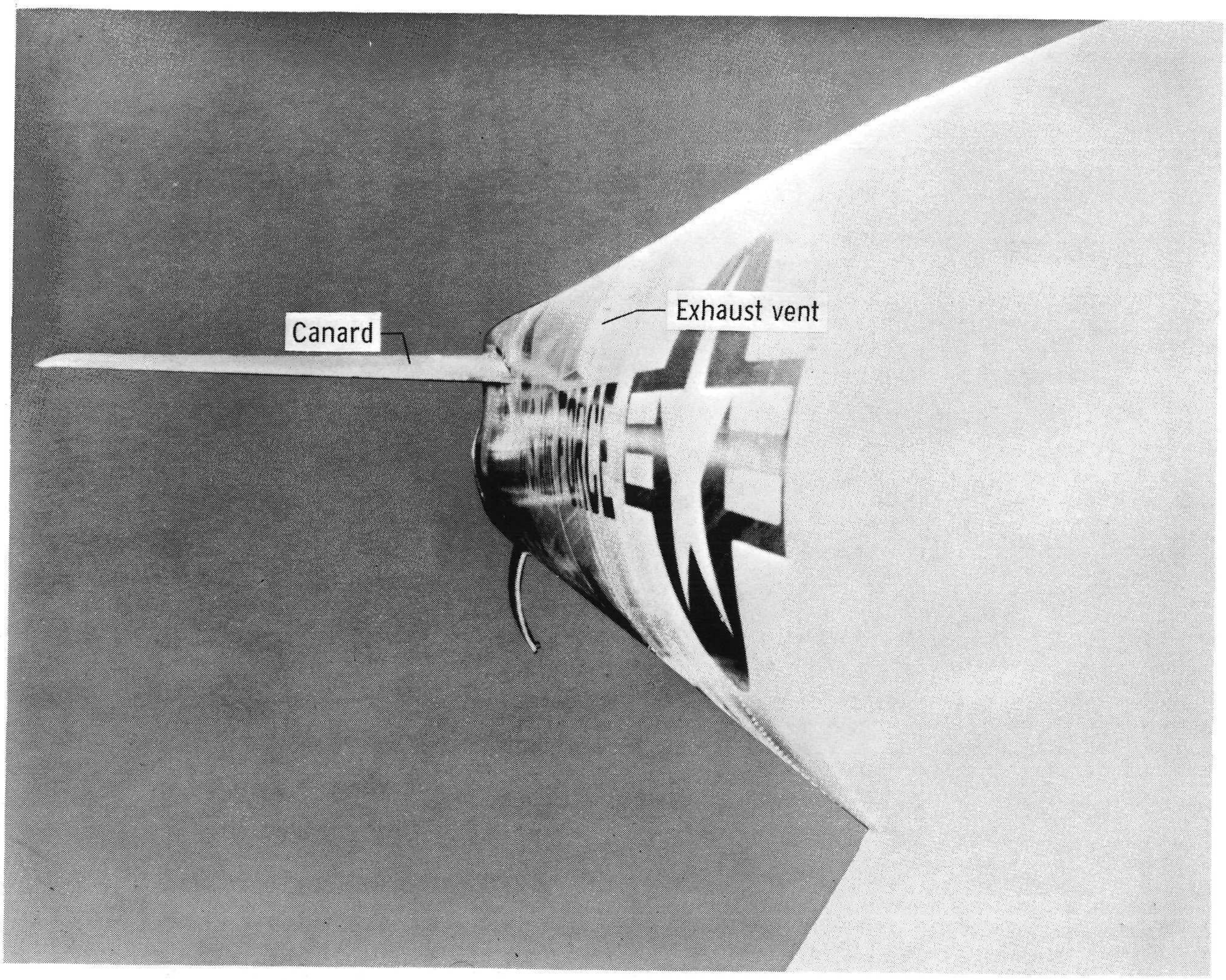

E-19795

(d) View looking forward, on left side, to area ahead of rear fuselage complex.

Figure 3. Continued.

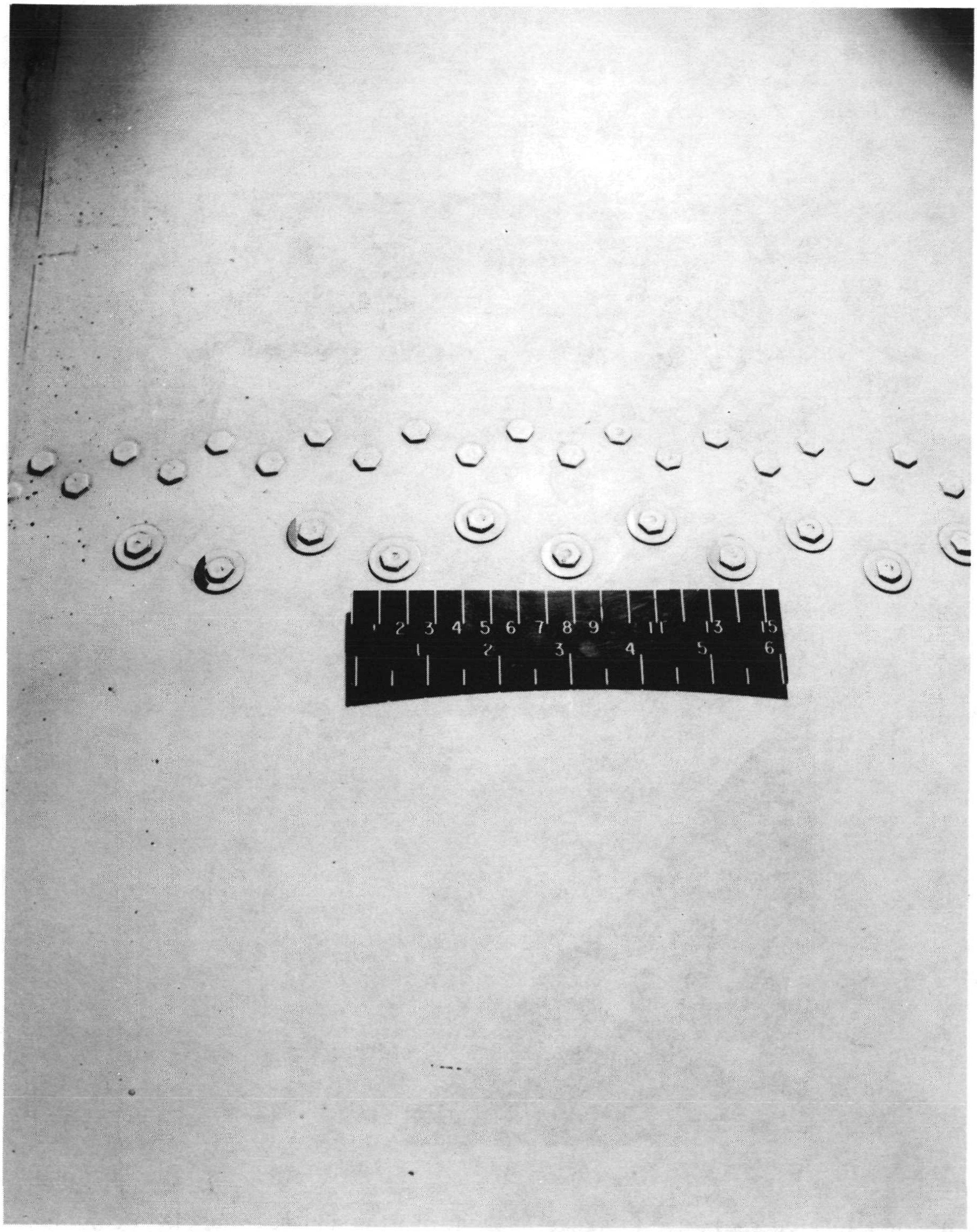

E-19806

(e) Typical screwhead roughness on the fuselage.

Figure 3. Continued.

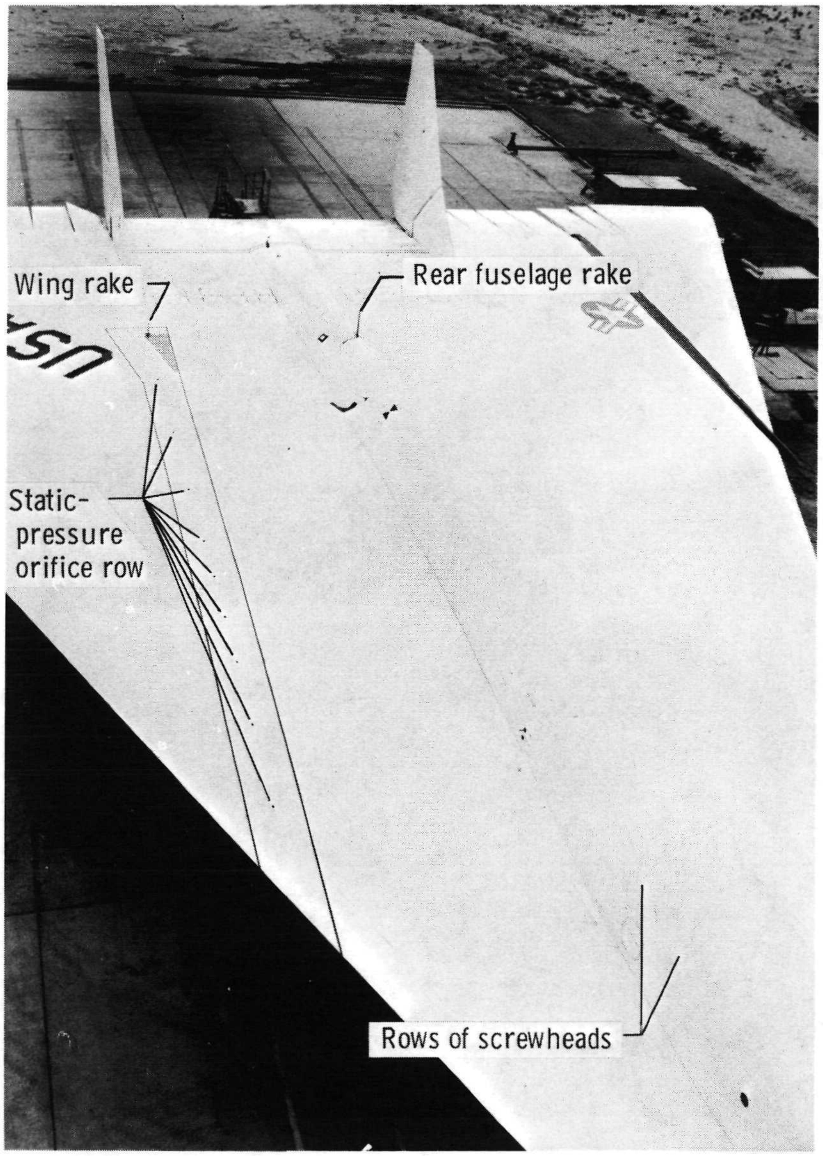

E-16563

(f) View looking rearward to areas in front of wing and rear fuselage complexes.

Figure 3. Continued.

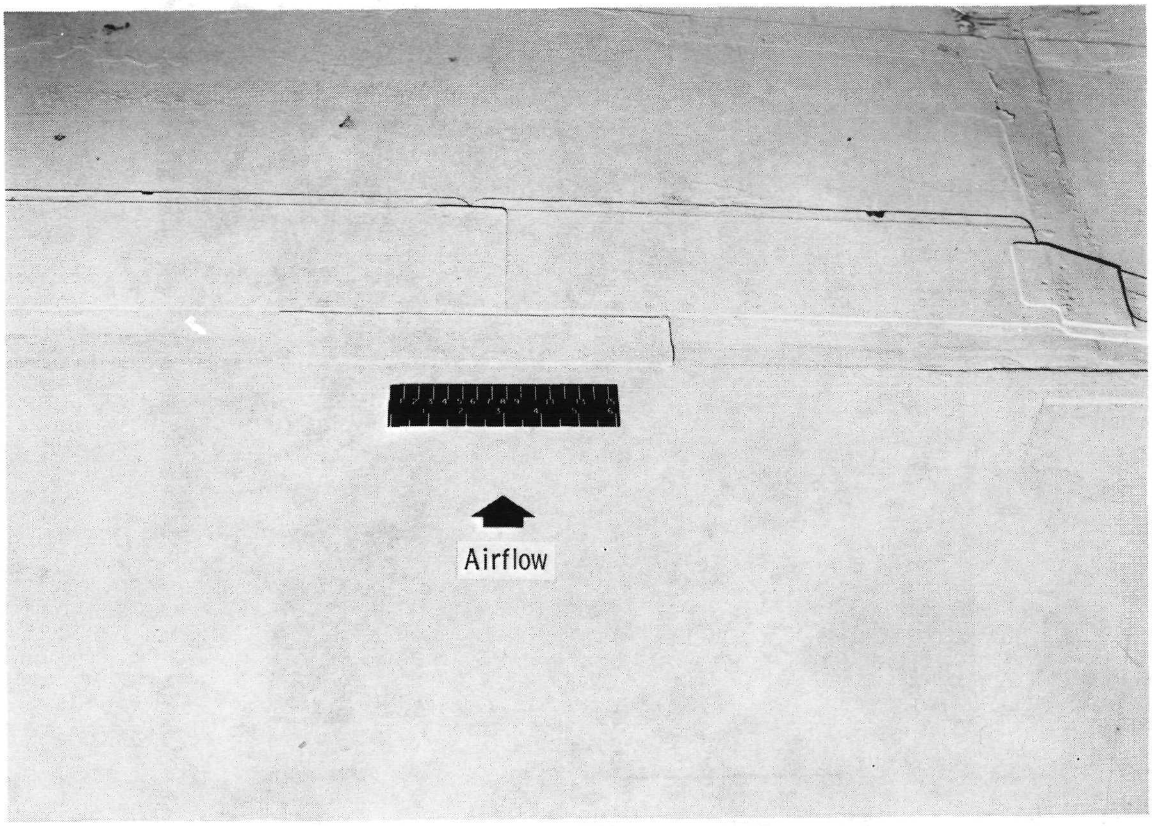

E-19805

(g) Typical lap joint (wing).

Figure 3. Concluded.

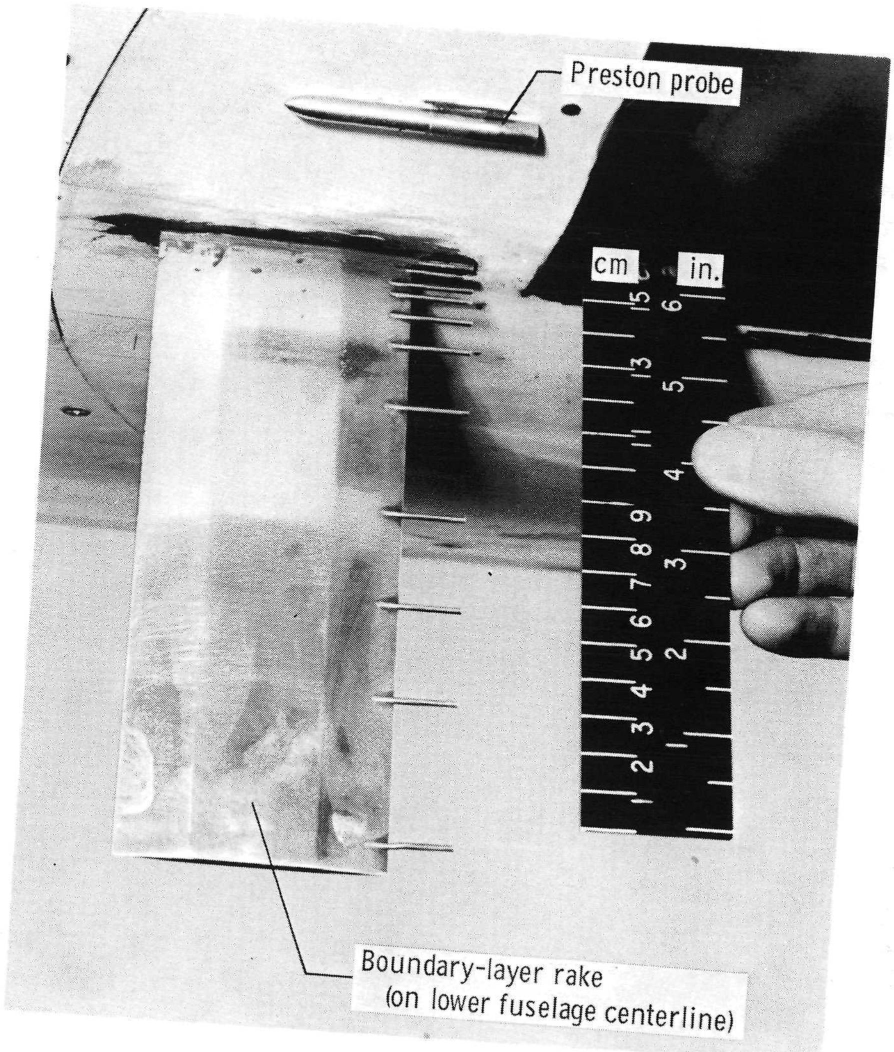

(a) Closeup view of nose rake and Preston probe. E-19729

Figure 4. Nose sensor complex.

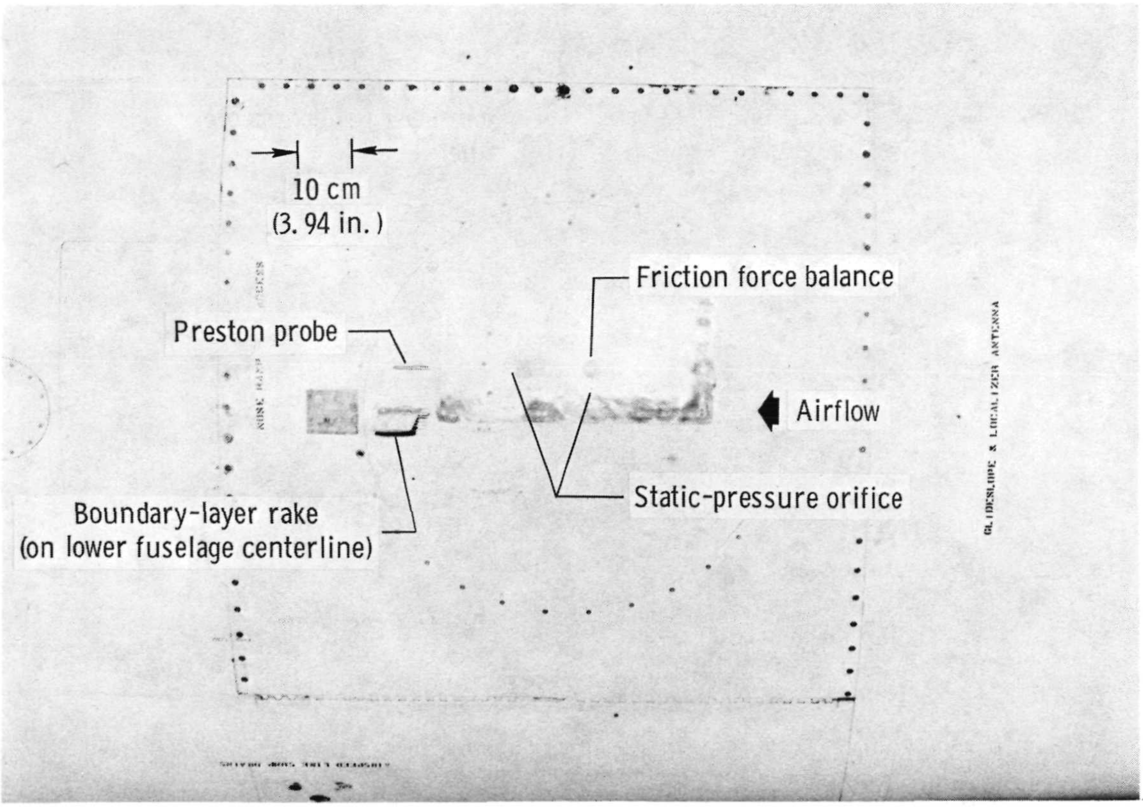

E-19822

(b) View from below.

Figure 4. Concluded.

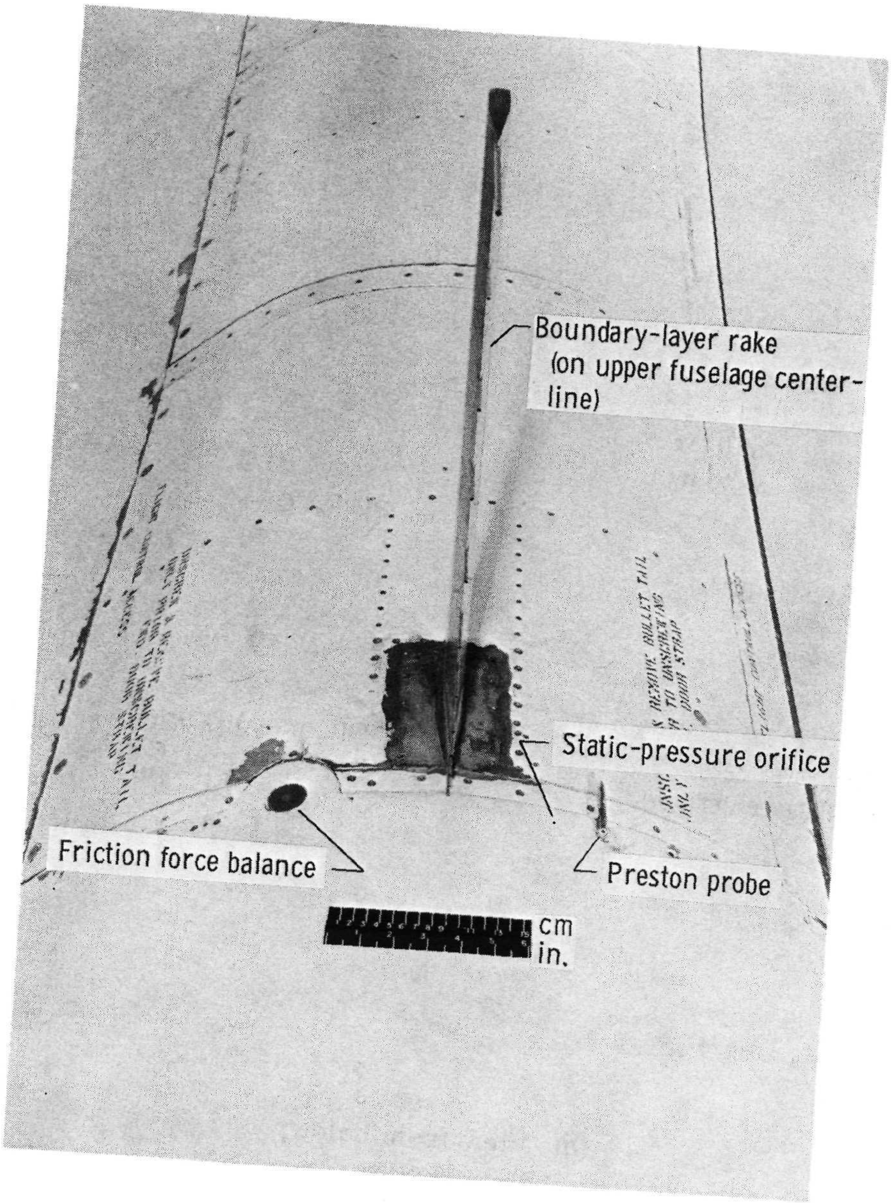

E-19727

(a) Front view.

Figure 5. Rear fuselage sensor complex.

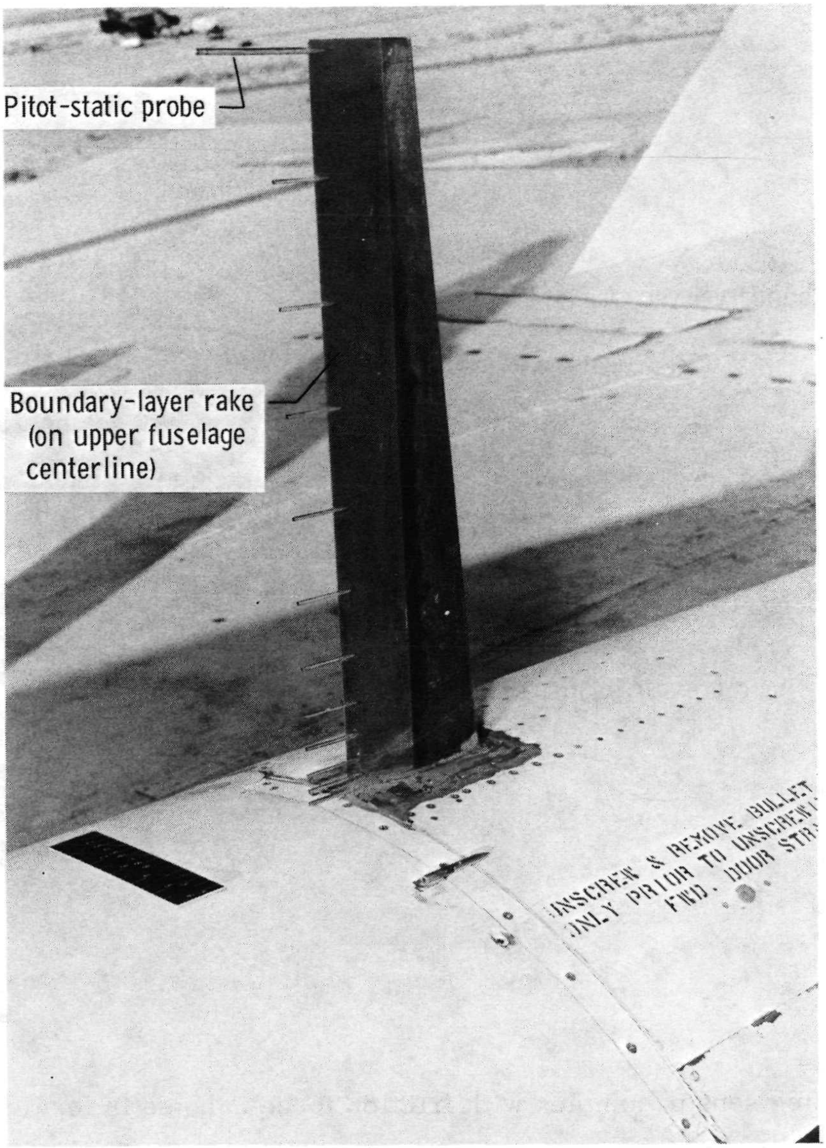

E-19723

(b) Three-quarter view.

Figure 5. Concluded.

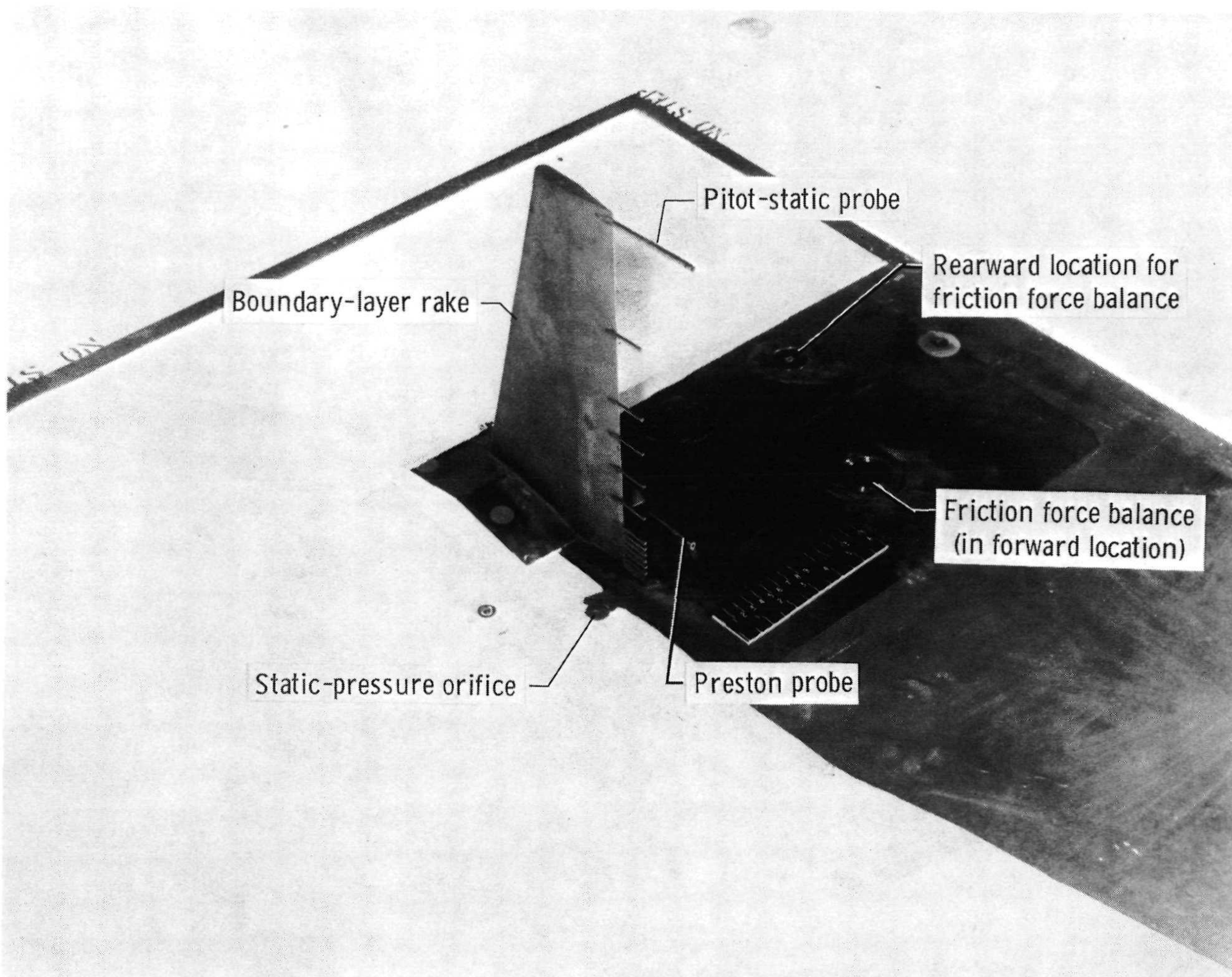

E-19726

Figure 6. Wing sensor complex with friction force balance in forward position.

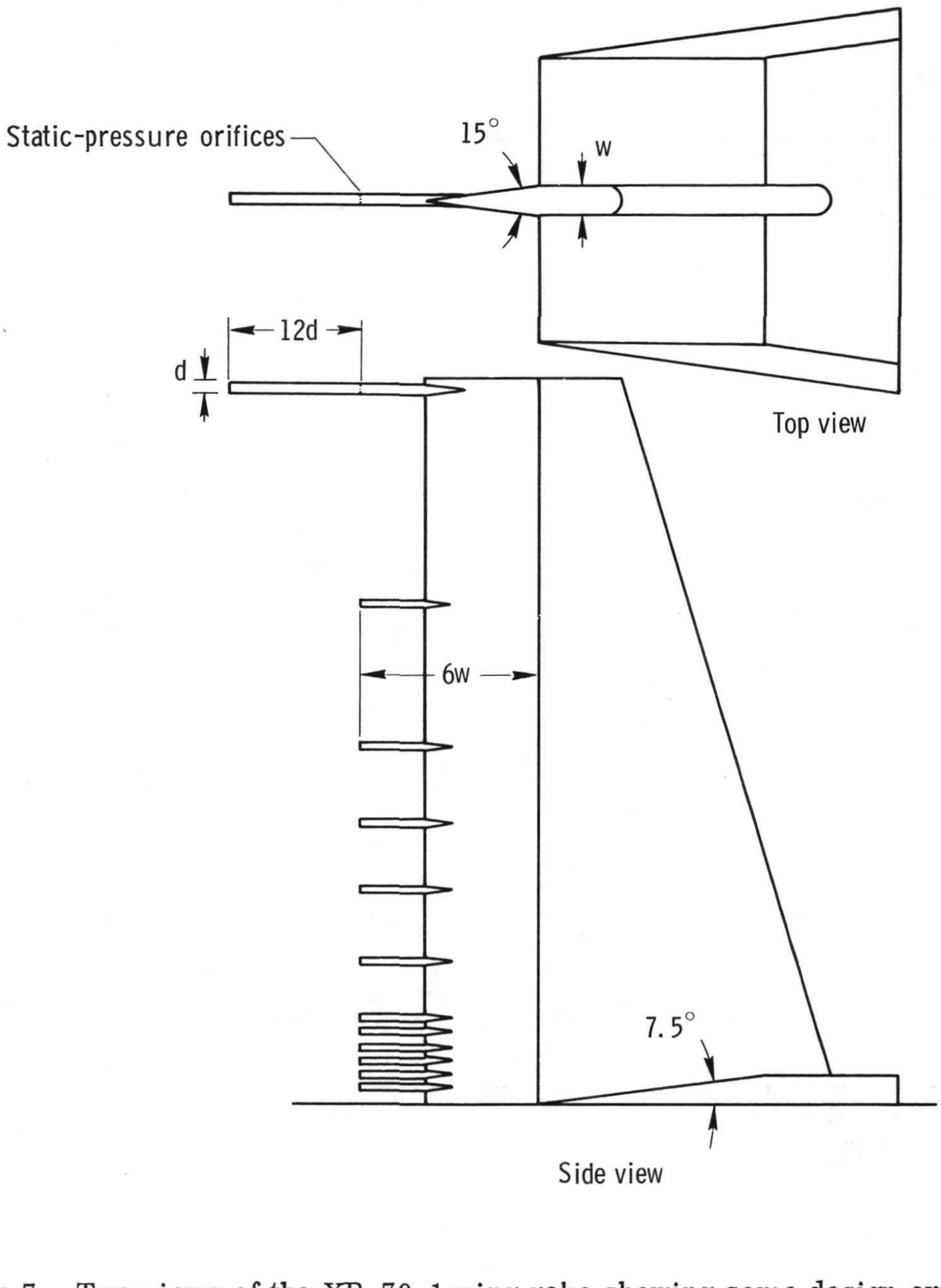

Figure 7. Two views of the XB-70-1 wing rake showing some design criteria.

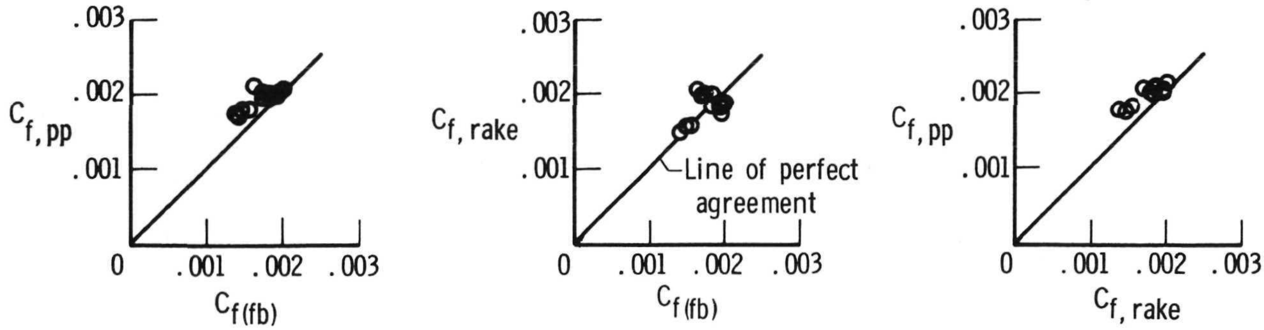

(a) Nose.

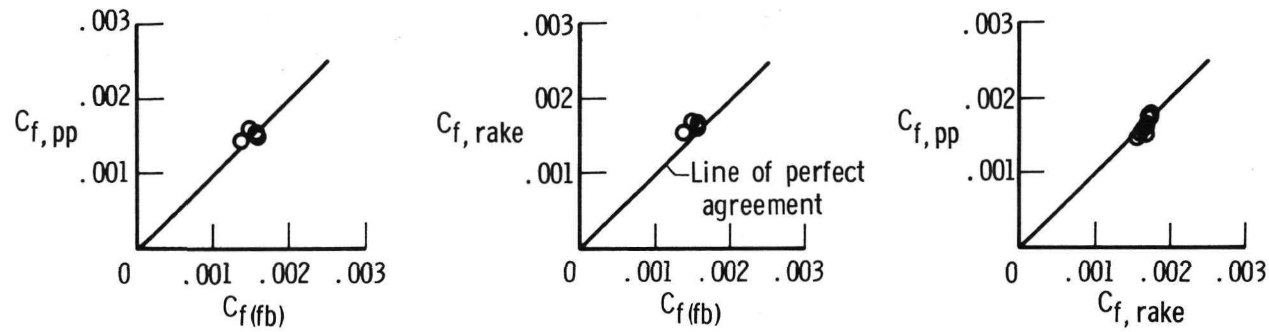

(b) Rear fuselage.

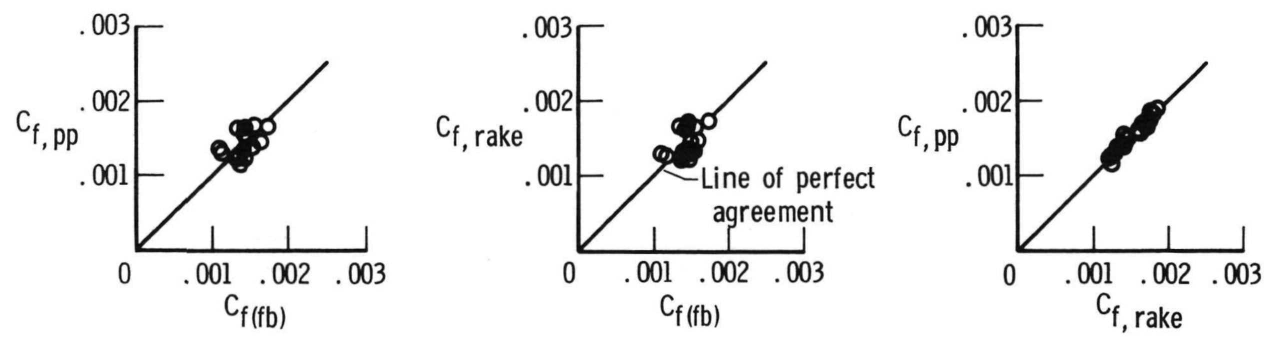

(c) Wing.

Figure 8. Comparison of data obtained with the three methods of determining local skin friction coefficient at the three locations investigated.

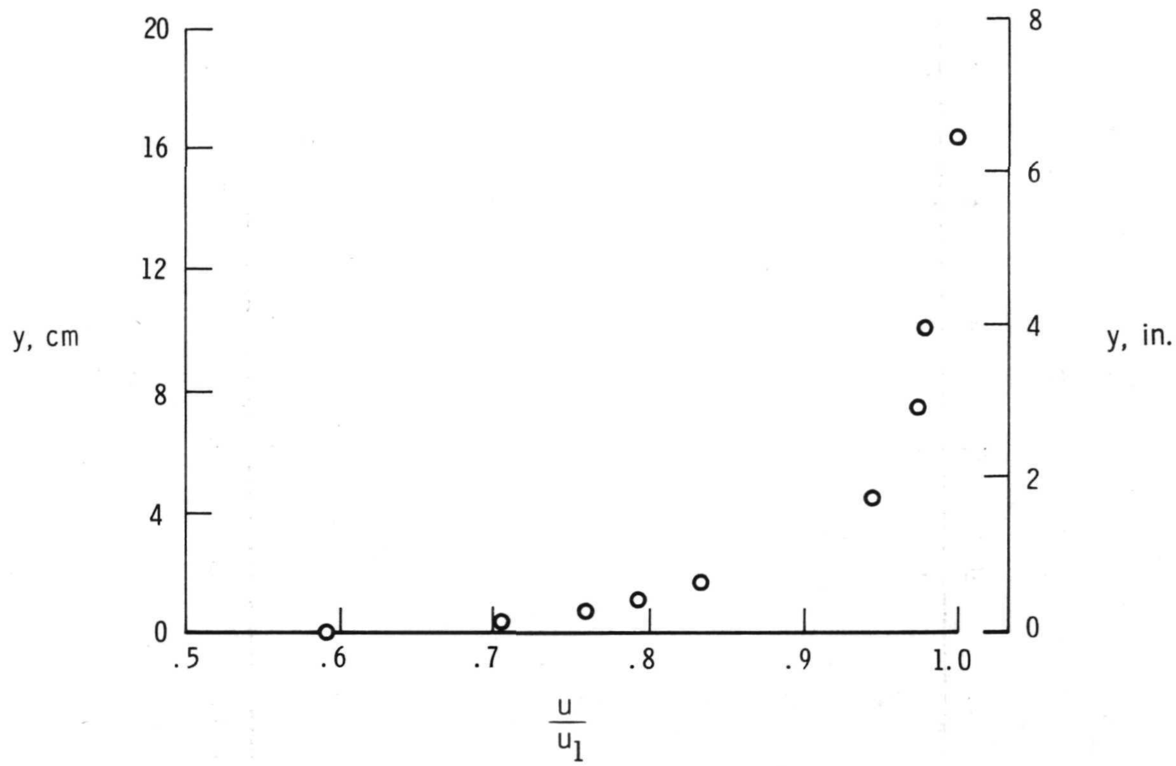

(a) Nose; $M_1 = 2.13$.

Figure 9. Typical boundary-layer velocity profiles for the three locations.

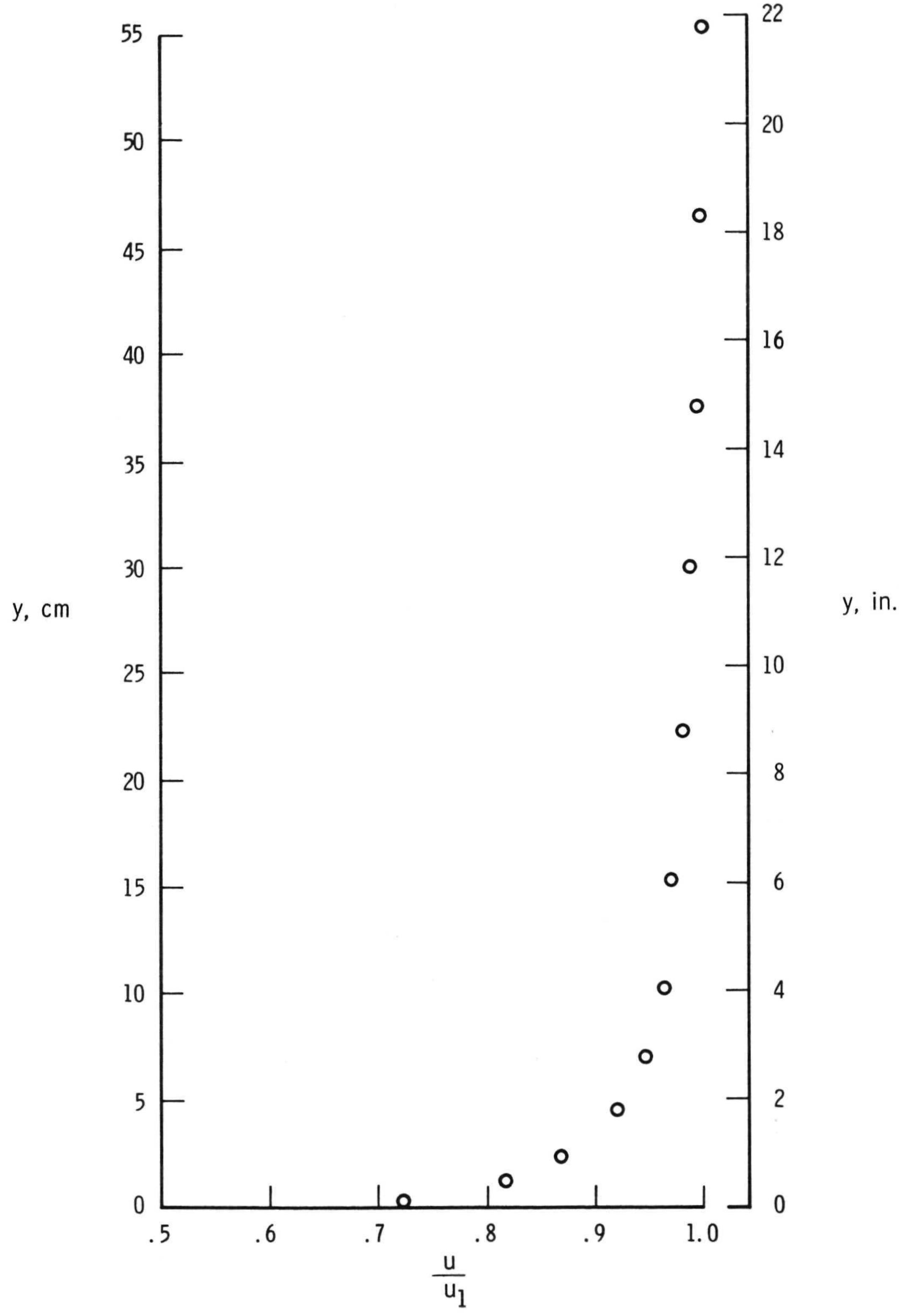

(b) Rear fuselage; $M_1 = 2.24$.

Figure 9. Continued.

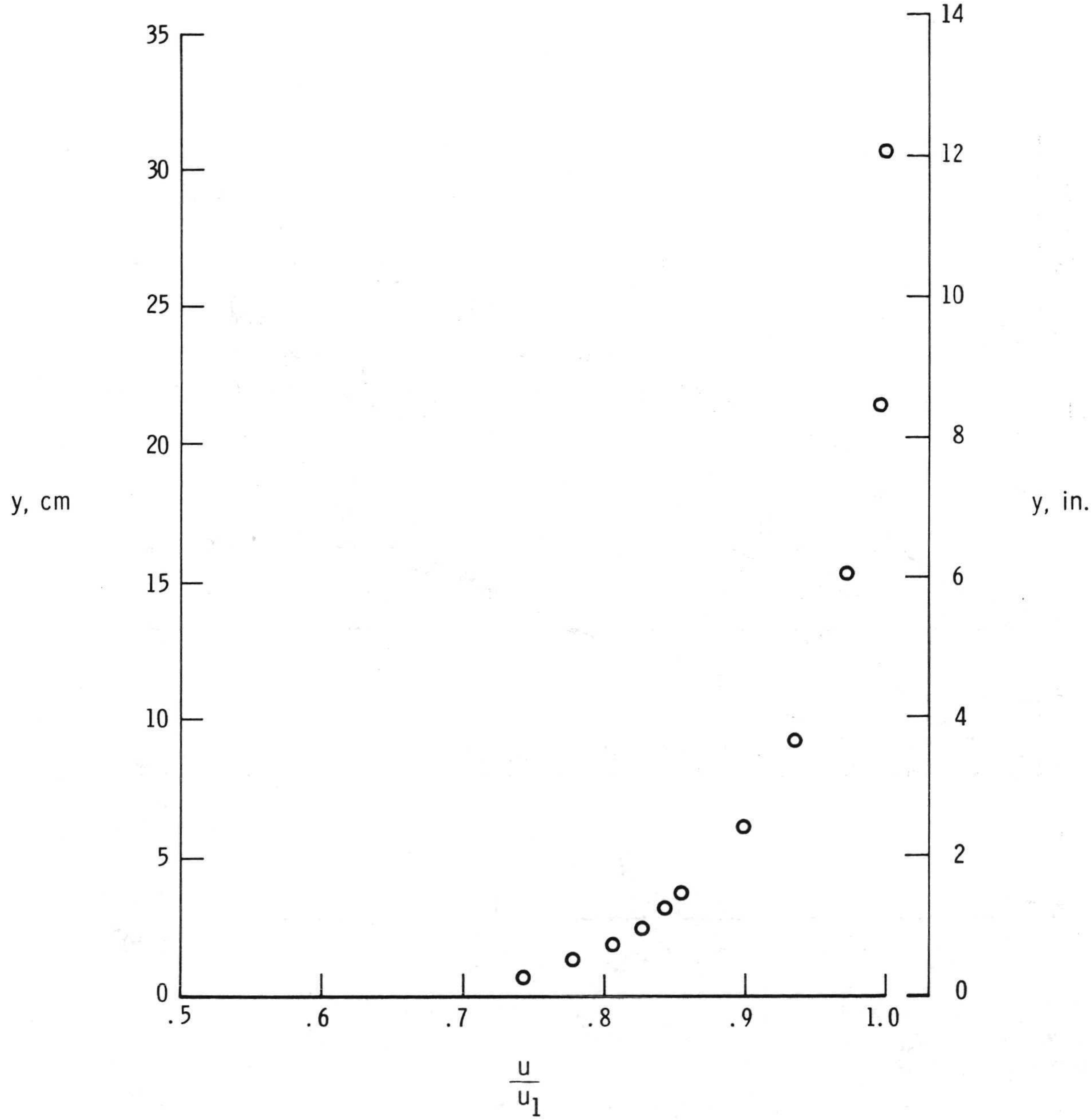

(c) Wing; $M_1 = 2.41$.

Figure 9. Concluded.

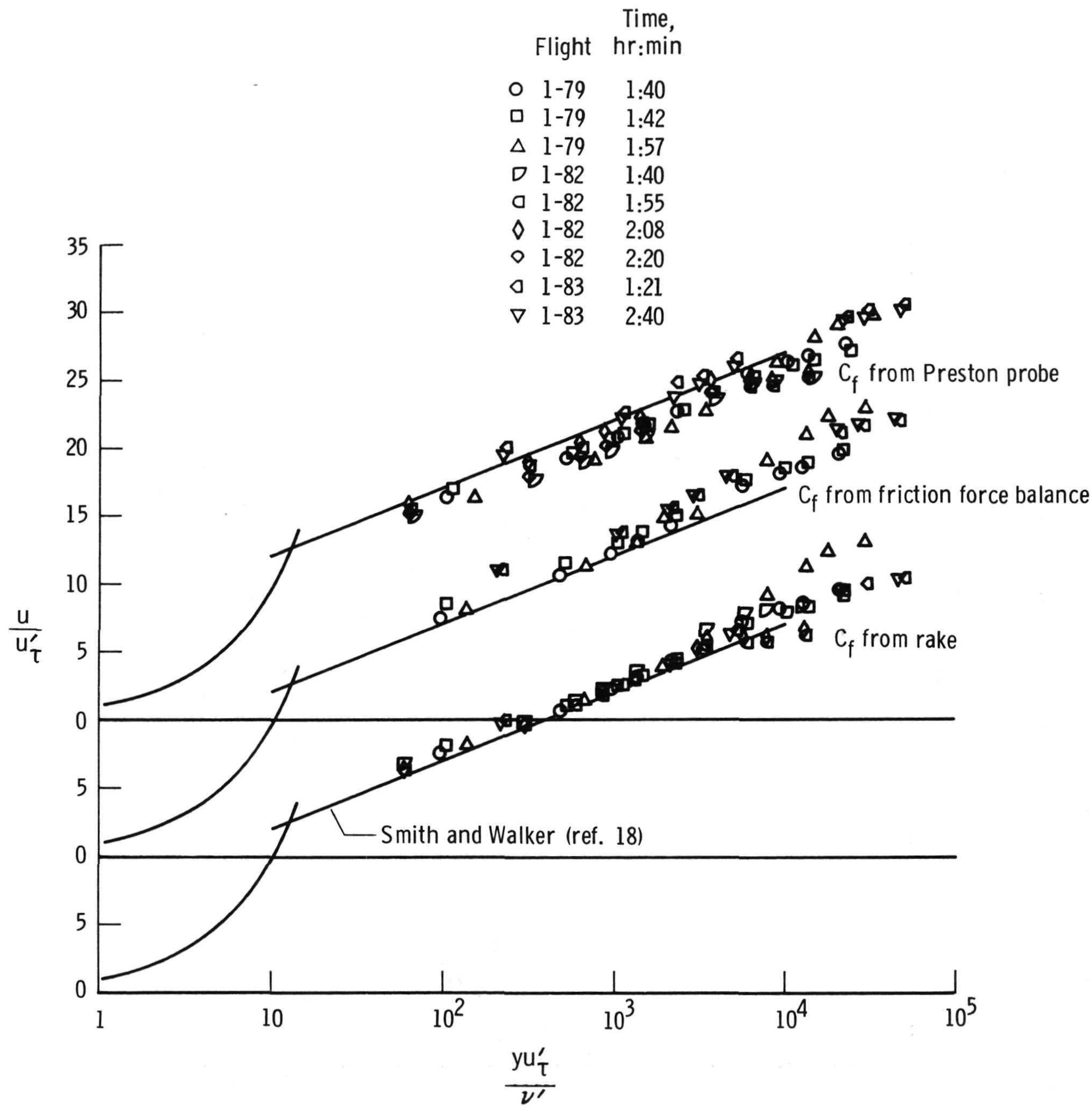

(a) Nose.

Figure 10. Law-of-the-wall velocity profiles for the three locations.

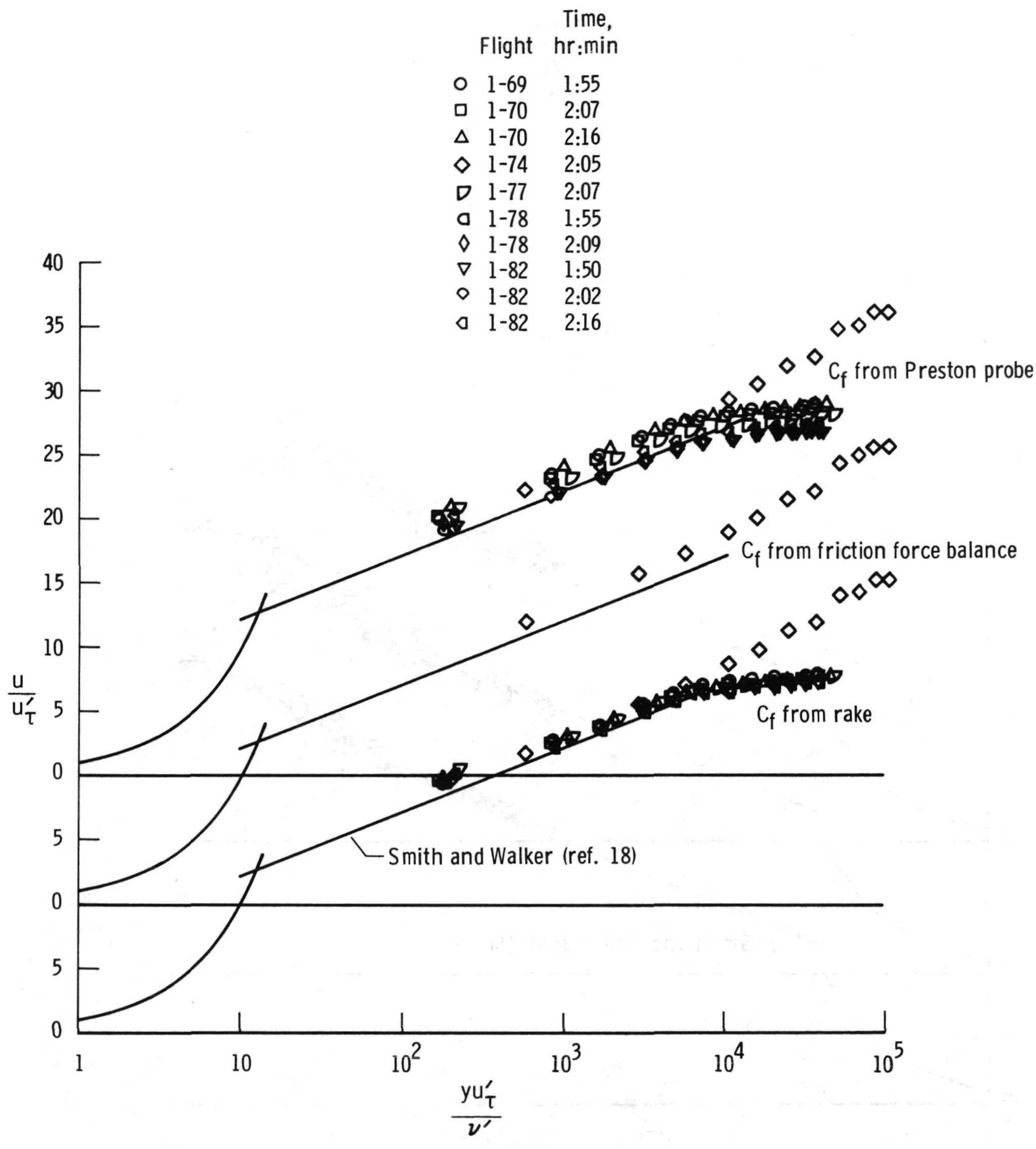

(b) Rear fuselage.

Figure 10. Continued.

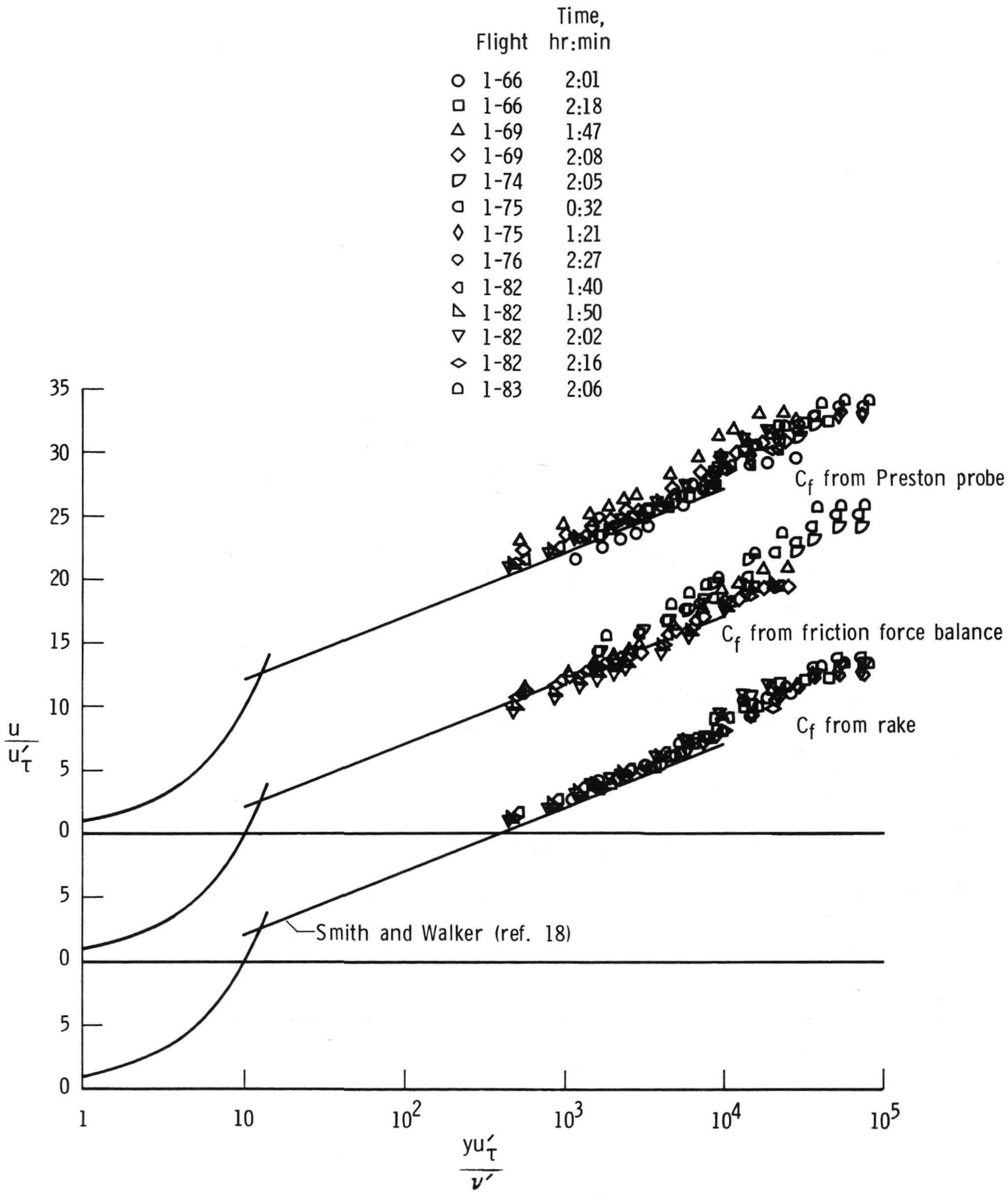

(c) Wing.

Figure 10. Concluded.

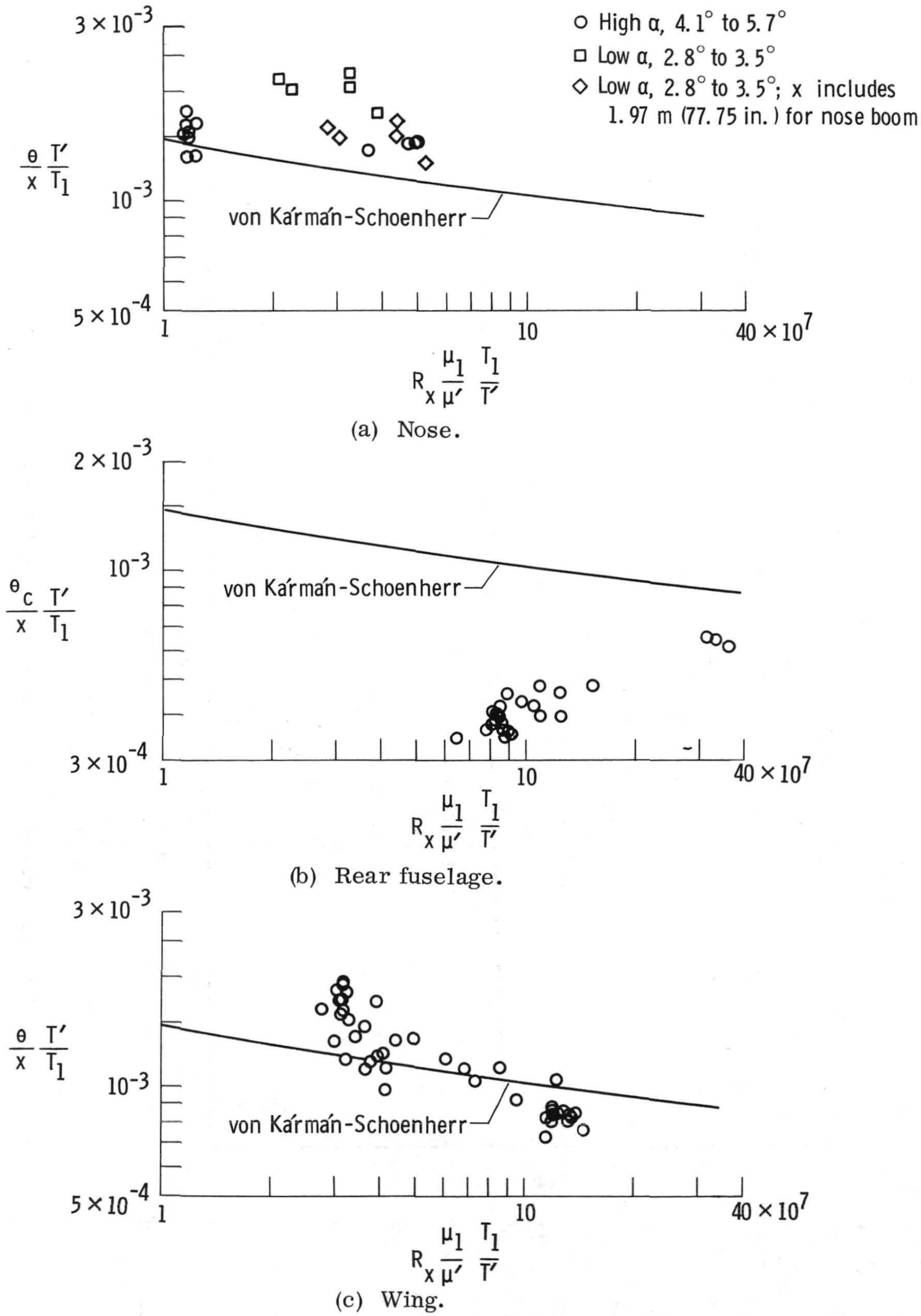

Figure 11. Variation of the transformed ratio Θ/x with transformed Reynolds number and comparison with the von Kármán-Schoenherr theory (ref. 21) for the three locations.

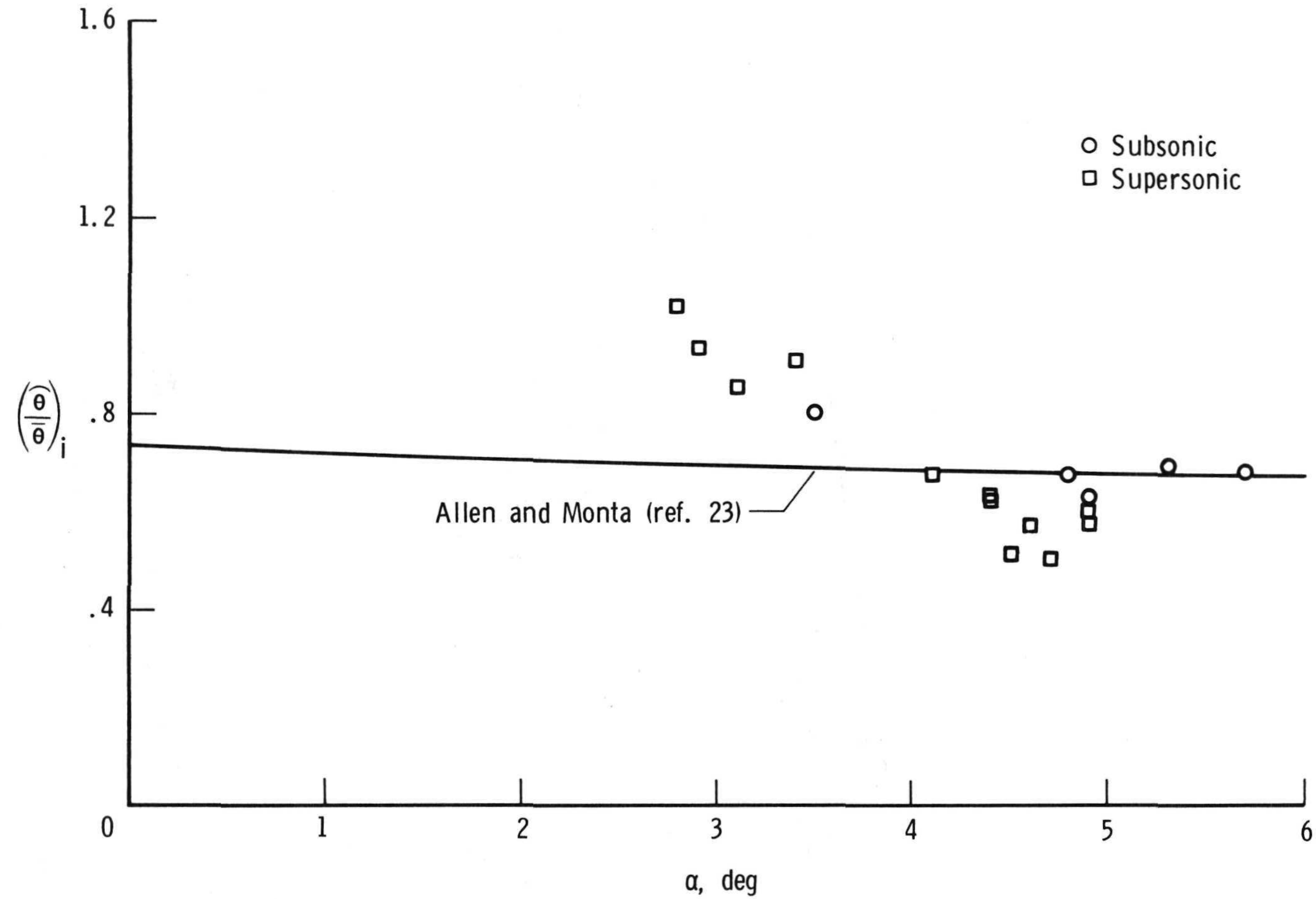

Figure 12. Variation of the momentum thickness ratio with angle of attack at the nose location.

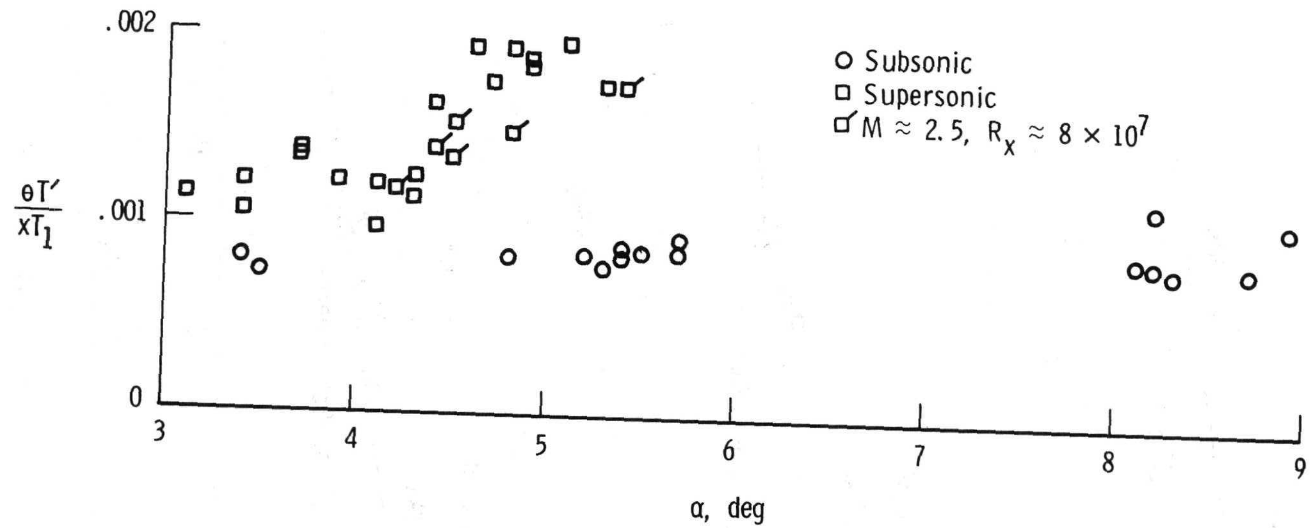

Figure 13. Variation of the transformed momentum thickness ratio, $\frac{\Theta T'}{xT_1}$ with angle of attack at the wing location.

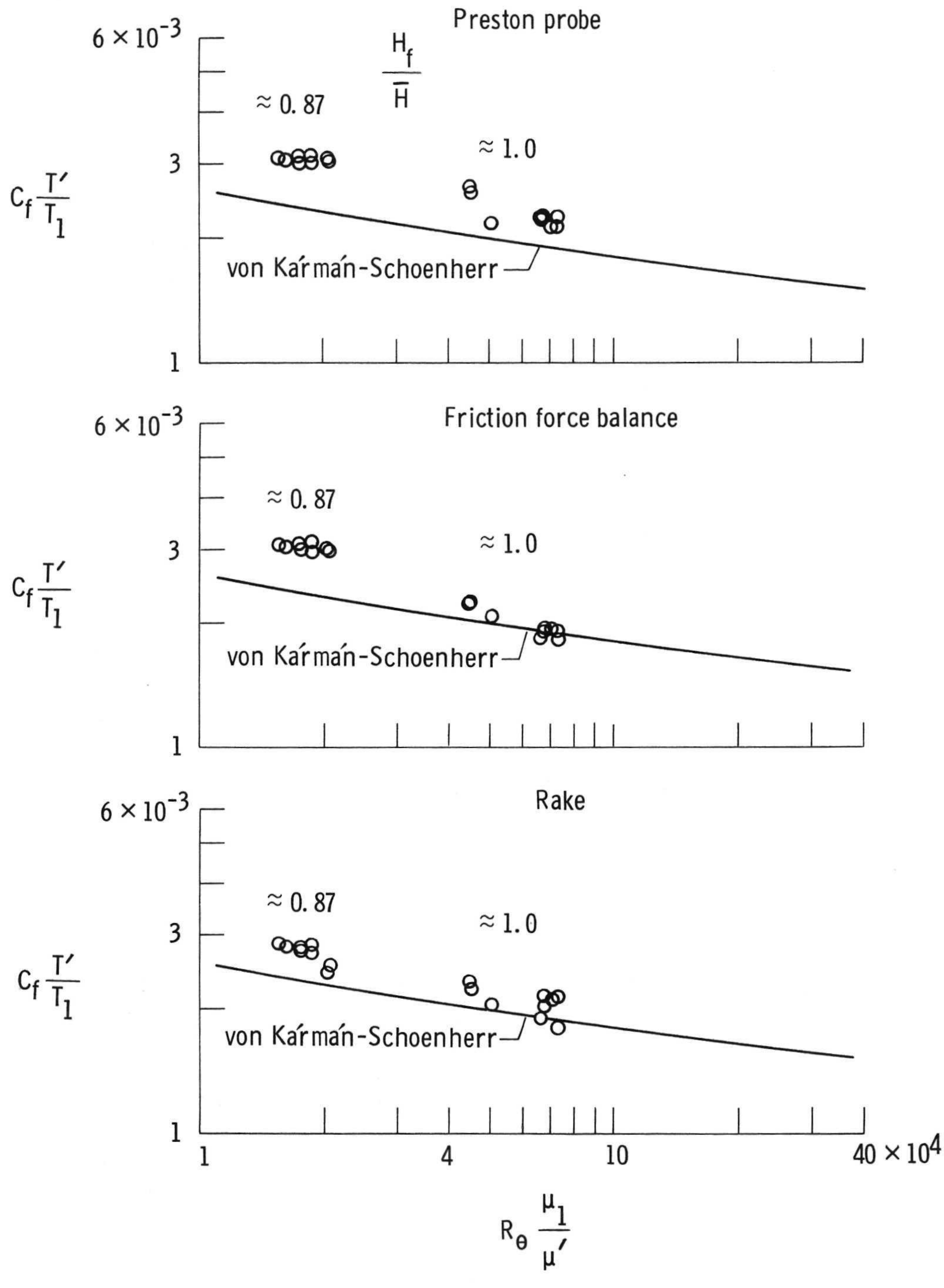

(a) Nose.

Figure 14. Variation of local skin friction coefficient with momentum thickness Reynolds number for the three methods at the three locations and comparison with the von Kármán-Schoenherr theory (ref. 21).

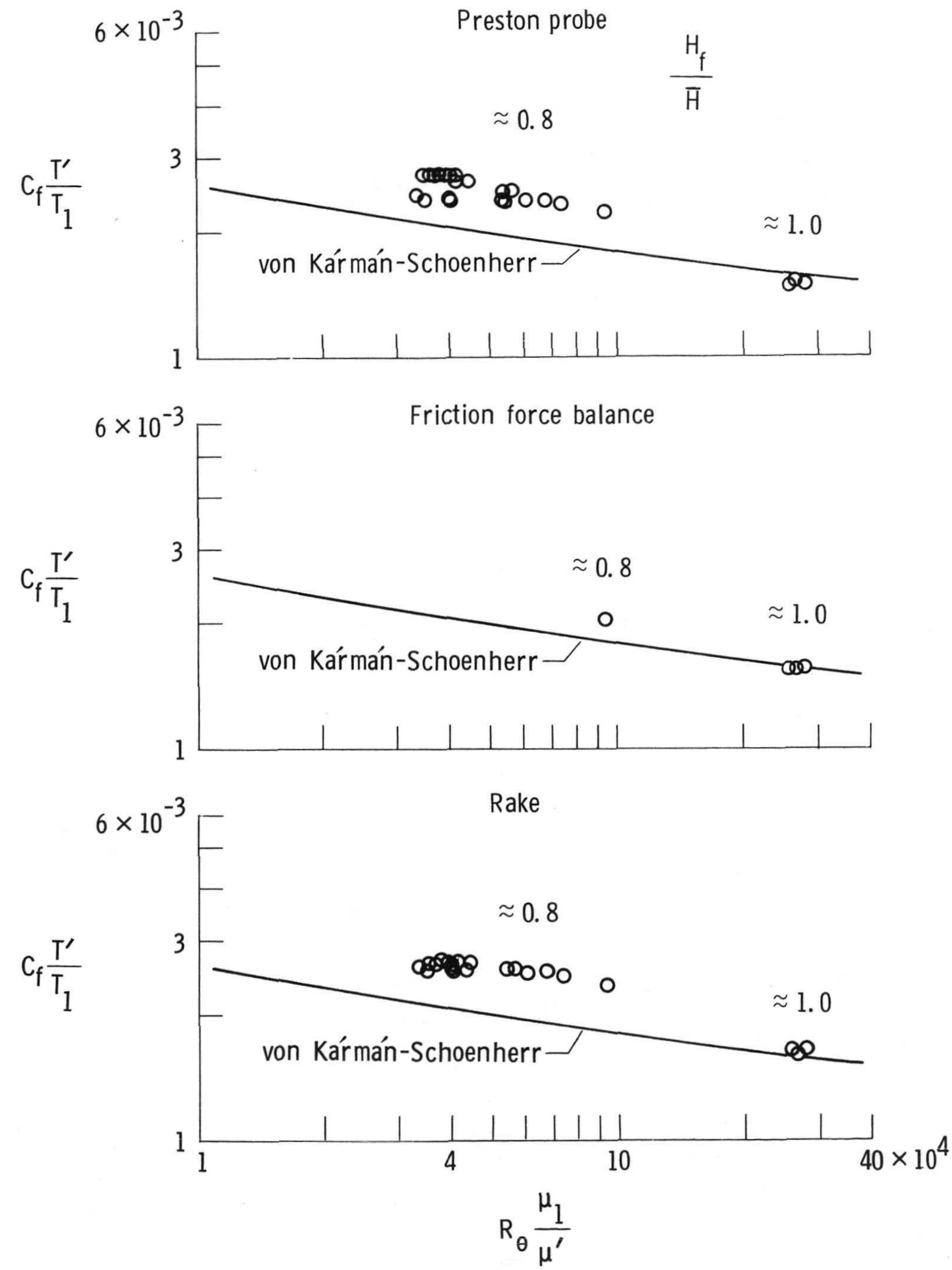

(b) Rear fuselage.

Figure 14. Continued.

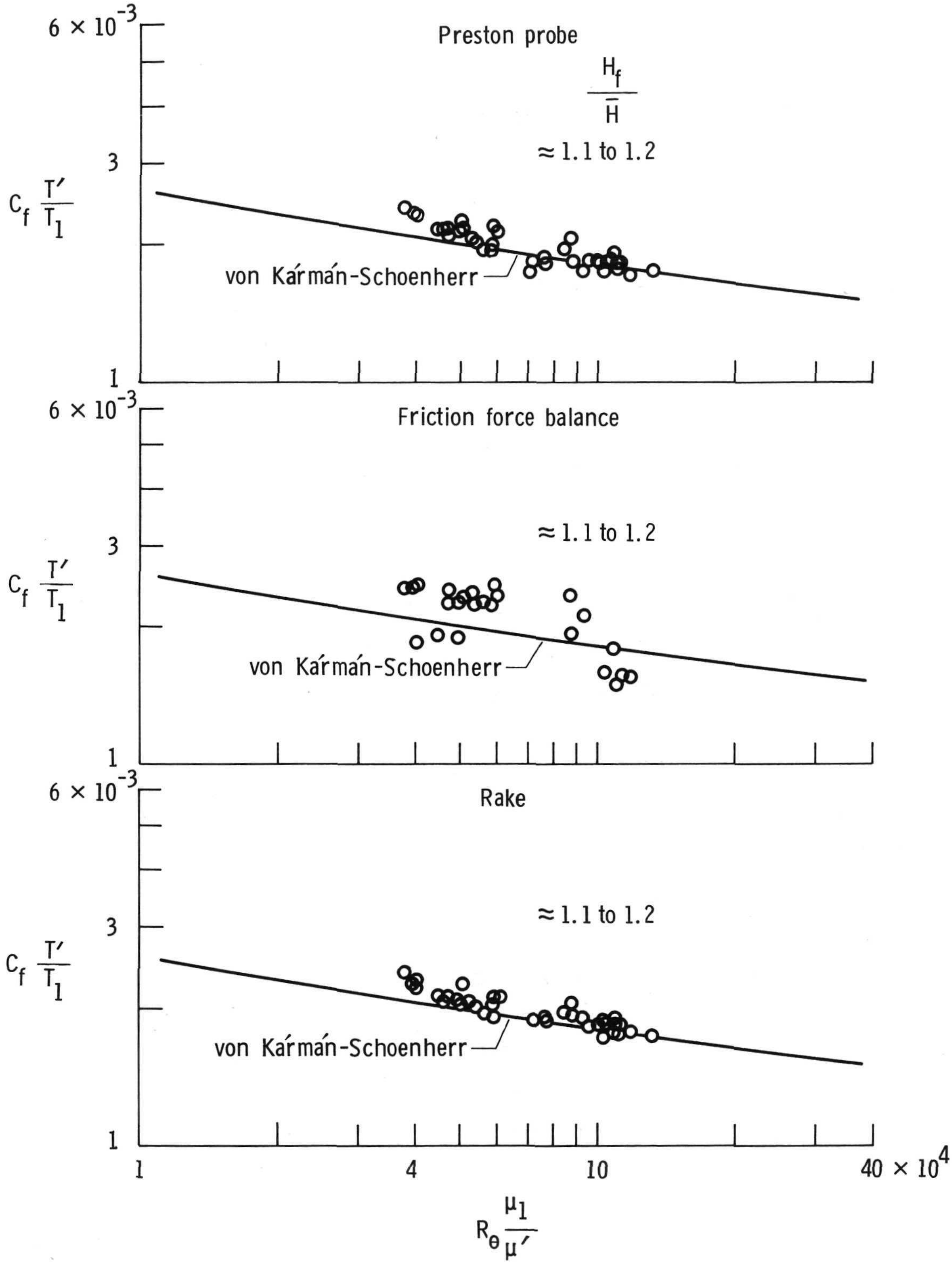

(c) Wing.

Figure 14. Concluded.

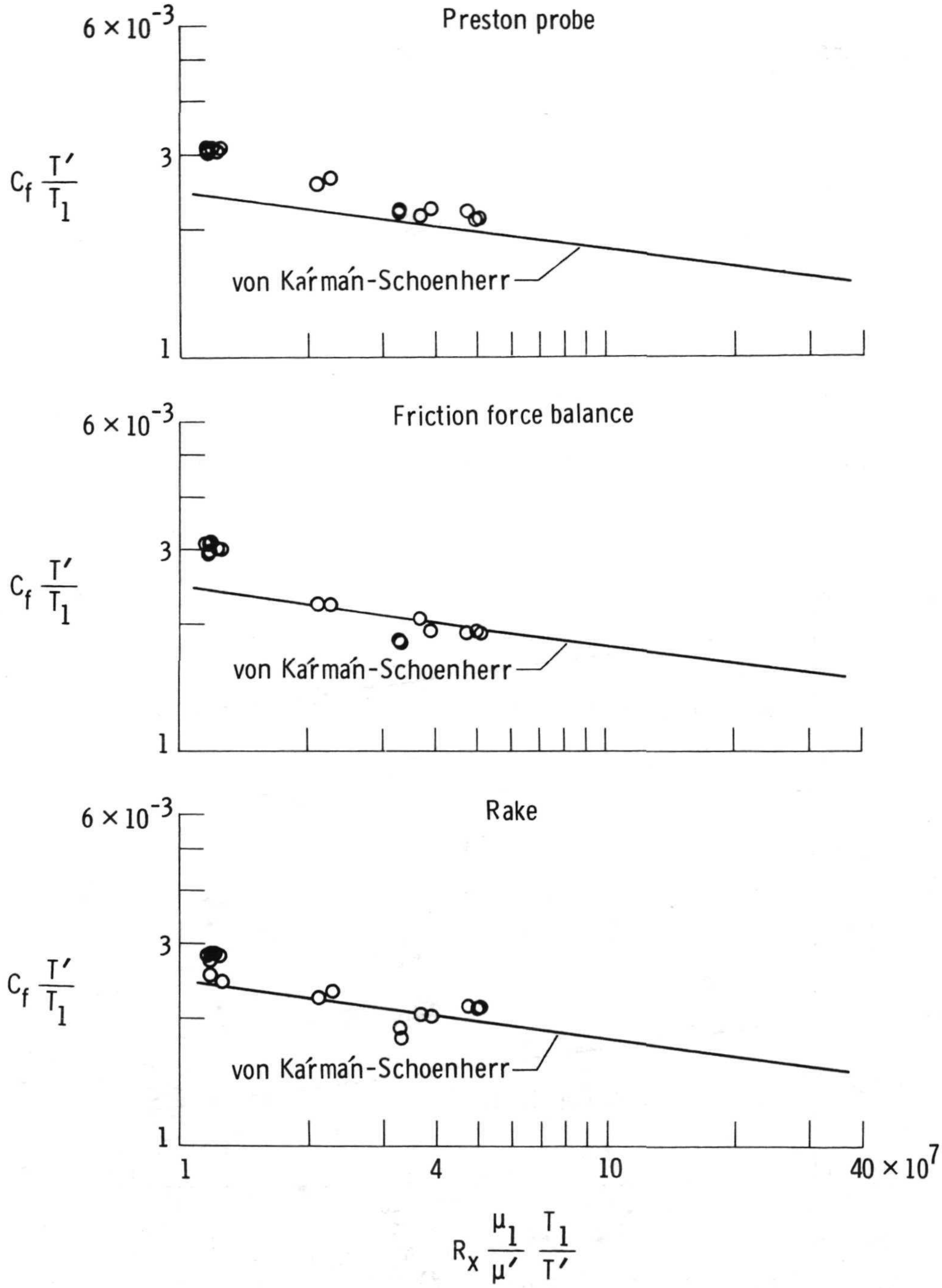

(a) Nose.

Figure 15. Variation of local skin friction coefficient with Reynolds number for the three methods at the three locations and comparison with the von Kármán-Schoenherr theory (ref. 21).

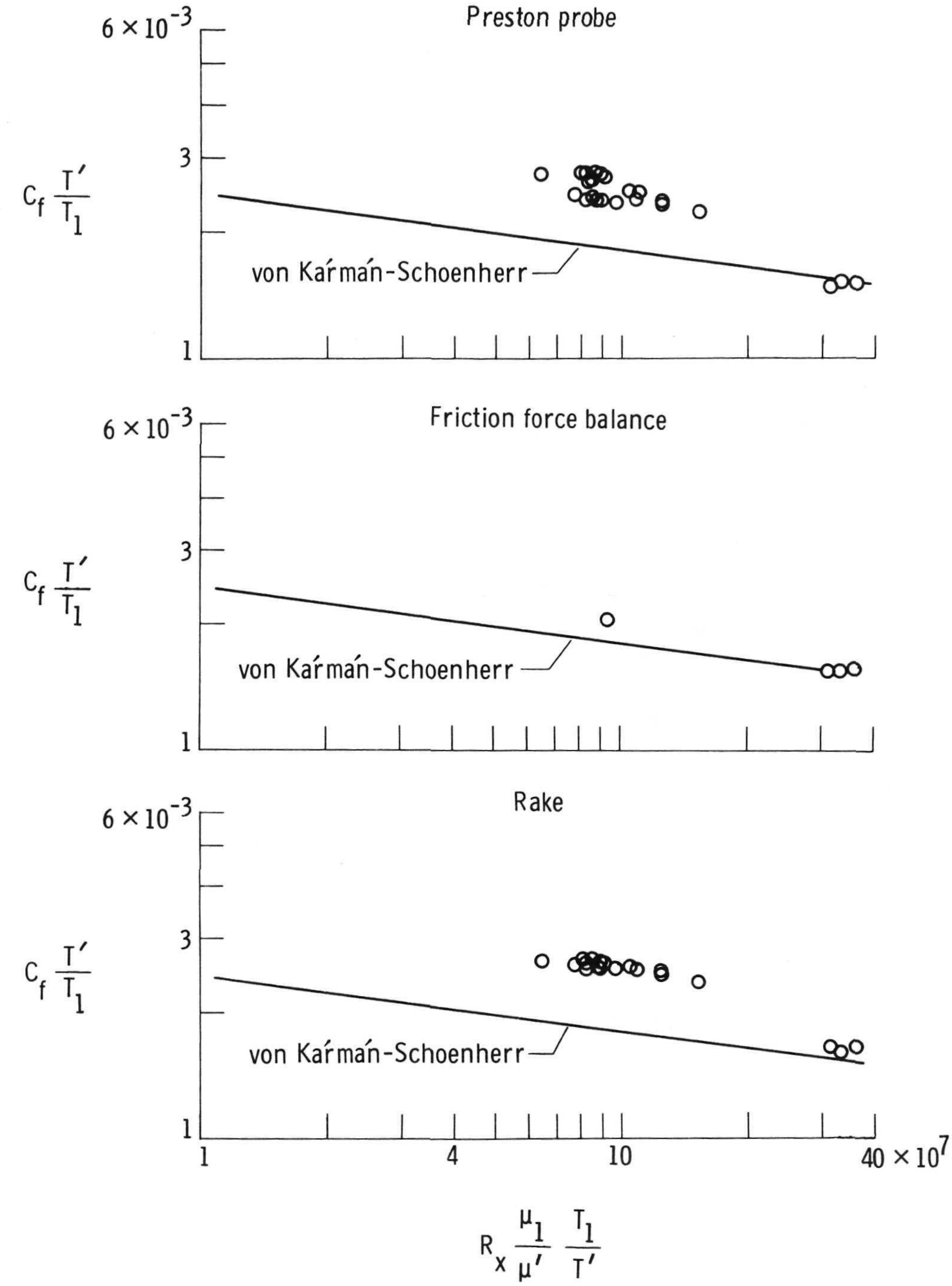

(b) Rear fuselage.

Figure 15. Continued.

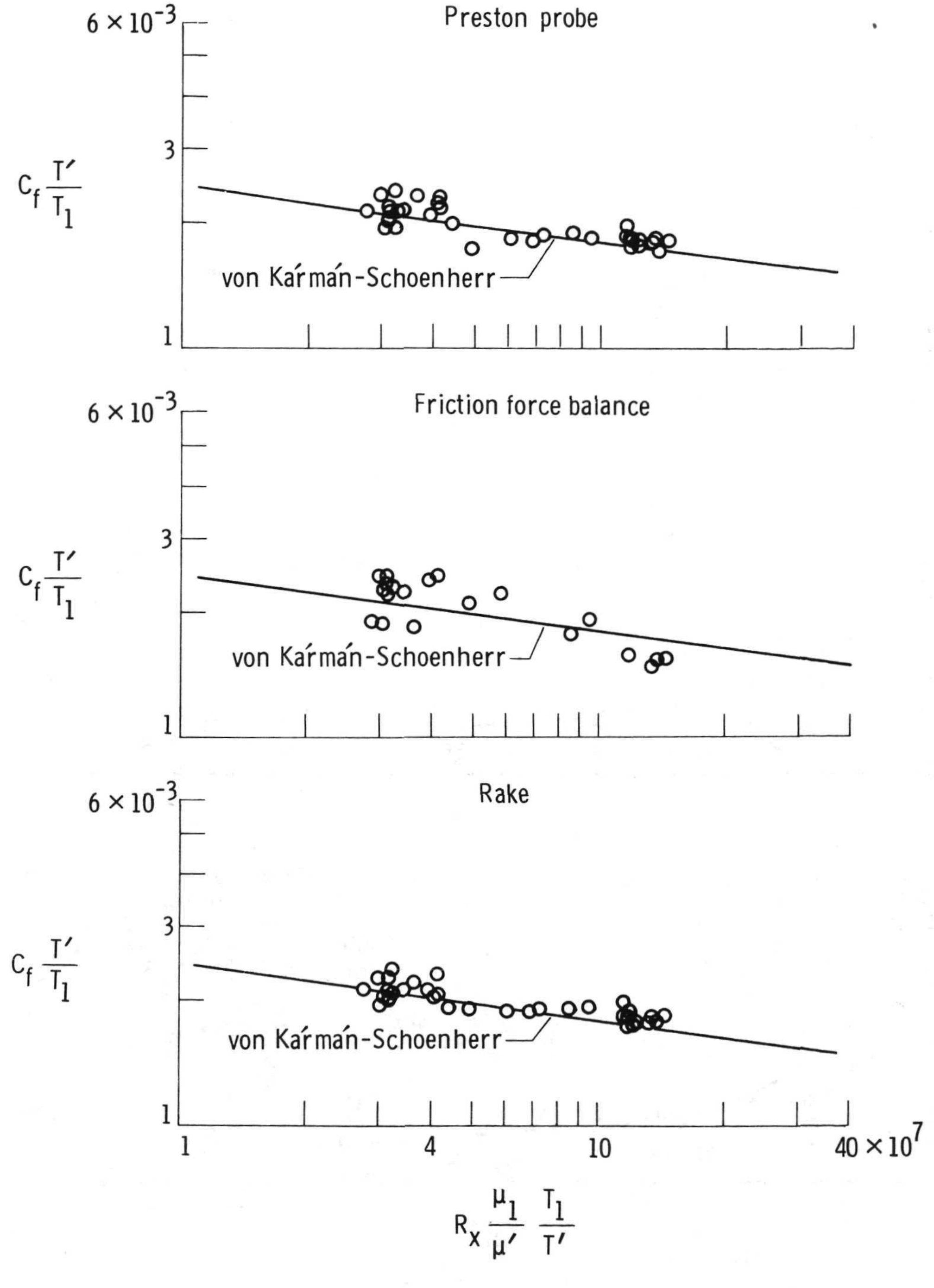

(c) Wing.

Figure 15. Concluded.

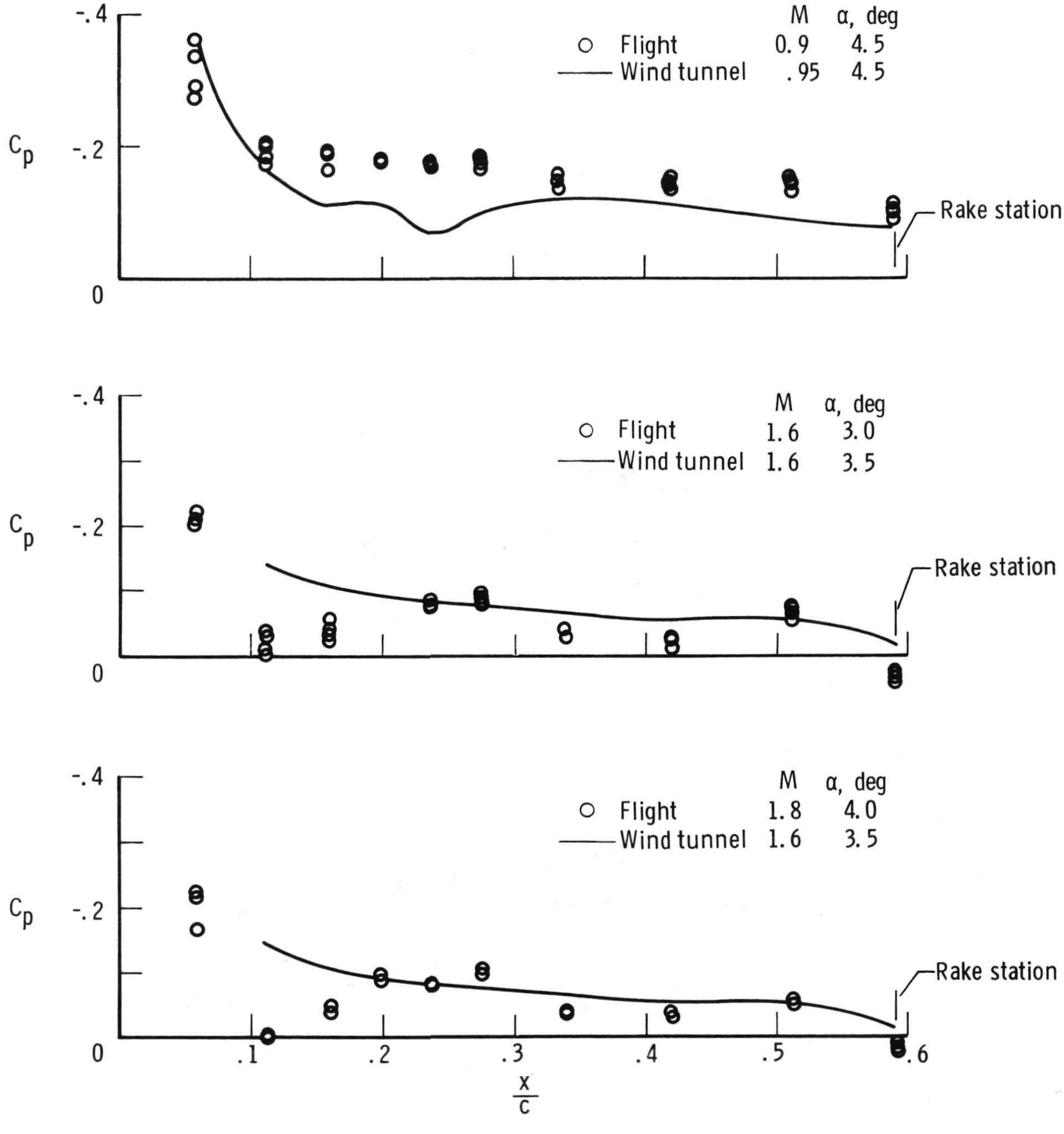

Figure 16. Comparison of flight and wind-tunnel-model wing pressure distribution ahead of wing sensor complex.

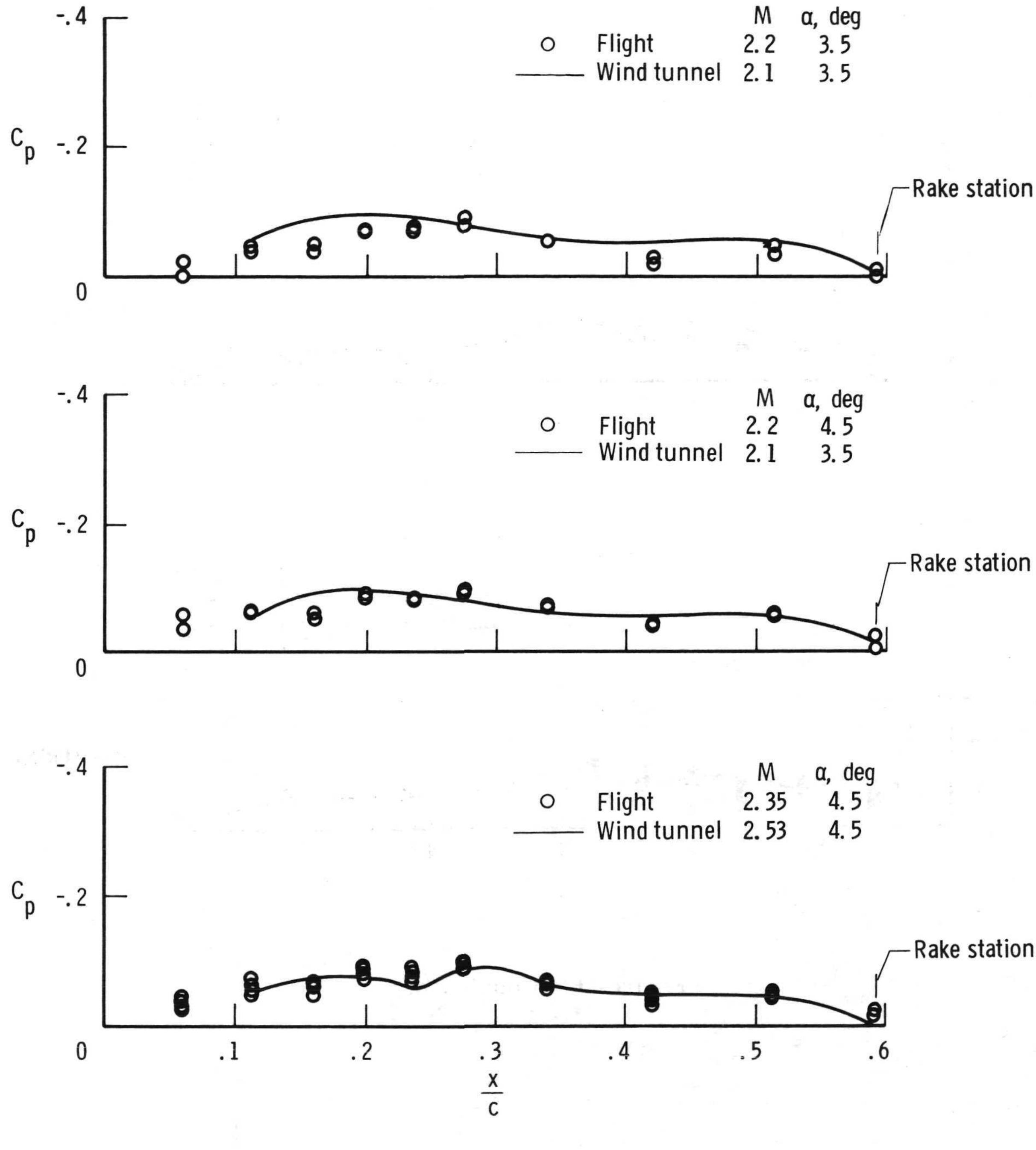

Figure 16. Continued.

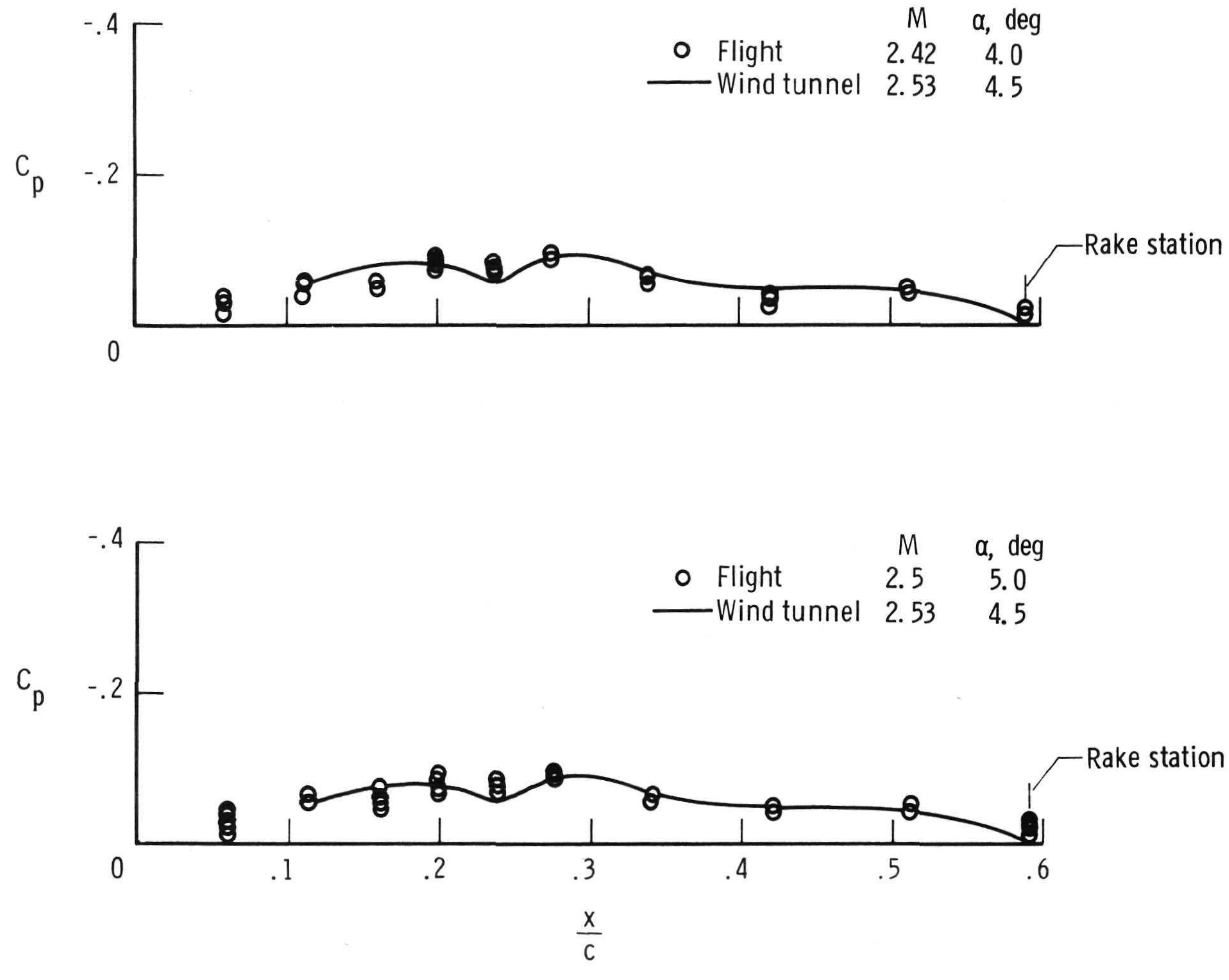

Figure 16. Concluded.

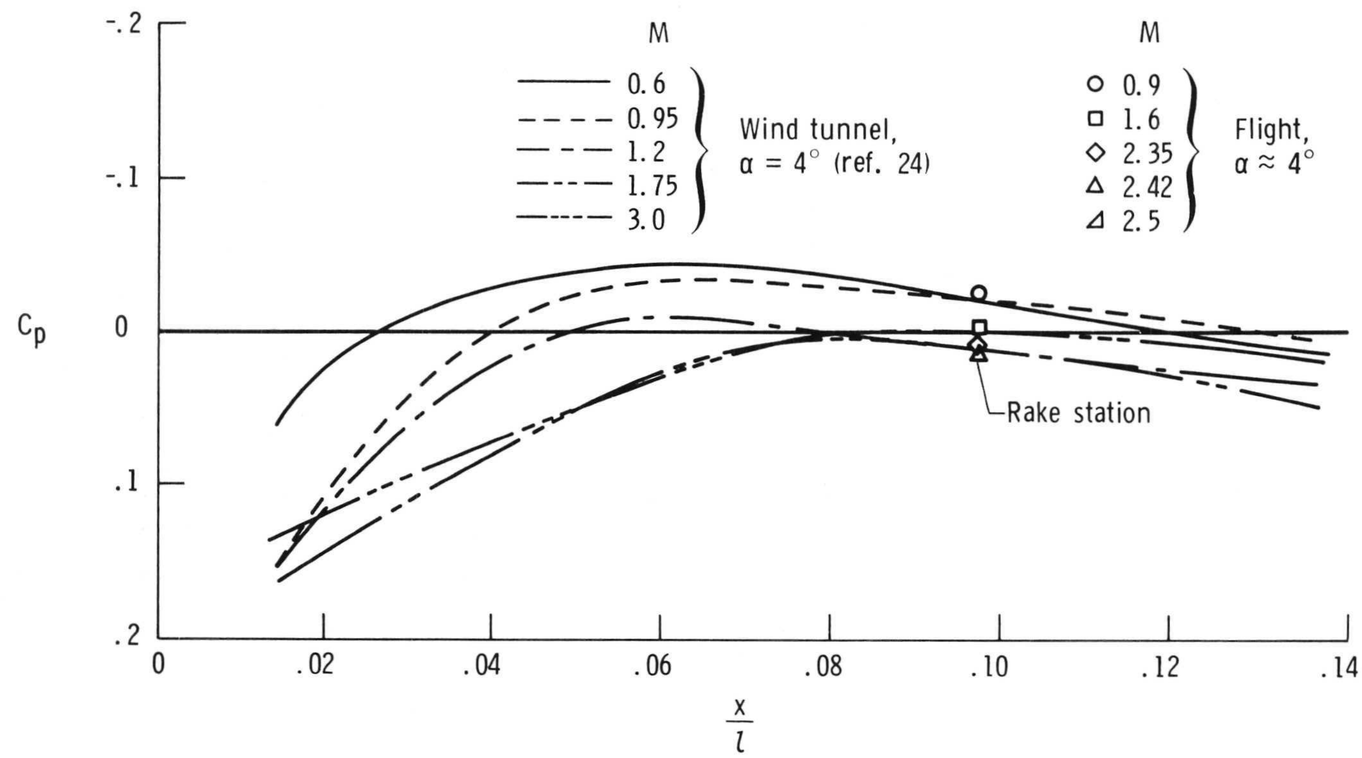

Figure 17. Wind-tunnel-measured pressure distribution on the fuselage lower surface and flight data for one location.

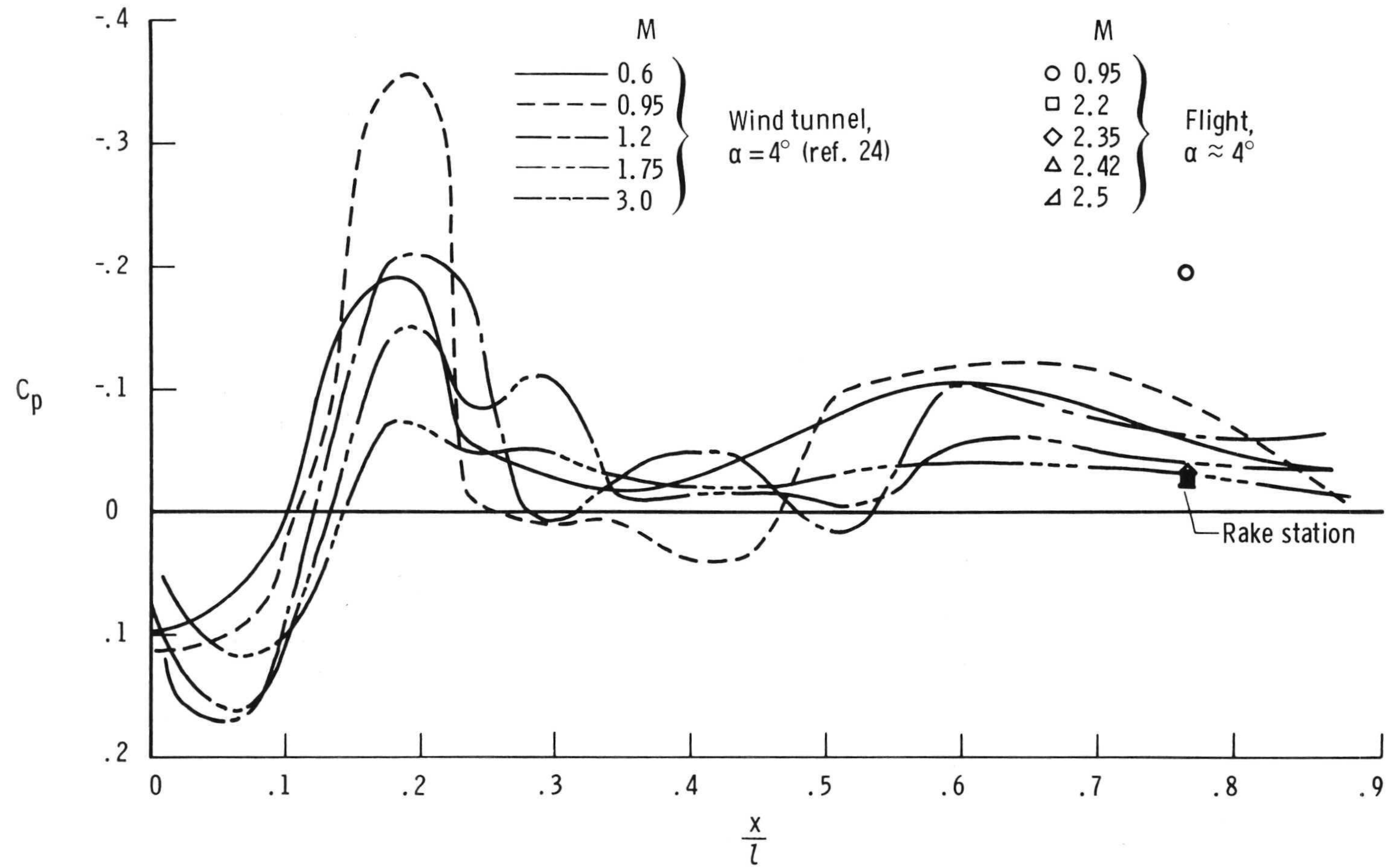

Figure 18. Wind-tunnel-measured pressure distribution on the fuselage upper surface and flight data for one location.

NASA-Langley, 1973 —— 12

"The aeronautical and space activities of the United States shall be conducted so as to contribute . . . to the expansion of human knowledge of phenomena in the atmosphere and space. The Administration shall provide for the widest practicable and appropriate dissemination of information concerning its activities and the results thereof."

—NATIONAL AERONAUTICS AND SPACE ACT OF 1958

NASA SCIENTIFIC AND TECHNICAL PUBLICATIONS

TECHNICAL REPORTS: Scientific and technical information considered important, complete, and a lasting contribution to existing knowledge.

TECHNICAL NOTES: Information less broad in scope but nevertheless of importance as a contribution to existing knowledge.

TECHNICAL MEMORANDUMS: Information receiving limited distribution because of preliminary data, security classification, or other reasons. Also includes conference proceedings with either limited or unlimited distribution.

CONTRACTOR REPORTS: Scientific and technical information generated under a NASA contract or grant and considered an important contribution to existing knowledge.

TECHNICAL TRANSLATIONS: Information published in a foreign language considered to merit NASA distribution in English.

SPECIAL PUBLICATIONS: Information derived from or of value to NASA activities. Publications include final reports of major projects, monographs, data compilations, handbooks, sourcebooks, and special bibliographies.

TECHNOLOGY UTILIZATION PUBLICATIONS: Information on technology used by NASA that may be of particular interest in commercial and other non-aerospace applications. Publications include Tech Briefs, Technology Utilization Reports and Technology Surveys.

Details on the availability of these publications may be obtained from:

SCIENTIFIC AND TECHNICAL INFORMATION OFFICE

NATIONAL AERONAUTICS AND SPACE ADMINISTRATION

Washington, D.C. 20546